

**CHARACTERIZATION OF REAL TIME PLATELET DEPOSITION ONTO OPAQUE  
SURFACES UNDER CLINICALLY-RELEVANT FLOW CONDITIONS**

by

Megan Ann Jamiolkowski

B.E. Biomedical Engineering, The Catholic University of America, 2010

Submitted to the Graduate Faculty of  
Swanson School of Engineering in partial fulfillment  
of the requirements for the degree of  
Doctor of Philosophy

University of Pittsburgh

2015

UNIVERSITY OF PITTSBURGH  
SWANSON SCHOOL OF ENGINEERING

This dissertation was presented

by

Megan Ann Jamiolkowski

It was defended on

November 9, 2015

and approved by

James Antaki, PhD

Professor, Departments of Biomedical Engineering and Computer Science, Carnegie Mellon University; Professor, Departments of Bioengineering and Surgery, University of Pittsburgh

Marina Kameneva, PhD

Professor, Departments of Surgery and Bioengineering and Director of the Artificial Blood Program, McGowan Institute for Regenerative Medicine, University of Pittsburgh

Alan Wells, D.M.Sc., M.D.

Professor and Vice-Chair, Department of Pathology, Professor, Department of Bioengineering, Executive Council, McGowan Institute for Regenerative Medicine,

University of Pittsburgh Cancer Institute

Dissertation Director: William Wagner, PhD,

Professor, Departments of Surgery, Bioengineering and Chemical Engineering, and Director, McGowan Institute for Regenerative Medicine, University of Pittsburgh

Copyright © by Megan Ann Jamiolkowski

2015

# **CHARACTERIZATION OF REAL TIME PLATELET DEPOSITION ONTO OPAQUE SURFACES UNDER CLINICALLY-RELEVANT FLOW CONDITIONS**

Megan Ann Jamiolkowski, PhD

University of Pittsburgh, 2015

Although the thrombogenic nature of the surfaces of cardiovascular devices is an important aspect of blood biocompatibility, few studies have examined platelet deposition onto opaque materials used for these devices in real time. This is particularly true for the metallic surfaces used in current ventricular assist devices (VADs). Using hemoglobin depleted red blood cells (RBC ghosts) and long working distance optics to visualize platelet deposition, we sought to perform such an evaluation. A titanium alloy (Ti6Al4V) and 5 alternative opaque materials were examined. Ti6Al4V had significantly increased platelet deposition relative to the majority of alternative materials.

Blood flow patterns are of particular concern for devices such as blood pumps where shearing forces can be high, volumes are relatively large, and the flow fields can be complex. However, few studies have examined the effect of geometric irregularities on thrombus formation on clinically relevant opaque materials under flow. The second objective of this report was to quantify human platelet deposition onto titanium alloys, as well as positive and negative control surfaces, in the region of crevices (~50-150  $\mu\text{m}$  in width) that might be encountered in many VADs. The results revealed that the largest crevice size was the least thrombogenic. At the higher shear rate, the most deposition occurred in the medium size crevice.

A third challenge in assessing the hemocompatibility of a blood-wetted device is understanding the functional relationship between shear stress, biochemical agonists, and artificial surfaces. The final objective of this report was to investigate the effect of sub-threshold concentrations of ADP in conjunction with flow on platelet deposition onto clinically relevant opaque materials. To achieve this aim, a membrane-based agonist delivery system was designed to evenly introduce specific concentrations of agonists into a flowing blood analog. The results showed that the addition of a sub-threshold level of ADP to the system resulted in nearly a 2.5 fold increase in deposition on the titanium surface. The data generated from this report could be used to improve the accuracy of a predictive model of thrombotic deposition in VADs.

## TABLE OF CONTENTS

<b>1.0</b>	<b>INTRODUCTION.....</b>	<b>1</b>
<b>1.1</b>	<b>SIGNIFICANCE.....</b>	<b>1</b>
<b>1.2</b>	<b>THROMBOSIS AND BLEEDING COMPLICATIONS ASSOCIATED WITH CONTINOUS FLOW VENTRICULAR ASSIST DEVICES .....</b>	<b>2</b>
<b>1.3</b>	<b>VIRCHOW’S TRIAD APPLIED TO VENTRICULAR ASSIST DEVICES.. .....</b>	<b>11</b>
<b>1.3.1</b>	<b>Biomaterial.....</b>	<b>11</b>
<b>1.3.2</b>	<b>Blood Flow.....</b>	<b>14</b>
<b>1.3.3</b>	<b>Blood Constitution.....</b>	<b>18</b>
<b>1.4</b>	<b>PREDICTIVE MODELS OF DEVICE THROMBOSIS .....</b>	<b>19</b>
<b>1.5</b>	<b>SUMMARY OF INTRODUCTION .....</b>	<b>20</b>
<b>1.6</b>	<b>OBJECTIVES.....</b>	<b>21</b>
<b>1.6.1</b>	<b>Objective # 1: Real time visualization and characterization of platelet deposition under flow onto clinically relevant opaque surfaces .....</b>	<b>22</b>
<b>1.6.2</b>	<b>Objective # 2: Visualization and Analysis of Biomaterial-centered Thrombus Formation within a Defined Crevice under Flow .....</b>	<b>22</b>
<b>1.6.3</b>	<b>Objective # 3: Characterizing the effect of sub-threshold concentrations of ADP on platelet deposition onto clinically relevant opaque materials.....</b>	<b>23</b>

<b>2.0</b>	<b>REAL TIME VISUALIZATION AND CHARACTERIZATION OF PLATELET DEPOSITION UNDER FLOW ONTO CLINICALLY RELEVANT OPAQUE SURFACES .....</b>	<b>24</b>
<b>2.1</b>	<b>INTRODUCTON.....</b>	<b>24</b>
<b>2.2</b>	<b>MATERIALS AND METHODS .....</b>	<b>25</b>
<b>2.2.1</b>	<b>Platelet Collection and Fluorescent Labeling .....</b>	<b>25</b>
<b>2.2.2</b>	<b>RBC Ghost Preparation and Characterization .....</b>	<b>26</b>
<b>2.2.3</b>	<b>Test Materials .....</b>	<b>27</b>
<b>2.2.4</b>	<b>Parallel Plate Flow Chamber.....</b>	<b>28</b>
<b>2.2.5</b>	<b>Blood Analogue Perfusion and Image Acquisition.....</b>	<b>28</b>
<b>2.2.6</b>	<b>Scanning Electron Microscopy.....</b>	<b>32</b>
<b>2.2.7</b>	<b>Flow Cytometry .....</b>	<b>33</b>
<b>2.2.8</b>	<b>Statistical Analyses .....</b>	<b>33</b>
<b>2.3</b>	<b>RESULTS .....</b>	<b>34</b>
<b>2.3.1</b>	<b>RBC Ghost Rheology.....</b>	<b>34</b>
<b>2.3.2</b>	<b>Acute Platelet Adhesion on Test Surfaces .....</b>	<b>35</b>
<b>2.3.3</b>	<b>Wall Shear Rate Effect on Platelet Adhesion.....</b>	<b>39</b>
<b>2.3.4</b>	<b>Surface Contact Angles, Scanning Electron Microscopy and Flow Cytometry .....</b>	<b>41</b>
<b>2.4</b>	<b>DISCUSSION.....</b>	<b>43</b>
<b>2.5</b>	<b>LIMITATIONS.....</b>	<b>47</b>
<b>2.6</b>	<b>CONCLUSIONS .....</b>	<b>49</b>

<b>3.0</b>	<b>VISUALIZATION AND ANALYSIS OF BIOMATERIAL-CENTERED THROMBUS FORMATION WITHIN A DEFINED CREVICE UNDER FLOW .....</b>	<b>50</b>
<b>3.1</b>	<b>INTRODUCTON.....</b>	<b>50</b>
<b>3.2</b>	<b>MATERIALS AND METHODS.....</b>	<b>51</b>
<b>3.2.1</b>	<b>Blood analog preparation .....</b>	<b>51</b>
<b>3.2.2</b>	<b>Parallel plate flow chamber .....</b>	<b>53</b>
<b>3.2.3</b>	<b>Blood analog perfusion and image acquisition .....</b>	<b>54</b>
<b>3.2.4</b>	<b>Fluorescent image analysis .....</b>	<b>55</b>
<b>3.2.5</b>	<b>Statistical analysis.....</b>	<b>56</b>
<b>3.3</b>	<b>RESULTS .....</b>	<b>56</b>
<b>3.3.1</b>	<b>Probability of acute platelet adhesion.....</b>	<b>56</b>
<b>3.3.2</b>	<b>Average intensity of deposited platelets.....</b>	<b>64</b>
<b>3.3.3</b>	<b>Representative real-time perfusion videos .....</b>	<b>68</b>
<b>3.4</b>	<b>DISCUSSION.....</b>	<b>69</b>
<b>3.5</b>	<b>LIMITATIONS.....</b>	<b>72</b>
<b>3.6</b>	<b>CONCLUSIONS .....</b>	<b>74</b>
<b>4.0</b>	<b>CHARACTERIZING THE EFFECT OF SUB-THRESHOLD CONCENTRATIONS OF ADP ON PLATELET DEPOSITION ONTO CLINICALLY RELEVANT OPAQUE MATERIALS.....</b>	<b>75</b>
<b>4.1</b>	<b>INTRODUCTON.....</b>	<b>75</b>
<b>4.2</b>	<b>MATERIALS AND METHODS.....</b>	<b>76</b>
<b>4.2.1</b>	<b>Blood analog preparation .....</b>	<b>76</b>

4.2.2	Parallel plate flow chamber and membrane based agonist delivery system .....	77
4.2.3	Blood analog and agonist perfusion .....	79
4.2.4	Image acquisition .....	80
4.2.5	Fluorescent image analysis .....	80
4.2.6	Statistical analysis .....	80
4.3	RESULTS .....	81
4.3.1	Acute platelet deposition .....	81
4.3.2	Representative real-time perfusion videos .....	85
4.4	DISCUSSION .....	87
4.5	LIMITATIONS .....	92
4.6	CONCLUSIONS .....	92
5.0	CONTINUED RESEARCH AND FUTURE DIRECTIONS .....	94
5.1	SYNERGISTIC EFFECT OF BIOCHEMICAL AGONIST ON PLATELET DEPOSITION ONTO CLINICALY RELEVENTS MATERIALS .....	94
5.2	CHARACTERIZING THE EFFECT OF GEOMETRIC IRREGULARITES ON PLATELET DEPOSTION ONTO CLINICALY RELEVENT SURFACES .....	95
5.2.1	Investigating the effect of crevice size and geometry .....	95
5.2.2	Pulsatile flow .....	96
5.3	COMPARATIVE ANALYSIS OF HUMAN, BOVINE AND OVINE BLOOD .....	97

<b>5.4</b>	<b>IN VIVO VALIDATION OF IN VITRO VISUALIZATION AND ANALYSIS OF BIOMATERIAL-CENTERED THROMBUS FORMATION WITHIN A DEFINED CREVICE .....</b>	<b>99</b>
<b>5.4.1</b>	<b>Visualization of platelet adhesion.....</b>	<b>99</b>
<b>5.4.2</b>	<b>Hematological analysis of test subject's blood .....</b>	<b>100</b>
<b>6.0</b>	<b>FINAL CONCLUSIONS .....</b>	<b>101</b>
	<b>APPENDIX A .....</b>	<b>105</b>
	<b>BIBLIOGRAPHY.....</b>	<b>109</b>

## **LIST OF TABLES**

Table 1. INTERMACS Profiles of Advanced Heart Failure. Manual of Operations and Procedures, Version 4.0. Available at <https://www.uab.edu/medicine/intermacs/mop-4-0> [15] ..... 8

## LIST OF FIGURES

- Figure 1.** Representative images of thrombosis in a continuous flow VAD (HeartMate II; Thoratec Corp, Pleasanton, CA, USA). A) Thrombosis in the bend relief and B) the pump. From Cheng et al. [15] ..... 4
- Figure 2.** Increase in confirmed HeartMate II pump thrombosis at three active implanting institutions after March 2011. From Starling et al. [32]..... 10
- Figure 3.** Representative digitized images of platelet adhesion on a) low-temperature isotropic carbon (LTIC) b) diamond-like carbon (DLC) c) Ti6Al4V (Ti). From Schaub et al. [43]..... 13
- Figure 4.** Scanning electron micrographs of platelets adhered to A) Ti6Al4V B) trimethoxy silane modified Ti6Al4V (Ti-TMSi) C) Silanated zwitterionic phosphorylcholine modified Ti6Al4V (Ti-PCSi) D) Silanated sulfobetaine modified Ti6Al4V (Ti-SBSi). Platelet deposition is reduced when the titanium alloy is modified by PCSi and SBSi. From Ye et al. [46]..... 14
- Figure 5.** High-speed flow visualization of flow within the HeartMate II pump utilizing flow fluorescent particles. Pump was run at clinically relevant speeds. Areas of erratic flow found near the bearings and after the stator. From Yang et al. [57] ..... 16
- Figure 6.** The design challenge of continuous flow ventricular assist devices. (a) A section of rotary blood pump; (b) ring thrombus formed at the transition between metal barb and polymer cannula of a pediatric continuous flow blood pump; (c) exaggerated magnified view of the irregular geometries located at the seams of blood-wetted devices; (d) well-known flow separation downstream of a backward step. From Zhao et al. [49] ..... 17
- Figure 7.** Parallel plate flow chamber and experimental set up. A) The circular metallic piece and rectangle were secured around the flow chamber with screws. B) The flow path was formed from a silicon gasket. Thin aluminum shim stock can be seen along the length of either side of the silicone gasket to ensure a precise chamber height. C) The blood analogue was perfused through the chamber and across the sample for 5 min. Images were acquired, in real time, 4mm from the inlet by a CCD camera. The transparent blood analogue and long working distance objective allowed for real time visualization of adherent fluorescent platelets through the flow path onto the opaque test surface. .... 30

**Figure 8.** Image analysis to quantify the percent platelet surface coverage. A) Original fluorescent image of platelets adhered to SiC after 5 min of perfusion, B) binary image rendered by the MatLab program, C) original fluorescent image overlaid with the outline of the binary image. Scale bar = 40  $\mu\text{m}$ . ..... 31

**Figure 9.** A) Comparing the viscosity of native and ghost RBCs in human plasma at a matched hematocrit of 27%. B) Mixture of native and ghost RBCs subjected to a wall shear rate of 1100  $\text{sec}^{-1}$ . Red and blue arrows indicate a native and ghost RBC respectively. Scale bar = 40  $\mu\text{m}$ . C) Deformability of native and ghost RBCs. .... 34

**Figure 10.** Representative fluorescent images of platelets adhered to A) Ti6Al4V, B) SiC, C) Al<sub>2</sub>O<sub>3</sub>, D) YZTP, E) ZTA, and F) MPC-Ti6Al4V after 5 min of perfusion. Scale bar = 40  $\mu\text{m}$ ... 36

**Figure 11.** Acute platelet adhesion on test materials perfused at a wall shear rate of 400  $\text{sec}^{-1}$ . Images were acquired at 4mm distance from the inlet of the parallel plate flow chamber..... 37

**Figure 12.** Acute platelet adhesion on test materials perfused at a wall shear rate of 1000  $\text{sec}^{-1}$ . Images were acquired 4mm from the inlet of the parallel plate flow chamber. .... 38

**Figure 13.** Comparison of the effect of wall shear rate on acute platelet adhesion. Note Ti6Al4V and SiC are scaled differently than the other materials.  $P < 0.01$  between shear rates for all materials except MPC-Ti6Al4V. .... 40

**Figure 14.** Representative scanning electron micrographs of platelets adhered to A) Ti6Al4V, B) SiC, C) Al<sub>2</sub>O<sub>3</sub>, D) YZTP, E) ZTA, and F) MPC-Ti6Al4V after 5 min of perfusion. Scale bar = 40  $\mu\text{m}$ . .... 42

**Figure 15.** Experimental Setup. A) Schematic of the flow path utilized in this study with magnified view of the rectangular crevice. The arrow indicates the direction of flow B) Photograph of parallel plate chamber with magnified view of the rectangular crevice. C) Schematic of the experimental layout. D) Photograph of the actual experimental layout. .... 54

**Figure 16.** Color maps depicting the local probability of platelet deposition within each crevice size, over time, at a perfusion rate of 125  $\mu\text{L}/\text{min}$  and a wall shear rate of 400  $\text{sec}^{-1}$ . The direction of flow is down for the main channel, outside of the crevice. .... 57

**Figure 17.** Color maps depicting the probability of platelets depositing within each crevice size, over time, at a perfusion rate of 310  $\mu\text{L}/\text{min}$  and a wall shear rate of 1000  $\text{sec}^{-1}$ . The direction of flow is down for the main channel, outside of the crevice. .... 58

**Figure 18.** Color maps depicting the probability of platelets depositing on each material, over time, at a perfusion rate of 125  $\mu\text{L}/\text{min}$  and a wall shear rate of 400  $\text{sec}^{-1}$ . Crevice size of  $90 \pm 12 \mu\text{m}$ . The direction of flow is down for the main channel, outside of the crevice. .... 59

**Figure 19.** Color maps depicting the probability of platelets depositing on each material, over time, at a perfusion rate of 310  $\mu\text{L}/\text{min}$  and a wall shear rate of 1000  $\text{sec}^{-1}$ . Crevice size of  $90 \pm 12 \mu\text{m}$ . The direction of flow is down for the main channel, outside of the crevice. .... 60

**Figure 20.** The percent of the surface covered by deposited platelets. A) The effect of crevice size on platelet surface coverage at a wall shear rate of 400  $\text{sec}^{-1}$ . B) The effect of material on platelet surface coverage at a wall shear rate of 400  $\text{sec}^{-1}$ . Crevice size of  $90 \pm 12 \mu\text{m}$ . C) The effect of crevice size on platelet surface coverage at a wall shear rate of 1000  $\text{sec}^{-1}$ . D) The effect of material on platelet surface coverage at a wall shear rate of 1000  $\text{sec}^{-1}$ . Crevice size of  $90 \pm 12 \mu\text{m}$ . .... 61

**Figure 21.** Effect of wall shear rate on platelet surface coverage. A)  $137 \pm 10 \mu\text{m}$ . B)  $90 \pm 12 \mu\text{m}$ . C)  $53 \pm 7 \mu\text{m}$ . D) Collagen. E) MPC-Ti6Al4V. .... 63

**Figure 22.** Color maps depicting the average intensity of the platelet deposition within each crevice size, over time, at a perfusion rate of 125  $\mu\text{L}/\text{min}$  and a wall shear rate of 400  $\text{sec}^{-1}$ . The direction of flow is down for the main channel, outside of the crevice. .... 65

**Figure 23.** Color maps depicting the average intensity of the platelet deposition within each crevice size, over time, at a perfusion rate of 310  $\mu\text{L}/\text{min}$  and a wall shear rate of 1000  $\text{sec}^{-1}$ . The direction of flow is down for the main channel, outside of the crevice. .... 66

**Figure 24.** The direction of flow is down. Color maps depicting the average intensity of the platelet deposition on each material over time, at a perfusion rate of 125  $\mu\text{L}/\text{min}$  and a wall shear rate of 400  $\text{sec}^{-1}$ . Crevice size of  $90 \pm 12 \mu\text{m}$ . .... 67

**Figure 25.** The direction of flow is down. Color maps depicting the average intensity of the platelet deposition on each material over time, at a perfusion rate of 310  $\mu\text{L}/\text{min}$  and a wall shear rate of 1000  $\text{sec}^{-1}$ . Crevice size of  $90 \pm 12 \mu\text{m}$ . .... 68

**Figure 26.** Membrane based biochemical agonist delivery system. A) Photo of the membrane based biochemical agonist delivery system. B) Schematic of the agonist delivery system. B.1) Side view of the system schematic. B.2) Front view of the system schematic. .... 78

**Figure 27.** Percent of the test surface covered by deposited platelets. A) Wall shear rate 400  $\text{sec}^{-1}$ . B) Wall shear rate 1000  $\text{sec}^{-1}$ . .... 82

**Figure 28.** Effect of wall shear rate on the percent of the test surface covered by deposited platelets. A) Ti6Al4V: 10 nM ADP. B) Ti6Al4V: 5 nM ADP. C) Ti6Al4V: 0 nM ADP. D) ZTA: 10 nM ADP ..... 83

**Figure 29.** Average area of individual thrombi over time. A) Wall shear rate 400  $\text{sec}^{-1}$ . B) Wall shear rate 1000  $\text{sec}^{-1}$  ..... 84

**Figure 30.** Effect of wall shear rate on average area of individual thrombi over time. A) Ti6Al4V: 10 nM ADP. B) Ti6Al4V: 5 nM ADP. C) Ti6Al4V: 0 nM ADP. D) ZTA: 10 nM ADP. 85

**Figure 31.** *Representative fluorescent images of embolization at a wall shear rate of 400 sec<sup>-1</sup>. Embolization was only seen when 10 nM of ADP was added to the blood analog perfusing over the Ti6Al4V surface. Scale bar = 40 μm* ..... 86

**Figure 32.** *Representative fluorescent images of embolization at a wall shear rate of 1000 sec<sup>-1</sup>. Embolization was seen when 5 nM or 10 nM of ADP was added to the blood analog perfusing over the Ti6Al4V surface. Scale bar = 40 μm.* ..... 87

**Figure 33.** *Method for in vivo visualization. A) Fiber optic remote microscope. B) Modified a polycarbonate centrifugal blood pump. From Wagner et al.[8]* ..... 100

## **1.0 INTRODUCTION**

### **1.1 SIGNIFICANCE**

Blood-contacting medical devices are often associated with thrombotic, and thromboembolic events that result in morbidity and mortality, which ultimately impedes the broader adoption of these technologies.[1-5] The propensity for platelet adhesion, activation and thrombus formation are key considerations in the design and selection of materials for blood-wetted devices. The majority of cardiovascular devices, such as vascular grafts, stents, and heart valves, are susceptible to thrombosis and thromboembolic events. In these devices platelets are subjected to areas of varying flow patterns, high wall shear stress, and exposure to a multitude of biochemical agonists (ADP, Ca<sup>++</sup>, thrombin, thromboxane A<sub>2</sub>, etc.).[6]+

Continuous flow ventricular assist devices (VADs) present particular blood biocompatibility challenges due to their complex blood flow pathways, supra-physiological shear rates, large blood contacting surface areas, and extended implant periods in patients with advanced cardiovascular disease. In the United States it is estimated that there are over 100,000 patients with end stage heart failure that could benefit from a heart transplant. However due to the limited organs available, only around 2200 transplants are likely to be performed in 2015.[7] VADs were originally designed to provide circulatory support to end stage heart failure patients while awaiting a heart transplant (bridge to transplant (BTT)) by mimicking the biphasic flow of

the native heart.[8, 9] However, the power and volume displacement necessary for pulsatile flow required these devices to be large, limiting their use in smaller heart failure patients. The introduction of rotary and centrifugal pumps decreased the size and power requirements of VADs, increasing the patient population eligible to receive the device. These pumps utilized a single rotating impeller to support the patient with continuous perfusion of blood, increasing their mechanical durability, allowing the device to be implanted for extended periods of time. These devices may also improve destination therapy (DT), a possibility for patients who do not qualify for heart transplantation.[10] This report focuses on continuous flow VADs. Despite improvement in VAD technology, the threat of thromboembolic events and pump thrombosis continues to be a major concern for these patients.[1, 2, 11, 12]

## **1.2 THROMBOSIS AND BLEEDING COMPLICATIONS ASSOCIATED WITH CONTINUOUS FLOW VENTRICULAR ASSIST DEVICES**

As more centers started implanting a variety of VADs, the need for a standardized definition of thromboembolic events and a method for analyzing these events in patients became apparent. To address this need, the Interagency Registry for Mechanically Assisted Circulatory Support (INTERMACS) was developed. INTERMACS is a national database sponsored by the National Heart, Lung and Blood Institute in partnership with the U.S Food and Drug Administration (FDA) and the Centers for Medicare and Medical Services.[1, 13, 14] This database provides a method for acquiring important VAD implant information, including adverse events and mortality rates. It also provides a standard definition for major adverse events like bleeding, neurological dysfunctions and pump thrombosis.[15]

In an INTERMACS report published in 2014, continuous flow VAD patients had a one year survival rate of 81%. [1] This is substantially higher than end stage heart failure patients who are not supported by a device who only have a 1 year survival rate of around 50%. [16] Continuous flow VAD patients also experienced a 89%, 83%, and 81% freedom from major neurological events at 1, 2, and 3 years of device support (N=5436). [13] The rate of neurological dysfunction within this patient population was 1.83 (events/ 100 patient months in the first 12 months after implantation). Bleeding and pump malfunction events were also reported, with a rate of 9.45 and 1.60 respectively (events/ 100 patient months in the first 12 months after implantation). [13] The overall survival for continuous flow VAD patients continues to be high with a 1 and 2 year survival rate of 80% and 70% respectively. [1] However their actual freedom from any major adverse event (infection, bleeding, device malfunction, stroke, or death) is only 48% after 3 months and only 14% after 3 years [13] Representative images of thrombus in continuous flow VADs are shown in **Figure 1**. [17]

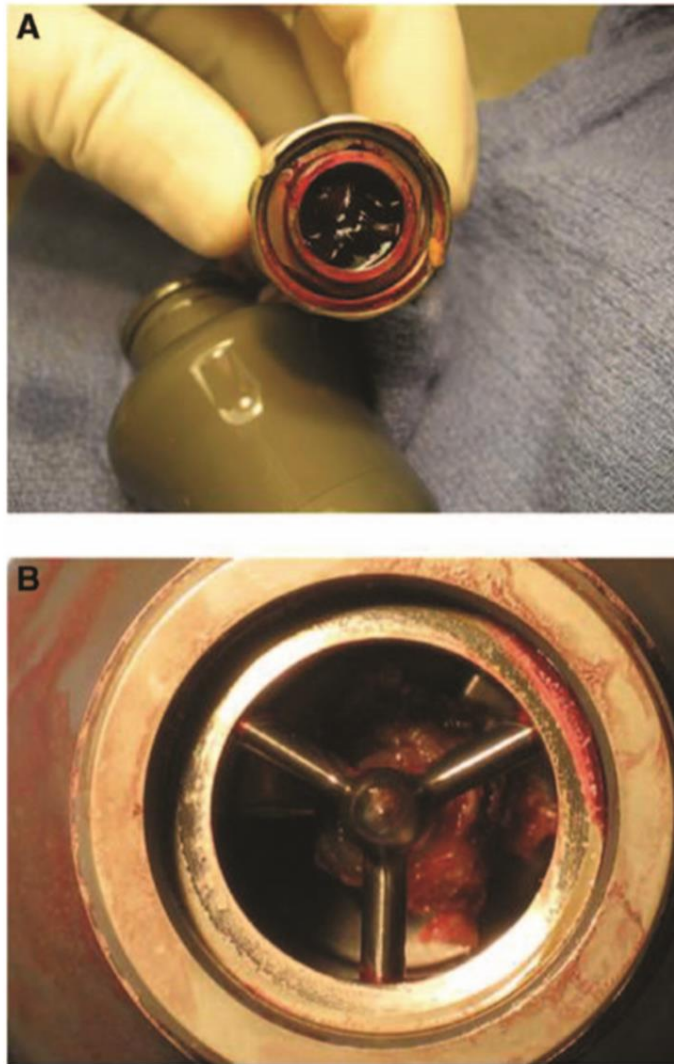


**Figure 1.** Representative images of thrombosis in a continuous flow VAD (HeartMate II; Thoratec Corp, Pleasanton, CA, USA). A) Thrombosis in the bend relief and B) the pump. From Cheng et al. [15]

Currently, one of the most widely used continuous flow VADs is the Thoratec HeartMate II (Thoratec Corp, Pleasanton, CA, USA) axial flow pump.[18, 19] Several studies have reported on adverse events experienced by patients who are supported by this device. Data reported in 2007 from the HeartMate II bridge to transplant (BTT) clinical trial found that 6% of the VAD recipients experienced ischemic strokes, 2% hemorrhagic stroke, 2% pump thrombosis requiring

pump replacement, and 84% of patients suffered a bleeding event, with 41% requiring re-operation (133 patients).[20] In 2009, a report by Pagani et al. published results gathered from the continuation of the HeartMate II BTT trial. This report revealed that the incidence of bleeding was decreased to 79%, with 26% requiring re-operation (1.67 and 0.45 events/patient year, respectively). The incidence of ischemic and hemorrhagic stroke remained essentially the same at 5% and 3% respectively (0.09 and 0.05 events/patient year respectively). 1% of the VAD patients had primary device thrombosis requiring surgical intervention (0.04 events/patient year; 281 patients).[21] The HeartMate II was approved by the FDA for BTT indications in 2008. A report on the post-approval trial by Starling et al. revealed the incidence of bleeding continued to be high, with 44% of HeartMate II patients experiencing a bleeding event (1.44 events/patient year). Furthermore, 4.7% of patients experienced an embolic stroke event (0.06 events/patient year) and 1.2 percent of patients suffered hemorrhagic stroke (0.01, 169 patients).[22]

The HeartMate II was approved for destination therapy (DT) indication in 2010 and it is currently the only continuous flow device approved for this purpose.[18] A 2009 report on the HeartMate II DT clinical trial revealed that 81% of the patients experienced a bleeding event (1.66 events/patient year) with another 30% requiring re-operation for bleeding (0.23 events/patient year). It was also reported that 18% of patients suffered a stroke, 8% of which were thromboembolic in nature. Another 4% had pump thrombosis (134 patients).[23] Since this study, the popularity of using VADs for DT has increased. The most recent INTERMACS report stated that nearly half of the continuous flow VADs implanted from 2011-2013 were for DT indications (41%). This report did show that the 2-year survival of patients supported for DT was 10% lower than that of patients supported for BTT (61% and 78% respectively). However, the 2-year survival rate of patients supported by the Heartmate II for DT is substantially higher than

the 2 year survival rate for the pulsatile VADs patient and patients receiving optimal medical management as reported in the Randomized Evaluation of Mechanical Assistance for the Treatment of Congestive Heart Failure (REMACH) Trial (23% and 8% respectively).[9]

Another continuous flow VAD that is widely used in clinics is the HeartWare HVAD (HeartWare Inc, Framingham, MA, USA). The HVAD is a centrifugal flow pump with magnetically and hydrodynamically levitated impeller. This impeller-levitating technology eliminates the need for mechanical bearings, improving the fluid dynamic design of the VAD. However, the HVAD and other 3rd generation pumps are still associated with hemocompatibility issues.[18, 24] In 2011, Strueber et al. reported that 12% of patients supported by the HVAD for BTT experienced stroke, 4% of which were ischemic, 30% had incidences of bleeding, with 20% needing re-operation, and another 8% needed a device replacement due to left heart embolus (N=50 patients).[25] The U.S. clinical trial for the use of the HVAD for BTT indicates that 14.8% of patients experienced bleeding events that necessitated re-operation, 12.7% experienced gastrointestinal bleeds, 15.3% suffered stroke with 7.5% being ischemic and 4.2% needed pump exchange due to expected or confirmed pump thrombosis. (N=332 patients).[26]

Due to the relative success of continuous flow VAD therapy, clinicians have considered implanting the devices in less sick patients.[1] The INTERMACS profile for advanced heart failure was developed to categorize the health status of heart failure patients, where a higher level indicates a more stable patient (**Table 1**).[15] INTERMACS data show that VAD patients whose INTERMACS profile level is greater than 2 at implantation have a 5%-8% increase in 1 year survival rate compared to those who are characterized as INTERMACS profile level 2 or lower.[9, 13] In a single center study of patients who received the HVAD for BTT, the outcomes for patients who were characterized as either INTERMACS level 1/level 2 or INTERMACS

level 3/level 4 at the time of implantation were compared. Patients who were INTERMACS level 3/level 4 had improved survival rates compared to the less stable patients (30 day survival rate of 90% and 50% respectively). The more stable patients also had a greater freedom from stroke at 81% compared to 48% with the INTERMACS level 1/level 2 patients (N=50 patients).[27] Despite these results, the risk of thrombotic and thromboembolic events remain high. In the same study they found that 22% of patients suffered ischemic stroke, 4% suffered hemorrhagic stroke, and 26% of patients experienced bleeding that required re-operation.[27] Another recent single center study reported by Wu et al. in 2013 found that 6.81% of patients suffered from a neurological dysfunction.[28] The substantial adverse events experienced by VAD patients are deterrents for implanting the device in healthier patients. This is particularly true because patients who receive optimal medical treatment (OMT) for heart failure tend to experience reduced incidence of these events. A study reported by Rogers et al. found that 11% of OMT patients treated for a comparable length of time as VAD implantation experienced stroke while 0% experienced bleeding (N=18 patients).[29] Similarly, Rose et al. found neurological dysfunction at a rate of 0.09 events/patient year and no bleeding events (61 patients).[30] Furthermore, Witt et al. performed a meta-analysis that found only 5% of heart failure patients experienced ischemic stroke within the first 5 years of diagnosis.[31] Therefore, these hematological adverse events associated with VADs deter the broader acceptance of this technology for use in less-sick patients.

**Table 1.** INTERMACS Profiles of Advanced Heart Failure. Manual of Operations and Procedures, Version 4.0.

Available at <https://www.uab.edu/medicine/intermacs/mop-4-0> [15]

<b>INTERMACS Profiles of Advanced Heart Failure</b>
<p><b>INTERMACS® 1:</b> Critical cardiogenic shock describes a patient who is “crashing and burning”, in which a patient has life-threatening hypotension and rapidly escalating inotropic pressor support, with critical organ hypoperfusion often confirmed by worsening acidosis and lactate levels.</p>
<p><b>INTERMACS® 2:</b> Progressive decline describes a patient who has been demonstrated “dependent” on inotropic support but nonetheless shows signs of continuing deterioration in nutrition, renal function, fluid retention, or other major status indicator. Patient profile 2 can also describe a patient with refractory volume overload, perhaps with evidence of impaired perfusion, in whom inotropic infusions cannot be maintained due to tachyarrhythmias, clinical ischemia, or other intolerance.</p>
<p><b>INTERMACS® 3:</b> Stable but inotrope dependent describes a patient who is clinically stable on mild-moderate doses of intravenous inotropes (or has a temporary circulatory support device) after repeated documentation of failure to wean without symptomatic hypotension, worsening symptoms, or progressive organ dysfunction (usually renal). It is critical to monitor nutrition, renal function, fluid balance, and overall status carefully in order to distinguish between a patient who is truly stable at Patient Profile 3 and a patient who has unappreciated decline rendering them Patient Profile 2. This patient may be either at home or in the hospital.</p>
<p><b>INTERMACS® 4:</b> Resting symptoms describes a patient who is at home on oral therapy but frequently has symptoms of congestion at rest or with activities of daily living (ADL). He or she may have orthopnea, shortness of breath during ADL such as dressing or bathing, gastrointestinal symptoms (abdominal discomfort, nausea, poor appetite), disabling ascites or severe lower extremity edema. This patient should be carefully considered for more intensive management and surveillance programs, which may in some cases, reveal poor compliance that would compromise outcomes with any therapy.</p>
<p><b>INTERMACS® 5:</b> Exertion Intolerant describes a patient who is comfortable at rest but unable to engage in any activity, living predominantly within the house or housebound. This patient has no congestive symptoms, but may have chronically elevated volume status, frequently with renal dysfunction, and may be characterized as exercise intolerant.</p>
<p><b>INTERMACS® 6:</b> Exertion Limited also describes a patient who is comfortable at rest without evidence of fluid overload, but who is able to do some mild activity. Activities of daily living are comfortable and minor activities outside the home such as visiting friend or going to a restaurant can be performed, but fatigue results within a few minutes of any meaningful physical exertion. This patient has occasional episodes of worsening symptoms and is likely to have had a hospitalization for heart failure within the past year.</p>
<p><b>INTERMACS® 7:</b> Advanced NYHA Class 3 describes a patient who is clinically stable with a reasonable level of comfortable activity, despite history of previous decompensation that is not recent. This patient is usually able to walk more than a block. Any decompensation requiring intravenous diuretics or hospitalization within the previous month should make this person a Patient Profile 6 or lower.</p>

A 2013 report by Starling et al. showed a concerning and sudden increase in HeartMate II pump thrombosis across three major implant centers: the Cleveland Clinic, Washington University Barnes-Jewish Hospital, and Duke University. The data showed that before 2011 only 2.2% of patients experienced pump thrombosis within 3 months of support, while this number increased four-fold to 8.4% of patients implanted from 2011 to 2013 (837 patients, **Figure 2**).<sup>[32]</sup> It is not known why this increase has occurred. Since the device has been approved for destination therapy, the device has most likely been implanted in sicker patients (patients who do not qualify for transplantation). It is also possible that pump thrombosis was originally underreported because it is difficult to diagnose without explanting the device. Pump thrombosis is particularly concerning because the 1 year patient survival rate decreases with each device replacement at 80% with the original device, to 65% after the second implant, and only 50% after the third implantation.<sup>[1]</sup> This and similar reports that have shown an unexpected increase in thromboembolic events in patients who have received HeartMate II and HVAD <sup>[32, 33]</sup>, has led the FDA to issue a safety communication stating the potential risk associated with the use of these devices is greater than originally reported at the time of regulatory approval.<sup>[34]</sup> Thus, the timeliness of a more thorough investigation into the potential triggers for thrombotic deposition in VADs is clear and this challenge extends to several other blood-contacting medical devices.

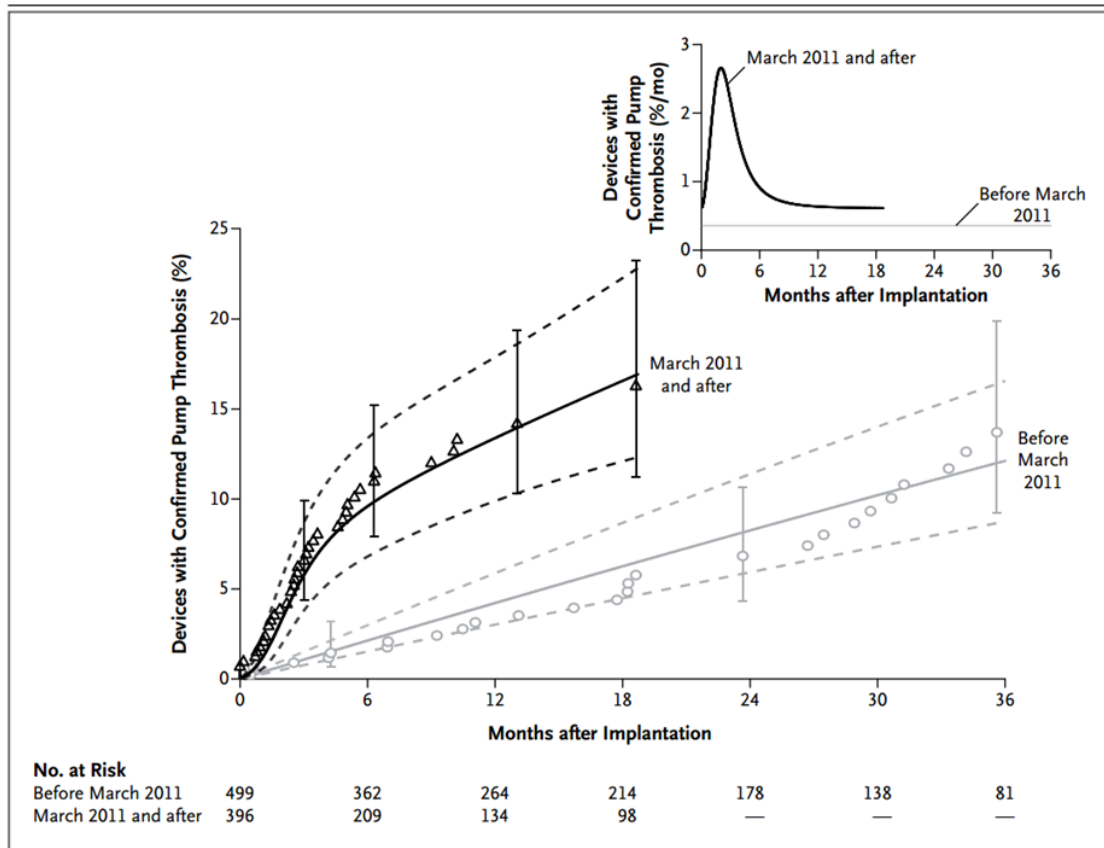


**Figure 2.** Increase in confirmed HeartMate II pump thrombosis at three active implanting institutions after March 2011. From Starling et al. [32]

DeVore et al. reported that the HeartMate II destination therapy trial determined that the cost for continuous flow VADs is \$190,148 per quality-adjusted life year (QALY). This does not, however, meet the cost-effectiveness metric for the U.S.[35] Puehler et al. reported a similar statistic stating that the mean cost for continuous flow support is \$193,812 per QALY.[9] One method to improve the cost effectiveness of continuous flow VADs is to develop more biocompatible VADs. In order to achieve this goal, further investigation into how fluid dynamics, material selection, and hemostatic condition of the patient affect the potential for device thrombosis is needed.

### **1.3 VIRCHOW'S TRIAD APPLIED TO VENTRICULAR ASSIST DEVICES**

Virchow's triad is a summation of factors that cause the development of thrombosis. According to this triad, these three components are abnormalities in the vessel wall, abnormalities in the blood constitution, and abnormalities in the blood flow. Although Virchow first published his work in 1856, the concept is still applicable today and can be translated to explain the factors involved in device thrombosis.[36] When applying Virchow's triad to cardiovascular devices such as VADs, the three factors that affect thrombosis development are: the reactivity of the biomaterial, the hemostatic state of the patient's blood, and the blood flow.[37, 38] As stated earlier, continuous flow VADs have complex blood flow pathways, supra-physiological shear rates, large blood contacting surface areas, and are often implanted in patients with pro-thrombotic conditions. Therefore, to fully investigate the thrombotic and thromboembolic issues associated with continuous flow VADs all three factors of the triad must be analyzed as well as their functional relationship with each other.

#### **1.3.1 Biomaterial**

When blood comes into contact with an artificial material, proteins quickly adhere to the surface. Initially the surface becomes covered in proteins that are in the highest concentration within the plasma or smaller proteins that are easily diffused towards the surface. However, over time these proteins are replaced by larger less diffusible proteins that have a higher affinity for the surface. This is known as the Vroman effect.[39] Blood interaction within the VAD occurs between the absorbed proteins and the patient's blood. Platelets adhere to blood-contacting surfaces through receptors that bind with specific absorbed plasma proteins. The most common platelet adhesion

receptors are glycoprotein IIb/IIIa (GP  $\alpha_{IIb}\beta_3$ ) that binds to absorbed fibronectin, fibrinogen, and von Willebrand factor and glycoprotein Ib (GP Ib). At higher shear rates GP Ib is the dominant receptor whereas at lower shear rates binding is dependent on GP IIb/IIIa. [39, 40] The surface chemistry of the biomaterial dictates the conformation of the absorbed proteins. Consequently, it is the surface chemistry that dictates whether the appropriate binding sites will be exposed to the blood in order to initiate platelet adhesion.[41]

A substantial portion of biomaterials research has been devoted to developing methods to reduce the thrombogenicity of these devices through their design and surface manipulation.[6, 10, 40, 44, 45] Numerous reports have focused on developing inert, nonfouling materials to prevent platelet adhesion and subsequent thrombus formation. For example, the anticoagulant heparin has been immobilized through covalent bonding, ionic bonding, and physical adsorption.[6, 10, 44, 45] To reduce platelet deposition onto common metallic biomaterials, coatings such as diamond like carbon (DLC) and 2-methacryloyloxyethyl phosphorylcholine (MPC) polymers have been investigated.[10, 40, 44] Although a wide array of approaches have been investigated to reduce material thrombogenicity, thrombosis complications remain of clinical significance for many devices. Thus surfaces with improved biocompatibility, as well as methods to quantify such improvements, remain of interest to the cardiovascular device community.

Continuous flow VAD manufacturers often use a polished titanium alloy (Ti6Al4V) as the blood contacting surface due to its desirable mechanical properties, resistance to corrosion and tolerable blood compatibility.[42] However, *in vitro* studies have shown that this alloy exhibited elevated acute thrombogenicity compared to other coated surfaces (e.g., polyethylene glycol and diamond-like carbon coatings) or related alloys (Ti6Al7Nb).[6, 43-45] Representative images of the thrombogenicity of Ti6Al4V compared to other materials and surface coatings are displayed in **Figures 3 and 4**.[43, 46]

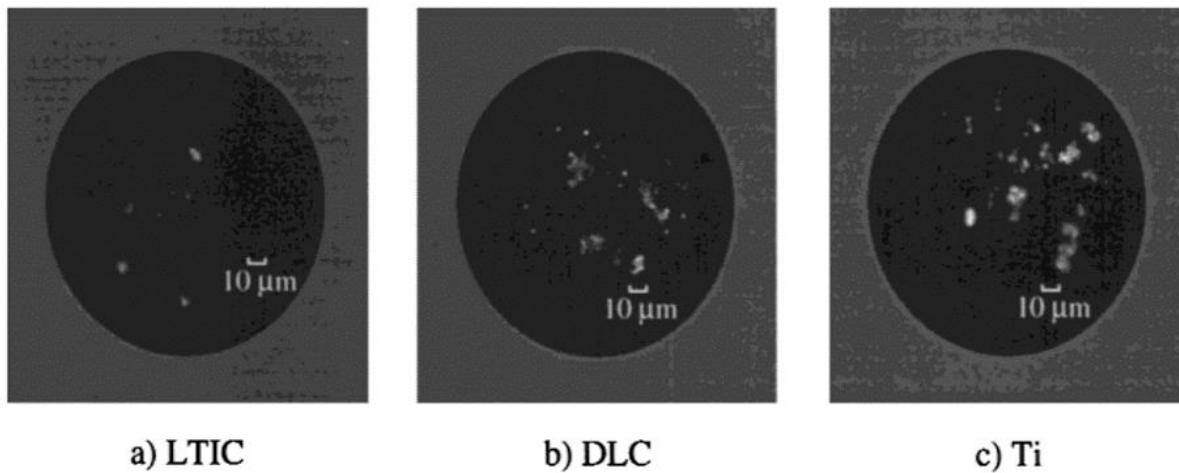


**Figure 3.** Representative digitized images of platelet adhesion on a) low-temperature isotropic carbon (LTIC) b) diamond-like carbon (DLC) c) Ti6Al4V (Ti). From Schaub et al. [43]

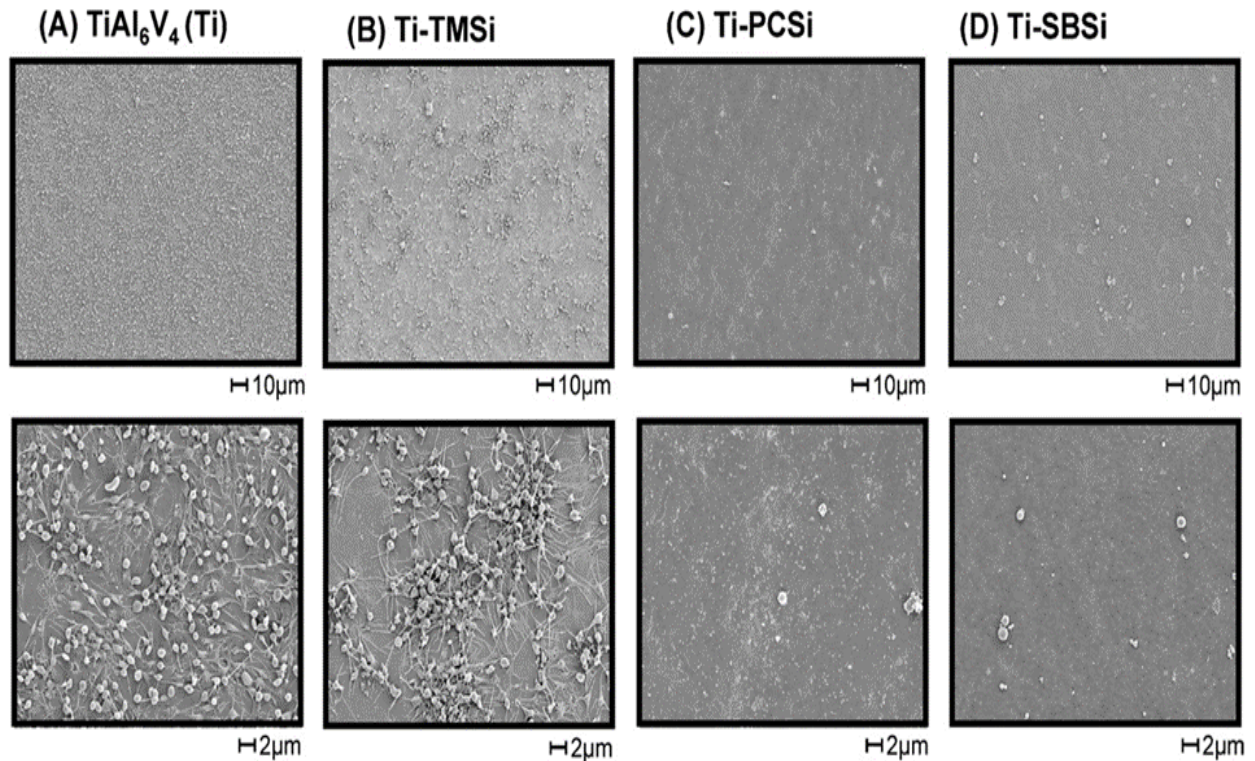


**Figure 4.** Scanning electron micrographs of platelets adhered to A) Ti6Al4V B) trimethoxy silane modified Ti6Al4V (Ti-TMSi) C) Silanated zwitterionic phosphorylcholine modified Ti6Al4V (Ti-PCSi) D) Salanated sulfobetaine modified Ti6Al4V (Ti-SBSi). Platelet deposition is reduced when the titanium alloy is modified by PCSi and SBSi.

From Ye et al. [46]

### 1.3.2 Blood Flow

Platelet deposition is dependent upon the transport of platelets from the bulk phase to the surface.[39, 40] At higher shear regions ( $> 30$  dyne/cm<sup>2</sup>), platelet aggregation is mediated by platelets binding to vWF through the GP IB receptor. Continuous flow VADS contain regions of pathologically high shear stresses ( $>100$  dyne/cm<sup>2</sup>). Studies have shown that these high shear stresses can activate platelets and lead to thrombosis development in VADs.[47, 48]

The blood flow path plays a major role in the formation of thrombi. Areas of flow separation, recirculation, and stagnation lead to increased platelet adhesion and thrombus formation.[49-52] *In vivo*, thrombosis is often found in regions of irregular geometries such as bifurcations, stenosis and aneurism, which are characterized by hazardous flow fields.[49] These patterns occur when flowing blood is unable to follow the rapid changes in the contour of the flow path created by the irregular geometries, causing flow separation, stagnation and recirculation.[52] Similar to these pathological conditions, areas of flow separation, recirculation, and stagnation are produced in several blood-wetted devices, such as VADs, heart valves, stents, and vascular grafts, because of sudden changes in the shape of the blood flow path. [52-56] Yang et al. utilized fluorescent particles to visualize the flow patterns in the HeartMate II *in vitro*. The report revealed that when the pump is run at typical clinical conditions (3.0-4.0 L/min at 9000 rpm), areas of erratic flow are found near the bearings before and after the stator (**Figure 5**).[57]

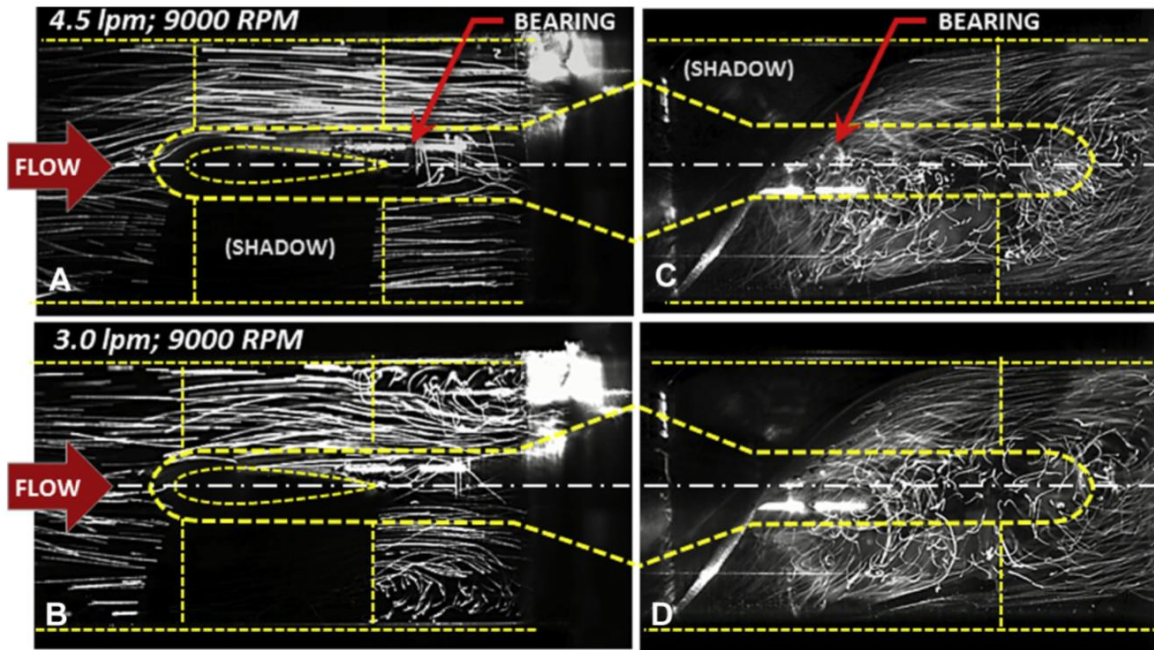


**Figure 5.** High-speed flow visualization of flow within the HeartMate II pump utilizing flow fluorescent particles. Pump was run at clinically relevant speeds. Areas of erratic flow found near the bearings and after the stator. From Yang et al. [57]

Geometric irregularities, such as steps and crevices, within the flow path of continuous flow VADs are known to serve as nidi for thrombus formation.[49] Because VADs are a complex assembly of multiple parts, the creation of internal steps and crevices is generally unavoidable. These features commonly occur at the sites where multiple components are mated. Manufacturers make a great effort to reduce the presence of these features within their devices through precise machining and polishing. Despite precautions, it is impossible to completely eliminate these unwanted topographies. This design challenge is illustrated in a figure (**Figure 6**) taken from Zhao et al.[49] **Figure 6A** shows the complexity of a rotary VAD design. An exaggerated view of the geometric irregularities that are created in the flow path of the pump due

to the combination of components is depicted in **Figure 6C**. These features are often the site of pump thrombosis because they cause flow separation, stagnation, and recirculation (**Figure 6D**). For example, **Figure 6B** shows that a ring thrombus formed at the transition between the metal barb and the polymer cannula of a pediatric VAD. A method for determining the effect of these erratic flow patterns on thrombus formation would be a useful tool in improving the design of VADs.

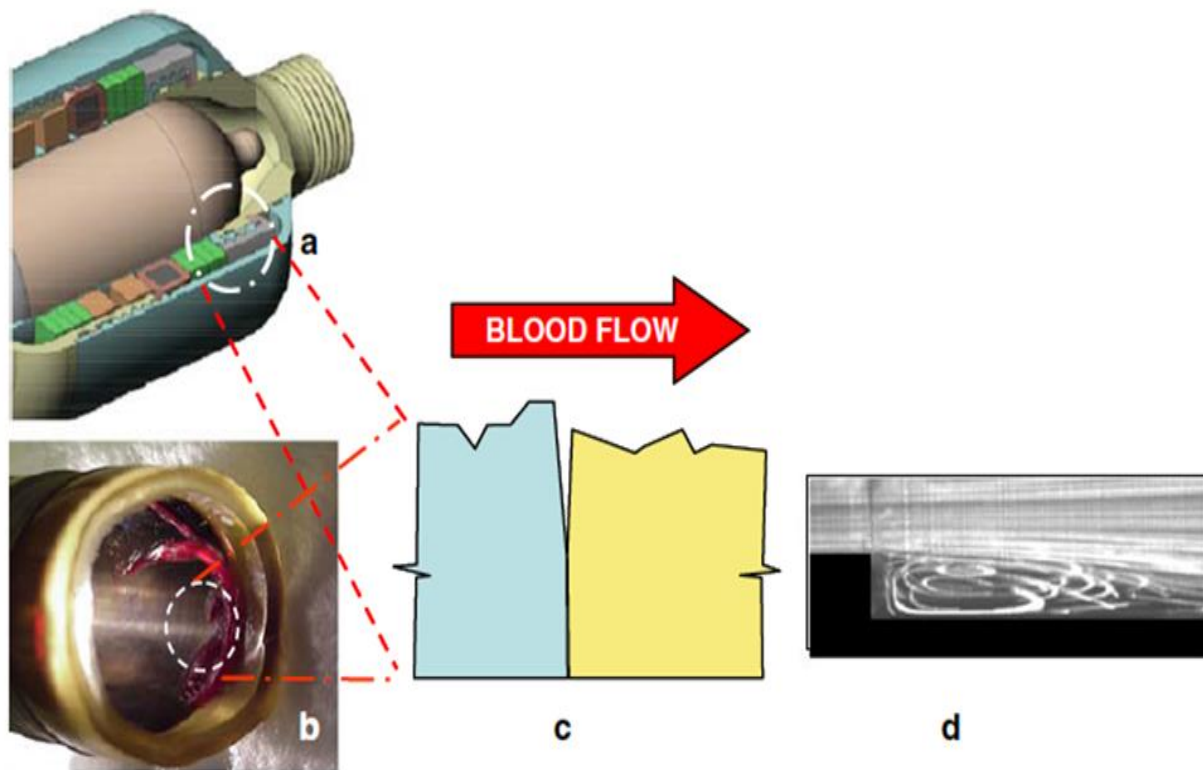


**Figure 6.** *The design challenge of continuous flow ventricular assist devices. (a) A section of rotary blood pump; (b) ring thrombus formed at the transition between metal barb and polymer cannula of a pediatric continuous flow blood pump; (c) exaggerated magnified view of the irregular geometries located at the seams of blood-wetted devices; (d) well-known flow separation downstream of a backward step. From Zhao et al. [49]*

### 1.3.3 Blood Constitution

Heart failure patients often have abnormal coagulation that increases their risk of stroke and thrombotic events prior to VAD implantation. This hypercoagulable state may be caused by many factors. Reduced myocardial contractility leads to low cardiac output and abnormal blood flow that can initiate coagulation.[58] Patients with heart failure often have dysfunctional endothelium, which can no longer act as an anticoagulant barrier. This dysfunction reduces the release of endothelium-derived nitric oxide (NO). NO acts to inhibit the platelet adhesion and activation *in vivo*, therefore a reduction of this factor increases the risk of thrombosis.[59, 60]

Another event that could lead to a hypercoagulable state in continuous flow VAD patients is infection. Infection occurs at a rate of 9.96 events/ 100 patient months in the first 12 months post-implant, and can elevate plasma levels of inflammatory cytokines such as tumor necrosis factor alpha and interleukin-1 (IL-1) that are known to initiate coagulation.[1, 58, 59] Investigating how pre-activation of platelets affects the formation thrombosis on biomaterials under flow could increase the understanding of device-centered thrombosis and lead to the development of more biocompatible VADs.

Due to the thrombogenic nature of continuous flow VADs, patients are on continuous anticoagulation and antiplatelet medications. Heparin is used preoperatively and during the initial recovery from implantation to get the patient's partial thromboplastin time (PTT) between 40-60 sec.[61] Heparin is a highly sulfated glycosaminoglycan that binds to and increases the activity of Antithrombin III, an enzyme inhibitor that inactivates thrombin. [62] Heparin is eventually replaced with warfarin and aspirin to get an international internalized ratio (INR) of 2.0-3.0.[61, 63-67] Warfarin is a vitamin K inhibitor, preventing the synthesis of several biologically active forms of calcium dependent clotting factors (Factor II, VII, IX and X).[68] Aspirin acts as an

anti-platelet medication by inhibiting cyclooxygenase (COX-1), which is necessary for platelet activation through the arachidonic acid pathway.[69] Clopidogral (Plavix), an anti-platelet medication that reduces platelet activation through inhibiting the P2Y<sub>12</sub> (ADP) receptor, is also sometimes utilized.[58] This therapy is a delicate balance between preventing thrombosis and causing bleeding. An investigation of the effect of anticoagulant medications on thrombus formation onto biomaterials under clinically relevant flow conditions may be utilized to develop improved therapies.

#### **1.4 PREDICTIVE MODELS OF DEVICE THROMBOSIS**

Trial and error is commonly used by device manufacturers to reduce the risk of biocompatibility complications. This method is time-consuming and expensive, with often unpredictable outcomes. With advancements in computer technology and mathematical modeling, several mathematical and computer models have been developed to predict platelet deposition and thrombus formation in blood wetted devices.[70-75] Such a model would reduce the time and cost of designing and producing safe, effective blood-wetted devices and could be used to determine thrombogenic areas of devices prior to implantation. However the accuracy of the current models is limited by the lack of experimental data characterization of platelet deposition onto opaque surfaces under clinically relevant flow conditions.

For example, in 1992 Fogelson et al. developed a set of convection-diffusion-reaction (CDR) equations to simulate the transport of thrombin and other platelet agonists in a growing thrombus. This model incorporated platelet activation kinetics, wherein resting platelets are

considered activated if exposed to threshold concentrations of agonist.[76] This model was further developed by Sorensen et al. by integrating several previously disjointed components such as the inclusion of both active and resting platelets, and various platelet agonists, platelet activation kinetics, agonist production and consumption, conversion of thrombin and antithrombin III (ATIII) into thrombin-antithrombin (TAT), platelet-surface reaction kinetics, and thrombin inhibition by heparin and direct inhibitors.[77, 78] Several investigators utilized the Sorensen model to simulate platelet deposition in saccular aneurysms [79], expanding channels [80], tube flow [81], and corrugated channels [82] In 2010 Leiderman et al refined the model to consider coagulation biochemistry, platelet activation, platelet deposition and the effect of the thrombus formation on the flow field. Although this model provides an excellent representation of thrombus growth due to exposed subendothelium, it limits platelet activation and coagulation events to a thin reaction zone, just above a small vascular injury, which is not applicable to blood-wetted devices with complex geometries and flow patterns.[83] Experimental data that quantifies the effect of clinically-relevant biomaterials and flow patterns on thrombus formation may be used to calibrate and validate a predictive model of thrombosis in VADs.

## **1.5 SUMMARY OF INTRODUCTION**

The incidence of thrombosis, bleeding, and neurologic dysfunction experienced by patients supported by continuous flow VADs continues to limit the cost-effectiveness and clinical acceptance of the technology. Biomaterial-centered thrombosis and its subsequent thromboembolism remain of high relevance as designers seek to improve the blood

biocompatibility of future generation VADs and other cardiovascular devices. The development of an experimental method to characterize platelet deposition onto opaque surfaces under clinically relevant flow conditions would be a useful tool in generating data to validate computation models of thrombosis in blood-wetted devices, enabling the design of more hemocompatible VADs.

## 1.6 OBJECTIVES

As discussed in the sections above, continuous flow VADs present several blood biocompatibility challenges making it difficult to predict thrombosis within these devices. Evaluating the time dependent, platelet adhesion onto the blood-contacting surfaces of cardiovascular devices, under clinically relevant flow conditions, could be a useful tool in designing more hemocompatible VADs. Despite the large volume of research dedicated to characterizing and improving the blood biocompatibility of biomaterials, few studies have been performed to assess time dependent platelet adhesion onto opaque materials. Furthermore, the majority of materials used for cardiovascular devices are opaque, making it difficult to image microscopic platelet deposition onto these surfaces in real time. The aim of this research is to characterize real time platelet deposition onto opaque surfaces under clinically relevant flow conditions, in order to generate data to advance the accuracy and utility of predictive models of thrombosis in blood-wetted cardiovascular devices. This was accomplished through *in vitro* studies composed of the following objectives:

### **1.6.1 Objective # 1: Real time visualization and characterization of platelet deposition under flow onto clinically relevant opaque surfaces**

Continuous flow VAD manufacturers often use a polished titanium alloy (TiAl6V4) as the blood-contacting surface of their devices. However, *in vitro* studies have shown TiAl6V4 to have elevated acute thrombogenicity compared to other candidate materials or coatings. Due to erythrocyte opacity it has been difficult to develop a method for assessing real time platelet deposition onto TiAl6V4 and other alternative opaque materials using whole blood. Employing the use of optically clear hemoglobin depleted red blood cells (RBC ghosts), a parallel plate flow chamber, and long working distance optics we sought to perform such an evaluation.

### **1.6.2 Objective # 2: Visualization and Analysis of Biomaterial-centered Thrombus Formation within a Defined Crevice under Flow**

Although the majority of VAD manufacturers attempt to make the blood contacting surfaces of their devices as smooth as possible, all VADs are composed of combined components that inevitably generate crevices and steps along the flow path. These regions produce areas of recirculating flow and are often the nidus of thrombus formation in these devices. A custom designed parallel plate chamber containing crevices of defined dimensions was employed to investigate the effect of crevice size on platelet adhesion to clinically relevant opaque materials.

### **1.6.3 Objective # 3: Characterizing the effect of sub-threshold concentrations of ADP on platelet deposition onto clinically relevant opaque materials**

Another challenge in assessing the hemocompatibility of a blood-wetted device is understanding the functional relationship between shear stress, biochemical agonists, and artificial surfaces. To perform such an analysis, a membrane based agonist delivery system was design to evenly introduce specific concentrations of agonist into the blood analog prior to the blood contacting the test material. Using this method, the affect of sub-threshold concentrations of ADP on platelet deposition onto clinically relevant opaque materials, under flow, was characterized.

## **2.0 REAL TIME VISUALIZATION AND CHARACTERIZATION OF PLATELET DEPOSITION UNDER FLOW ONTO CLINICALLY RELEVANT OPAQUE SURFACES**

(Note: A majority of this chapter was previously published as: Jamiolkowski MA, Woolley JR, Kameneva MV, Antaki JF, Wagner WR. Real time visualization and characterization of platelet deposition under flow onto clinically relevant opaque surfaces. Journal of biomedical materials research Part A. 2015;103:1303-11.)

### **2.1 INTRODUCTON**

The manufacturers of the Heartmate-II and other continuous flow VADs currently use a polished titanium alloy (Ti6Al4V) as the blood contacting surface due to its desirable mechanical properties, resistance to corrosion, and tolerable blood compatibility.[42] However, *in vitro* studies have shown that this alloy exhibited elevated acute thrombogenicity compared to other coated surfaces (e.g. polyethylene glycol and diamond-like coatings) or related alloys (Ti6Al7Nb).[43-45, 84] This study was therefore conducted to perform a systematic side-by-side comparison of six candidate biomaterials currently being considered for application in continuous-flow blood pumps. However, since these materials are opaque, traditional methods for real time visualization of platelet deposition, such as fluorescent microscopy utilizing whole

blood, are not readily applicable. The present study demonstrates a method to overcome this limitation through the use of a blood analogue containing *transparent*, hemoglobin depleted red blood cells (RBC ghosts) combined with fluorescently-labeled platelets. The experimental preparation consisted of a parallel plate flow chamber with epifluorescence microscopy having a long working-distance objective. This preparation permitted real-time observation of deposition and embolization to identify promising alternatives to Ti6Al4V to improve the overall blood compatibility of the device, reducing reliance on anticoagulation and anti-platelet agents.

## 2.2 MATERIALS AND METHODS

### 2.2.1 Platelet Collection and Fluorescent Labeling

Fresh whole blood was collected after informed consent from 27 healthy donors (13 male, 14 female), who had refrained from taking any platelet altering medications 14 days prior to collection, with a mean age of  $35 \pm 12$  years in accordance with Institutional Review Board guidelines. Platelet-rich-plasma (PRP) was collected by centrifuging citrated blood (5 mL Vacutainer tubes, [0.105M] citrate, BD, Franklin Lakes, NJ, USA) at 250xg for 15 min. Platelets ( $2.7 \pm 0.30 \times 10^8$  per mL) were fluorescently labeled by the addition of quinacrine dihydrochloride (0.5  $\mu$ M final concentration, Sigma-Aldrich, St. Louis, MO, USA) to the PRP. Quinacrine dihydrochloride was chosen because studies have shown that platelet function is not affected when a final concentration  $< 20 \mu$ M is used.[85, 86]

### 2.2.2 RBC Ghost Preparation and Characterization

Packed RBCs (type O-, Valley Biomedical Products & Services, Inc., Winchester, VA, USA) were converted into RBC ghosts through the modification of established protocols.[87-90] Briefly, the RBCs were rinsed and centrifuged (2000×g, 15 min) three times with phosphate buffered saline without Ca<sup>2+</sup> or Mg<sup>2+</sup> (PBS, VWR International LLC., Radnor, PA, USA) and then suspended in PBS at a 50% hematocrit. While incubated between 0-6°C, 1 mL of RBC suspension was added to every 9 mL of a lysing solution composed of 4mM MgSO<sub>4</sub>, 5X concentrated PBS (25 mL per L distilled water), and acetic acid (Sigma-Aldrich, 80 µL per L of distilled water) in distilled water with a final osmolality of 40 mOsm and pH of 5.0-5.2. After 5 min incubation, osmolality and pH were increased to physiologic norms (300 mOsm and 7.8, respectively) by the addition of 0.3 mL of 5X concentrated PBS and 2µL of 1M Tris buffer (Thermo Fisher Scientific Inc., Pittsburgh, PA, USA) per mL of cell suspension and stored at 0-6 degrees C for 8 hrs. The cells were then resealed by incubation at 37°C for 1 hr. The suspension was centrifuged at 25400×g for 30 min and the supernatant was discarded. The cells were washed 3 times with PBS (25400×g for 30 min) and stored in PBS with 100 mg/L gentamicin (Thermo Fisher Scientific). The resulting RBC ghosts were observed to be translucent. The donor PRP was utilized within 6 hr after being drawn to minimize platelet activation. Therefore RBC ghosts were prepared prior to the blood draw and added to the donor PRP. Blood type O<sup>-</sup> RBCs were used to create RBC ghosts cells to allow mixing with any donor PRP blood type. The RBC ghosts were stored up to 2 wk at 4-6°C and a final hematocrit of ≥ 95%. These cells were utilized in the perfusion experiments within this time.

Prior to RBC ghost creation, an aliquot of native RBCs was set aside for comparative rheological testing in the Kameneva laboratory. The viscosity of RBC ghosts in human plasma

was measured using a cone and plate viscometer (Brookfield Digital Rheometer, Model DV-III, Brookfield Engineering Laboratories, Inc., Stoughton, MA, USA) and compared to native RBCs at the same hematocrit. The elongation of RBC ghosts and native RBCs at various wall shear rates was measured using an optical rheology system (CSS-450, Linkam Scientific Instruments Ltd., Tadworth, Surrey, UK) and analyzed using ImageJ (NIH). The elongation index was calculated as  $(L-W)/(L+W)$  where L and W are the major and minor axes of the ellipse representing elongated RBC, respectively.

### **2.2.3 Test Materials**

Ti6Al4V and 5 alternative materials or coatings were analyzed: Ti6Al4V (Supra Alloys Inc., Camarillo, CA, USA), a modified 2-methacryloyloxyethyl phosphorylcholine polymer coated Ti6Al4V (MPC-Ti6Al4V), silicon carbide (SiC; CoorsTek, Inc., Golden, CO, USA) alumina (Al<sub>2</sub>O<sub>3</sub>; CoorsTek), yttria partially stabilized zirconia (YZTP; CoorsTek), and Zirconia Toughened Alumina (ZTA; CoorsTek). All the materials had a mirror polish finish. MPC-Ti6Al4V was prepared in the authors' laboratory using previously reported protocols.[46] The materials evaluated were selected for their physical characteristics, which were generally compatible with use as blood contacting materials in a continuous flow VAD. A contact angle goniometer (VCA optima, AST Product Inc., Billerica, MA) was used to measure the contact angle of 1  $\mu$ L of distilled water at room temperature on each surface. All samples were cleaned with Simple Green® (Thermo Fisher Scientific Inc.) and Tergazyme® (Alconox, Inc., White Plains, NY, USA) and then sonicated three times with distilled water prior to testing using a protocol based on the cleaning methods utilized for continuous flow VADs undergoing preclinical testing.[91]

#### 2.2.4 Parallel Plate Flow Chamber

The parallel plate flow chamber design was similar to that described by Kent et al.[92] The top plate was clear acrylic with angled nylon inflow and outflow luer connectors, and the bottom plate was the interchangeable test material. A simple clamping mechanism held the plates together, with a silicone gasket outlining the channel width and length (5 x 8 mm). Aluminum shim stock was placed between the plates to provide a precisely defined channel height of 0.076 mm (**Figure 7A-7B**). The flow within this chamber was assumed to be one-dimensional laminar parallel plate flow (Reynolds numbers between 0.1 and 0.4).[43, 92]

#### 2.2.5 Blood Analogue Perfusion and Image Acquisition

The experimental flow path is presented in **Figure 7C**. All non-test surfaces were passivated by incubation with 1% bovine serum albumin (BSA, microbiological grade powder; MP Biomedicals, LLC, Solon, OH, USA) in PBS for 20 min prior to perfusion. To verify passivation, platelet deposition onto the acrylic top plate was qualitatively assessed after the perfusion experiments. Few to no adherent platelets were found. Quinacrine dihydrochloride - labeled PRP was mixed with RBC ghosts to produce an end hematocrit of 25% and a final platelet concentration of  $2.0 \pm 0.2 \times 10^8$  platelets/mL. This suspension was collected into a 20 mL polystyrene syringe (BD Biosciences) and pulled through the parallel plate flow chamber by a syringe pump (Harvard Apparatus, Holliston, Massachusetts, USA) for 5 min at flow rates of 0.118 and 0.295 mL/min (wall shear rates of  $400 \text{ sec}^{-1}$  and  $1000 \text{ sec}^{-1}$  respectively). These wall shear rates were chosen to represent a low ( $400 \text{ sec}^{-1}$ ) and high ( $1000 \text{ sec}^{-1}$ ) physiological rate. Continuous flow VADs produce a wide range of wall shear rates within the pumps, including

supra-physiological wall shear rates of  $>25000 \text{ sec}^{-1}$  (shear stress  $> 100 \text{ N/m}^2$ ).[93-95]  
However, the wall shear rates represented in this study are characteristic of those produced within the inlet and outlet regions and along the outer wall of centrifugal VADs (e.g. the clinically utilized HeartWare) [93, 94] and near the inlet in a region called the inducer in axial flow VADs (e.g. the clinically utilized HeartMate II).[95]

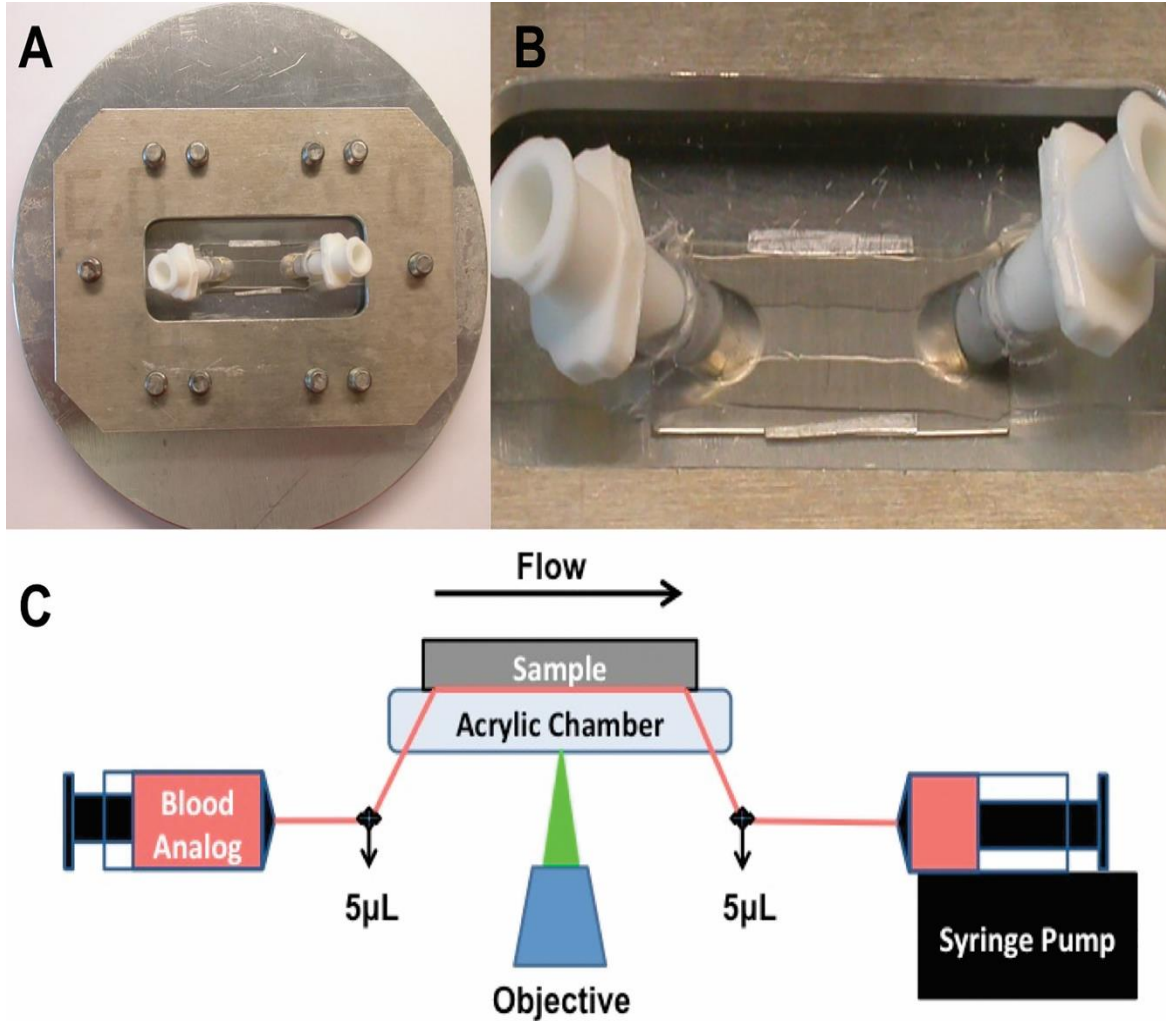


**Figure 7.** Parallel plate flow chamber and experimental set up. A) The circular metallic piece and rectangle were secured around the flow chamber with screws. B) The flow path was formed from a silicon gasket. Thin aluminum shim stock can be seen along the length of either side of the silicone gasket to ensure a precise chamber height. C) The blood analogue was perfused through the chamber and across the sample for 5 min. Images were acquired, in real time, 4mm from the inlet by a CCD camera. The transparent blood analogue and long working distance objective allowed for real time visualization of adherent fluorescent platelets through the flow path onto the opaque test surface.

Platelet adhesion was visualized within a 200x200 micron region of interest, located 4 mm downstream from the inlet connector, in real time, using an inverted epifluorescence microscope (Olympus IX FLA, Olympus Corporation, Shinjuku, Tokyo, Japan) with a 40x super long working distance objective (PlanFL, phase contrast, working distance 6.5 mm - 8.3 mm, numerical aperture 0.55, and maximum acceptable coverslip thicknesses of 2.6 mm; Olympus Corporation) and a 103W HBO short arc mercury lamp light source (OSRAM GmbH, Munich, Germany). Images were acquired every 0.4 sec beginning at one min after the start of perfusion using a CCD camera (PCO-TECH Inc., Romulus, Michigan, USA).

Images were analyzed by thresholding the intensity, subjectively to eliminate spurious artifacts (See **Figure 8A** and **8B**). The surface coverage (in percent) of deposited platelets was computed using a custom written program in MatLab (MathWorks, Inc., Natick, MA, USA). To visually determine the accuracy of the analysis the outline of the original image was overlaid onto the original image (**Figure 8C**).

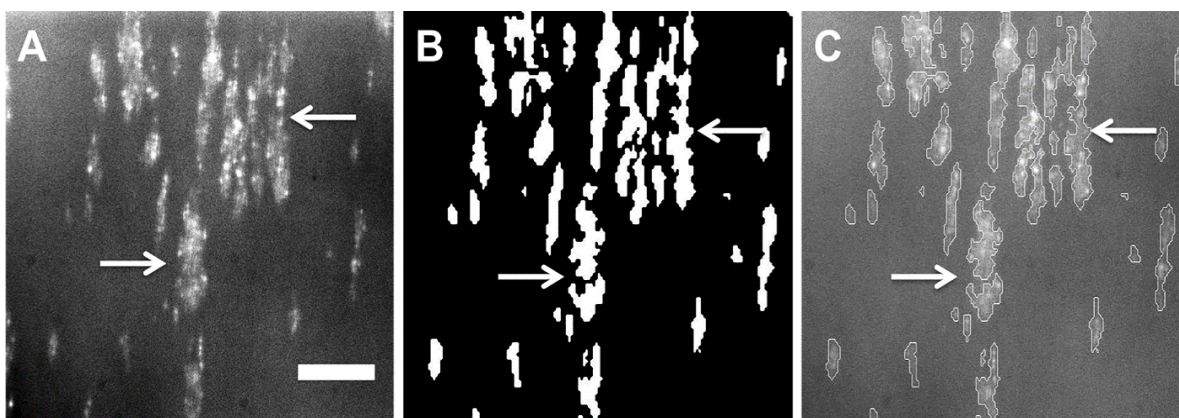


**Figure 8.** Image analysis to quantify the percent platelet surface coverage. A) Original fluorescent image of platelets adhered to SiC after 5 min of perfusion, B) binary image rendered by the MatLab program, C) original fluorescent image overlaid with the outline of the binary image. Scale bar = 40  $\mu$ m.

### **2.2.6 Scanning Electron Microscopy**

Following perfusion, samples were gently rinsed with PBS and incubated with glutaraldehyde (2.5% in PBS; Sigma-Aldrich) for 10 min. Next, the materials were washed 3 times with PBS and dehydrated in consecutive stages of increasing ethanol (Sigma-Aldrich) concentrations. The samples were then chemically dried with hexamethyldisilazane (Thermo Fisher). Finally, the samples were coated with gold-palladium (Hummer VI Sputtering System, TechnicsWest, Inc., San Jose, California, USA) and scanning electron micrographs (SEMs) were obtained (images obtained using scanning electron microscope model JSM6330F, JEOL, Tokyo, Japan).

### **2.2.7 Flow Cytometry**

Bulk phase activation of the platelets was measured by flow cytometry using previously described methods.[96] Briefly, blood was sampled from the exit port of the parallel plate chamber at two points in time: immediately after the sample initially crossed the test surface (determined visually) and also after 5 min perfusion. Aliquots of these samples were incubated in buffer solution (Tyrode's solution with 1% BSA, Electron Microscopy Science, Hatfield, PA, USA) with fluorescein isothiocyanate – conjugated mouse anti-human CD42b (CD42b, clone LG.3A10; AbD Serotec, Raleigh, NC, USA ) and either recombinant phycoerythrin–conjugated (RPE) mouse anti-human CD62P or RPE-conjugated isotype- matched control antibody (CD62P and Mouse IgG<sub>1</sub>, clones Psel.KO.2.5 and W3/25, respectively; both from AbDSerotec ) in the dark for 20 min. The cells were washed with Tyrode's solution with 1% BSA and 0.106 M sodium citrate dehydrate (Thermo Fisher), centrifuged, and the pellet isolated. The cells were re-suspended in 1% paraformaldehyde (Sigma-Aldrich) and stored at 4° C (<24 hr) until analyzed. CD42b+ events (>5000) were collected on a 3-color FACScan (BD Biosciences) and analyzed with WINList software (Verity Software House, Topsham, ME).

### **2.2.8 Statistical Analyses**

All data are presented as mean  $\pm$  standard error of the mean. Data were analyzed by two-way, repeated measures ANOVA with specific post-hoc (eliminated space after hypen) testing using the Bonferroni correction. SPSS v20 (IBM Corp, Armonk, NY) was used for all statistical analyses.

## 2.3 RESULTS

### 2.3.1 RBC Ghost Rheology

To verify that flow behavior of RBC ghosts is similar to that of native RBCs, the rheological properties of RBC ghost suspensions were examined by comparing their viscosity as a function of shear rate to that of native RBCs used for the ghost preparation. **Figure 9A** depicts the viscosity response of native and ghost RBCs in plasma over a range of shear rates. No difference between the two curves was found (**Figure 9A**,  $P=0.61$ ). Similarly, there was no difference found in deformability of the original RBCs and their ghosts (**Figure 9B**) and in their calculated elongation indices (**Figure 9C**;  $P = 0.41$ ). Additionally, no significant difference in bulk phase platelet activation was detected between PRP and PRP mixed with RBC ghosts ( $8.7 \pm 0.9\%$  and  $7.3 \pm 0.9\%$ , respectively;  $P=0.13$ ,  $N=5$ ).

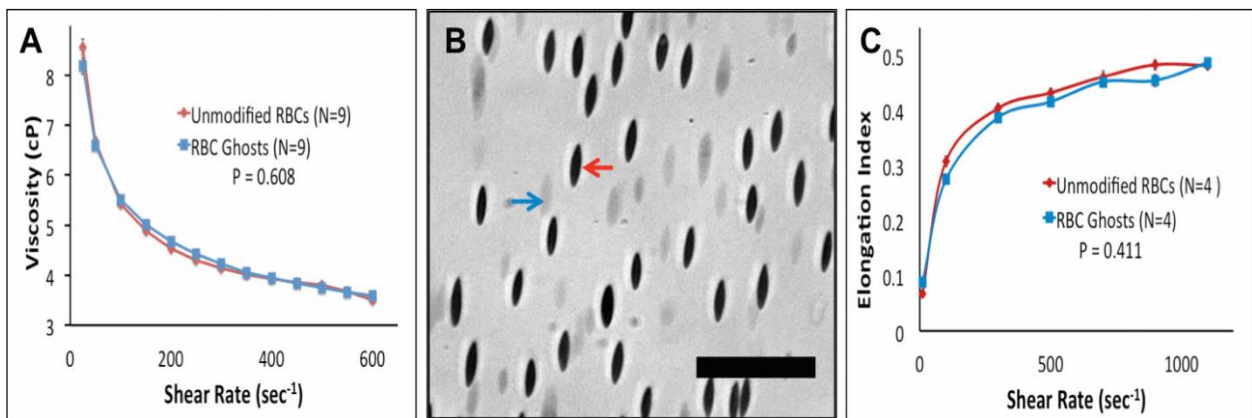


**Figure 9.** A) Comparing the viscosity of native and ghost RBCs in human plasma at a matched hematocrit of 27%. B) Mixture of native and ghost RBCs subjected to a wall shear rate of 1100 sec<sup>-1</sup>. Red and blue arrows indicate a native and ghost RBC respectively. Scale bar = 40  $\mu\text{m}$ . C) Deformability of native and ghost RBCs.

### 2.3.2 Acute Platelet Adhesion on Test Surfaces

Representative fluorescent images of platelet adhesion onto the 6 opaque test surfaces after 5 min of perfusion at wall shear rates of 400 and 1000  $\text{sec}^{-1}$  are shown in **Figure 10**. At the lower wall shear rate of 400  $\text{sec}^{-1}$ , Ti6Al4V had  $6.0\% \pm 2.0\%$  (n=7) platelet deposition after 60 sec of perfusion, which continued to increase throughout the test resulting in platelet surface area coverage of  $11.2 \pm 1.6\%$  (**Figure 11**). Similarly, SiC had  $5.5\% \pm 1.2\%$  (n=7) at 60 sec of perfusion which increased to  $15.6 \pm 2.2\%$  in 5 min. Platelet adhesion onto Ti6Al4V and SiC increased significantly with time and were not different from each other ( $P < 0.05$ ). In contrast,  $\text{Al}_2\text{O}_3$ , YZTP, ZTA, and MPC-Ti6Al4V all had significantly lower platelet adhesion ( $P < 0.005$ ) than the previous two surfaces, with average end platelet surface coverage of  $3.3 \pm 0.9\%$ ,  $2.5 \pm 1.1\%$ ,  $1.3 \pm 0.3\%$ , and  $1.2 \pm 0.5\%$ , respectively (**Figure 11**).

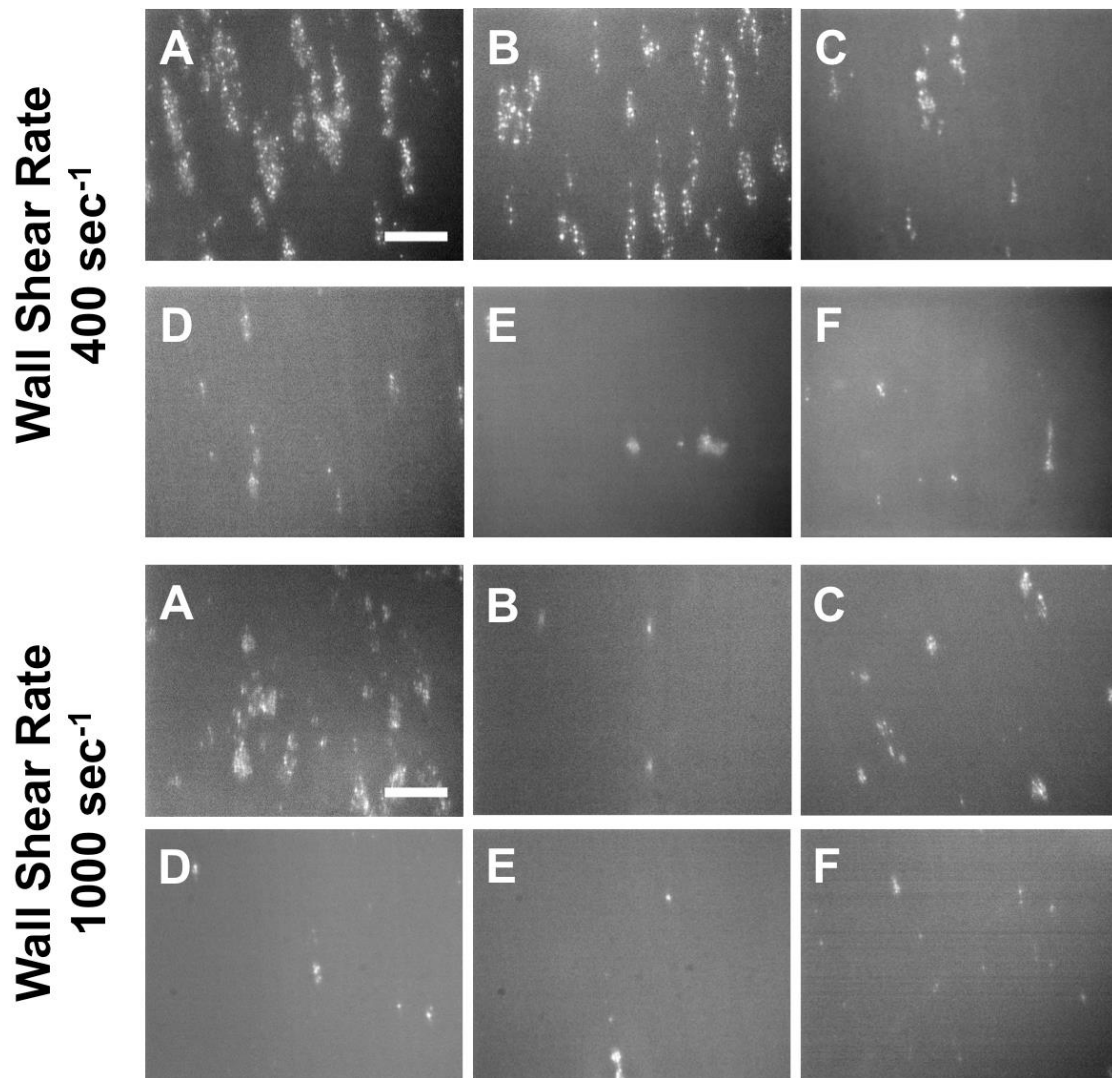


**Figure 10.** Representative fluorescent images of platelets adhered to A) Ti6Al4V, B) SiC, C) Al<sub>2</sub>O<sub>3</sub>, D) YZTP, E) ZTA, and F) MPC-Ti6Al4V after 5 min of perfusion. Scale bar = 40  $\mu$ m.

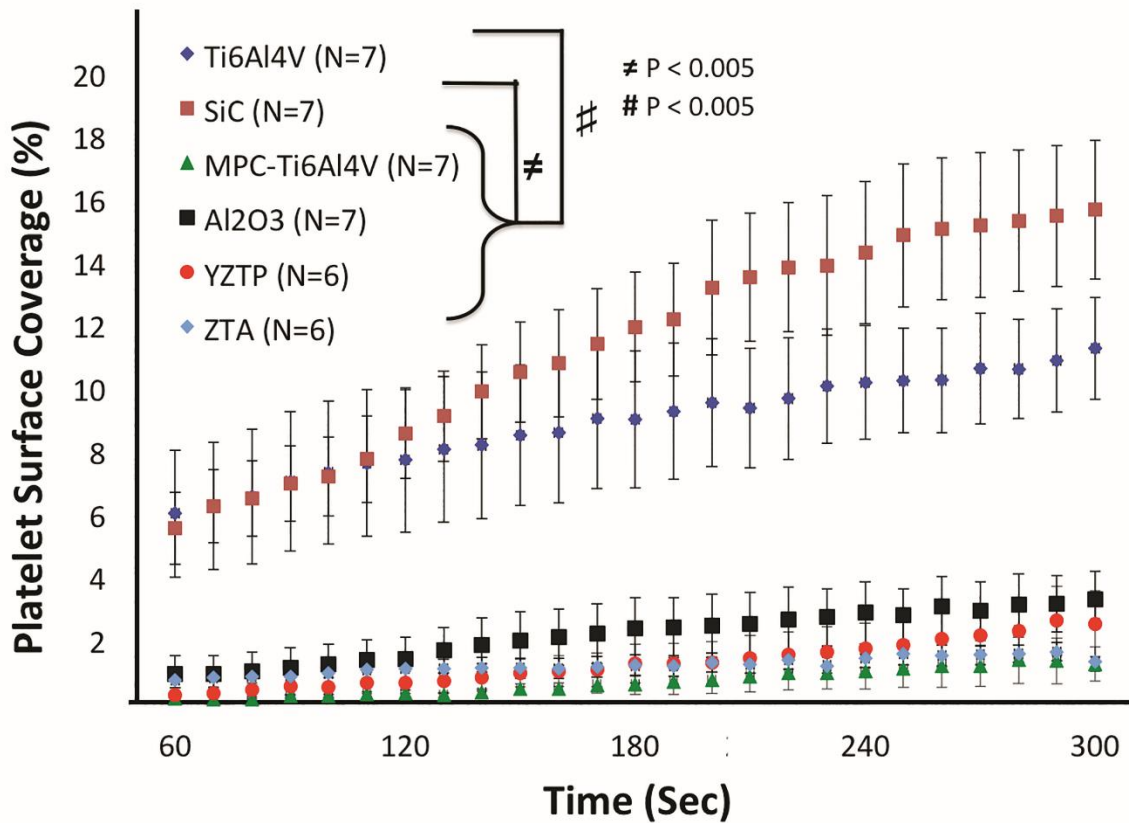


**Figure 11.** Acute platelet adhesion on test materials perfused at a wall shear rate of  $400 \text{ sec}^{-1}$ . Images were acquired at 4mm distance from the inlet of the parallel plate flow chamber.

At the higher wall shear rate of  $1000 \text{ sec}^{-1}$ , all of the test materials had significantly less platelet adhesion than Ti6Al4V ( $P < 0.001$ ) (**Figure 12**). After 5 min perfusion, Ti6Al4V had platelet surface coverage of  $4.8 \pm 1.0\%$ . In contrast, Al<sub>2</sub>O<sub>3</sub>, SiC, YZTP, ZTA, and MPC-Ti6Al4V had average end platelet surface coverage of  $1.2 \pm 0.3\%$ ,  $0.66 \pm 0.35\%$ ,  $0.60 \pm 0.17\%$ ,  $0.32 \pm 0.13\%$ , and  $0.63 \pm 0.23\%$ , respectively.

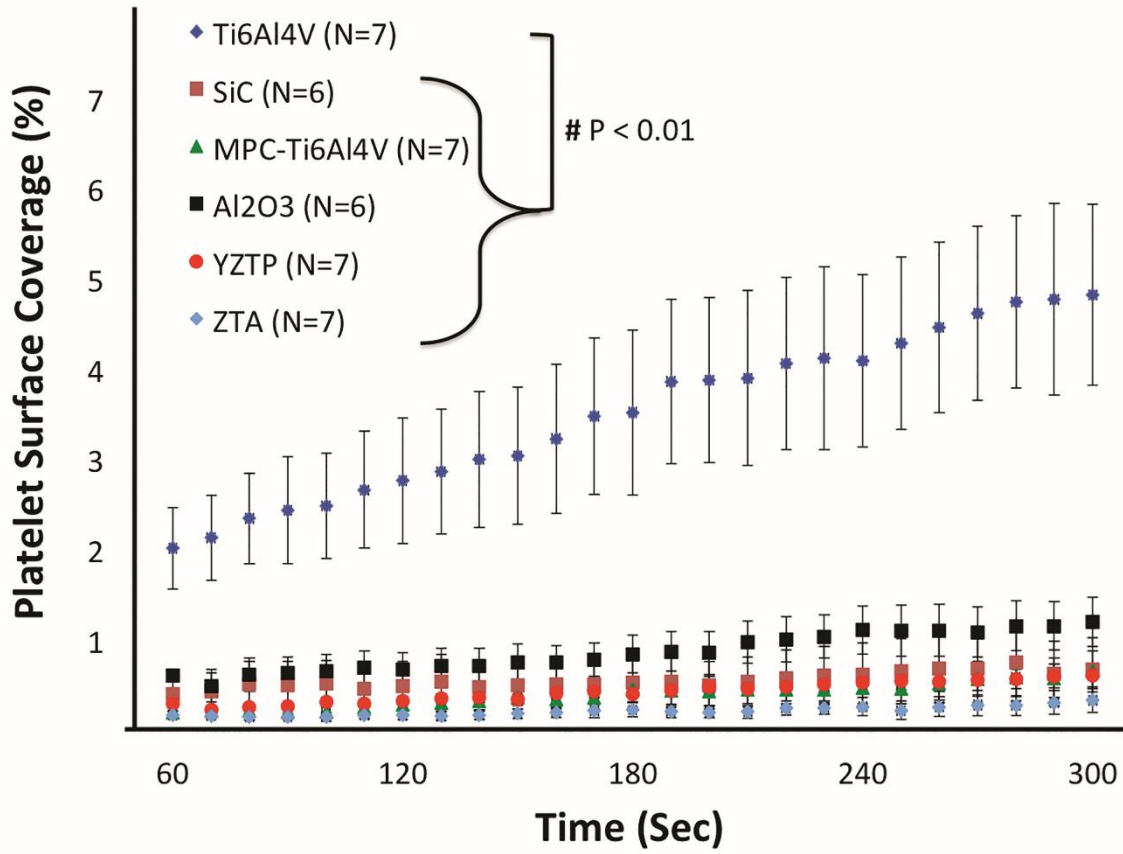


**Figure 12.** Acute platelet adhesion on test materials perfused at a wall shear rate of  $1000 \text{ sec}^{-1}$ . Images were acquired 4mm from the inlet of the parallel plate flow chamber.

Representative accelerated videos of real-time perfusion and platelets adhesion to all six surfaces, at wall shear rates of 400 or 1000  $\text{sec}^{-1}$  are available in the supplemental material of this report (**Video 2.1-2.12**). Although all materials had visible platelet deposition present during the experiments, the most pronounced thrombi formations were clearly observed with the Ti6Al4V samples at high and low wall shear rates and SiC samples at low wall shear rates. The thrombi grew in elliptical patterns, with the long axis aligned in the direction of flow. Embolization of fragments and entire thrombi were observed sporadically with the Ti6Al4V, SiC,  $\text{Al}_2\text{O}_3$ , and YZTP samples. Examination of the length of the flow path following perfusion indicated that platelets reacted uniformly with the test materials and were not diffusion-limited by the rapid depletion of platelets onto the surface at the inlet of the chamber.[77]

### **2.3.3 Wall Shear Rate Effect on Platelet Adhesion**

Curves comparing platelet adhesion to each of the six test surfaces at the two wall shear rates are presented in the supplemental material (**Figure 13**). Increasing the wall shear rate from 400 to 1000  $\text{sec}^{-1}$  produced a trend of decreased platelet adhesion to the test surfaces. This trend was significant for all of the surfaces, except MPC-Ti6Al4V ( $P < 0.05$ ). The largest change in platelet adhesion between wall shear rates occurred with SiC, in which a  $95 \pm 2\%$  decrease in platelet surface coverage was observed at  $t = 5$  min at the higher perfusion rate.

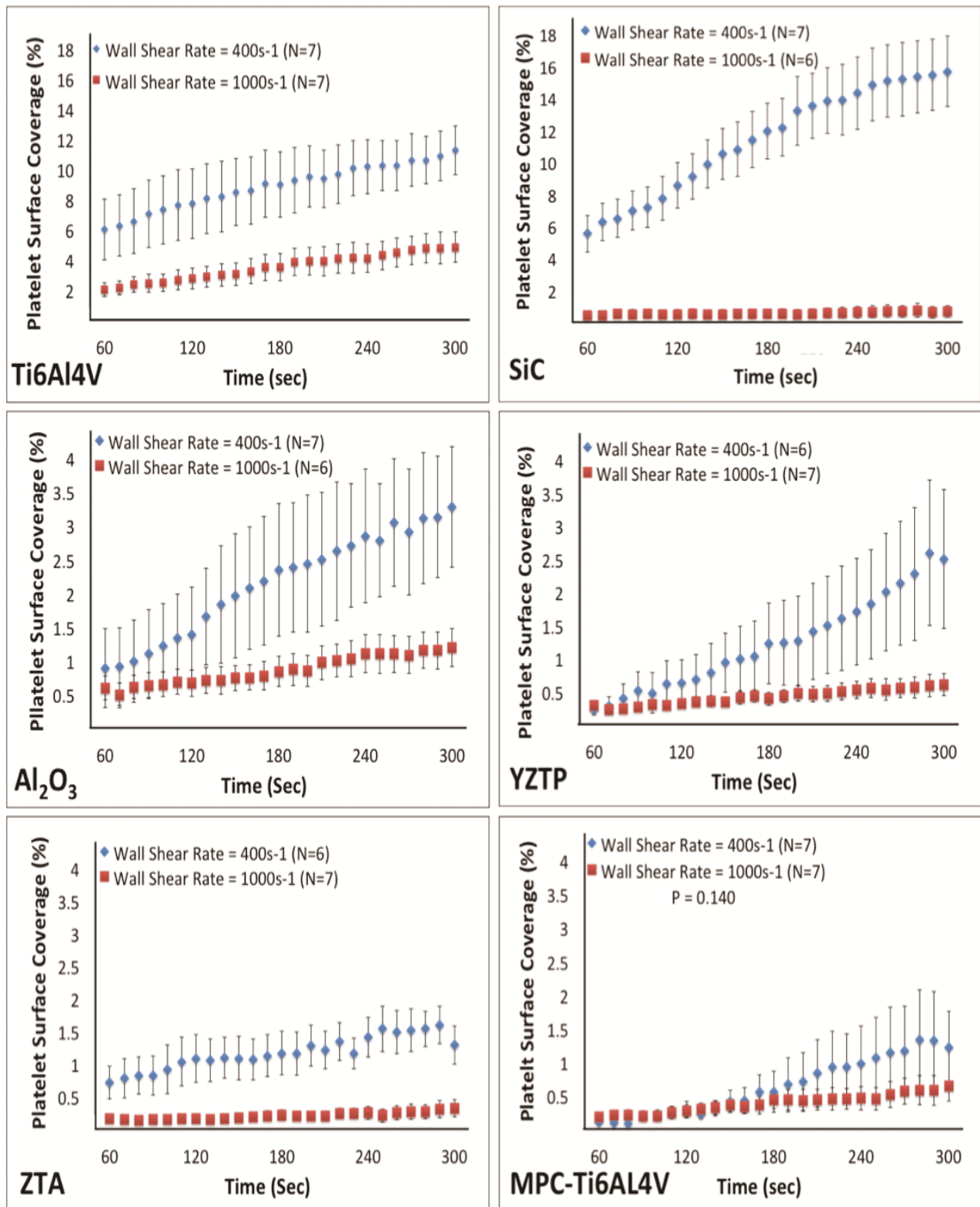


**Figure 13.** Comparison of the effect of wall shear rate on acute platelet adhesion. Note Ti6Al4V and SiC are scaled differently than the other materials.  $P < 0.01$  between shear rates for all materials except MPC-Ti6Al4V.

#### 2.3.4 Surface Contact Angles, Scanning Electron Microscopy and Flow Cytometry

Water contact angles of the materials measured prior to use were as follows; Ti6Al4V:  $55.3 \pm 3.1^\circ$ , SiC:  $72.14 \pm 3.6^\circ$ , Al<sub>2</sub>O<sub>3</sub>:  $69.2 \pm 2.7^\circ$ , YZTP:  $31.3 \pm 2.0^\circ$ , ZTA:  $42.0 \pm 2.1^\circ$ , and MPC-Ti6AL4V:  $20.6 \pm 2.1^\circ$ . Scanning electron micrographs of platelet deposition following blood analogue perfusion revealed similar adhesion patterns on the material surfaces as shown in the fluorescent images (**Figure 14**). Similar to the fluorescent images, the scanning electron micrographs revealed oval thrombi aligned in the direction of flow on the Ti6Al4V at both wall shear rates and on SiC at a wall shear rate of  $400 \text{ sec}^{-1}$ . Also, these micrographs verify that there is substantially less platelet deposition on the four other test surfaces. From the flow cytometry data, there was no difference found between materials or over the course of the perfusions in bulk phase platelet activation or circulating platelet-platelet microaggregate formation ( $P > 0.25$ ). The average percent of activated platelets and microaggregates across all of the materials at both time points were  $8.0 \pm 2.1\%$  and  $1.2 \pm 0.3\%$  respectively

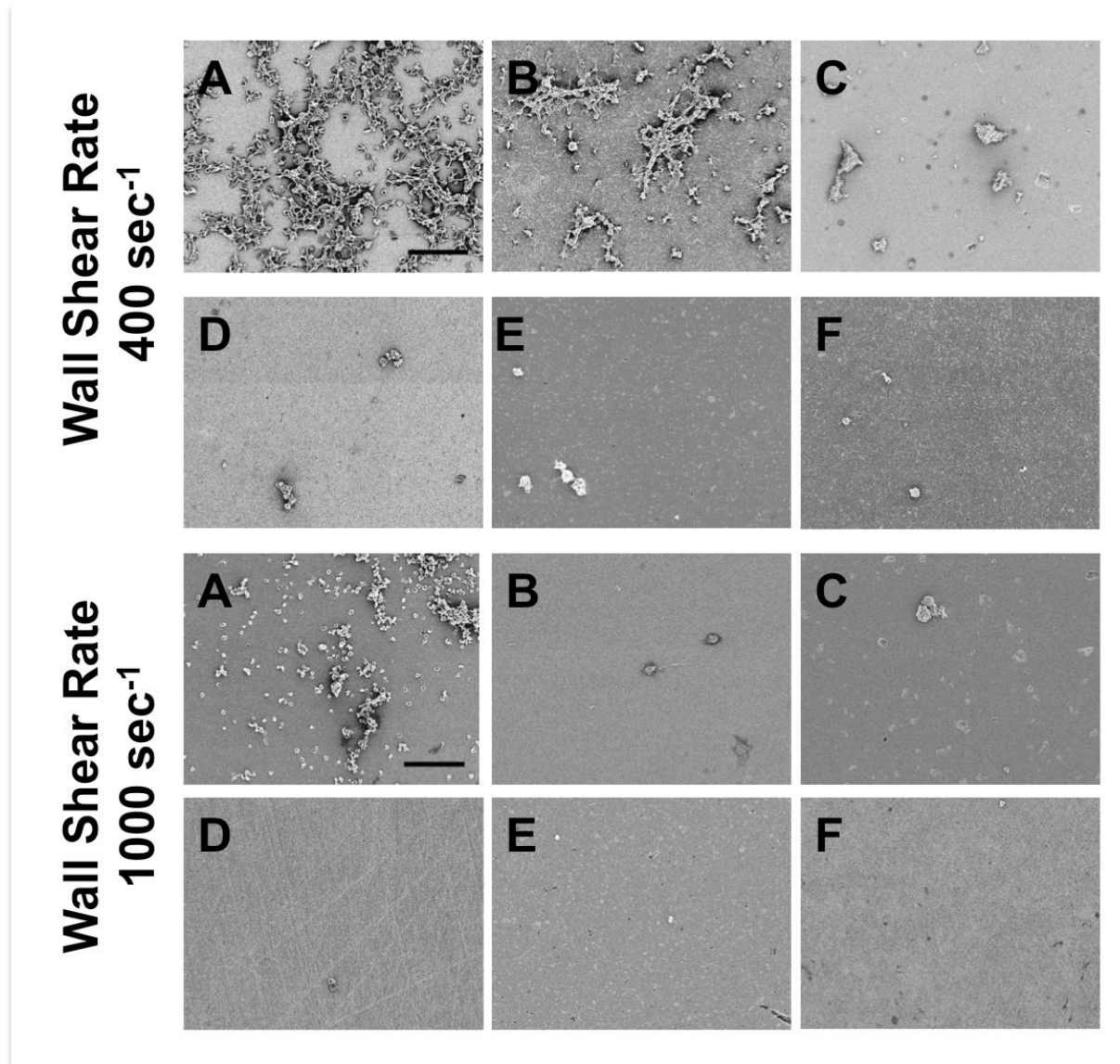


**Figure 14.** Representative scanning electron micrographs of platelets adhered to A) Ti6Al4V, B) SiC, C) Al<sub>2</sub>O<sub>3</sub>, D) YZTP, E) ZTA, and F) MPC-Ti6Al4V after 5 min of perfusion. Scale bar = 40  $\mu$ m.

## 2.4 DISCUSSION

Characterization of the *in vitro* thrombogenicity of surfaces is an important step in developing and selecting new materials for use in blood-wetted devices. Previous methods examining acute platelet deposition have utilized end-point analysis [97, 98] required the material to be transparent [99] or have used PRP instead of blood to perfuse over the surfaces.[100] The use of RBC ghosts mixed with PRP allows for a more physiologically relevant analysis of platelet deposition. Native RBCs have been shown to be involved in the transport of platelets to the vessel wall.[88] When blood flows through the microvessels the RBCs migrate towards the center of the vessels, crowding the platelets outward and increasing their concentration at the vessel wall.[49, 88] This phenomenon has also been observed with *in vitro* flow systems, where the increased platelet gradient near the test surfaces enhances platelet-surface interactions and increases the likelihood of platelet adhesion.[49, 101] A recent computational model of platelet adhesion in shear flow suggests that platelet adhesion is dependent upon near-wall collisions with RBCs.[102]

The axial migration of RBCs that promotes platelet transport away from the center of vessels is also dependent on the unique abilities of RBCs to deform and aggregate.[103, 104] The combination of aggregation and the deformability of RBCs are also responsible for the shear-thinning characteristics of whole blood.[105] Because the ghost RBCs produced in this study had an identical viscosity curve and deformability as native red blood cells they are expected to produce the same transport phenomena. Therefore, optically clear RBC ghosts were deemed acceptable substitutes for native RBCs in order to maintain the increased platelet concentration near the chamber walls while producing a transparent test fluid.

A parallel plate microfluidic device was chosen for this study because it provided one-dimensional, laminar flow and a defined wall shear rate.[43, 92] Szarvas et al. [106] found the parallel plate flow chamber to be superior to the cone and plate viscometer as the latter reduced surface-specific platelet deposition and experienced an increased reduction in single platelets with time. Other studies have utilized commercially available rotating disk or modified cone and plate viscometer systems to examine platelet adhesion to artificial surfaces with a wall shear stress gradient along the diameter of the disk or plate.[107-110] However, real-time videos of platelet deposition on opaque surfaces using whole blood with these systems have not yet been described. Uchida et al. used a cone and plate viscometer to show that time dependent platelet adhesion could be reduced by coating commercially pure titanium with apatite, and apatite composites. However, images were only acquired every 5 min for a total of 15 min and PRP was utilized instead of whole blood.[108] Furukawa et al. modified a cone and plate viscometer with transparent quartz glass which allowed for real time imaging of epifluorescent platelet deposition onto clear and opaque materials. However, PRP was still used as the perfusion fluid.[110]

Schaub et al. previously presented a method for visualization of time-dependent platelet deposition on opaque surfaces.[43] In that report platelet deposition was measured on opaque metallic and polymeric materials at discrete time points by introducing into the fluid path a fiber optic bundle coupled to an epifluorescent microscope. However, this technique allowed for only brief periodic visualization of platelet adhesion with a limited field of view (100  $\mu\text{m}$  diameter). Additionally, each time the fiber optic bundle was inserted into the chamber it altered the fluid dynamics of the system, potentially influencing subsequent observations. The methods described in this report avoid all these limitations by providing an increased field of view, improved image quality, and no disturbance to the flow field.

Variations in the extent and nature of protein adsorption, particularly fibrinogen, would be expected to be related to the variation in platelet adhesion observed between materials. Ye et al. previously incubated Ti6Al4V and MPC-Ti6Al4V in buffer solution containing ovine fibrinogen and quantified surface protein adsorption.[46] It was found that MPC-Ti6Al4V had significantly less fibrinogen adsorption than the unmodified titanium alloy, which could explain the marked reductions in platelet adhesion observed in this study.[46] While it has been demonstrated that fibrinogen from plasma dominates as the blood adsorbate driving platelet adhesion on artificial surfaces [111], a key factor is the conformational state of the adsorbed fibrinogen and not necessarily the total amount of adsorbed protein.[112] The employment of monoclonal antibodies specific for platelet binding sites on fibrinogen would be a means to investigate whether the trends in platelet adhesion observed in this study for the various opaque surfaces could be directly related back to fibrinogen adsorption and orientation on the surface.[112]

In this study, all materials exhibited an inverse relationship between wall shear rate and area of platelet coverage. Previous studies that investigated the effect of shear rate on platelet adhesion onto highly thrombogenic surfaces, such as type I collagen or tissue factor, showed that platelet deposition increased directly with shear rate.[113, 114] This may simply be due to higher shear rates being associated with greater platelet transport to these surfaces, which are highly platelet reactive.[77, 78] For the surfaces used in this study, the reduced platelet deposition at higher wall shear rates could be explained by shorter periods of interaction between near-wall platelets and surface-bound ligands or greater drag forces on platelets forming transient surface bonds.[77, 78] The results suggest that reducing device regions under a low wall shear rate may aid in lowering device thrombogenicity. Of particular note was the 23-fold drop in platelet coverage observed with the SiC samples at the end of the 5 min perfusion. While the results indicate less than 1% surface area coverage at the  $1000 \text{ sec}^{-1}$  wall shear rate, the videos show transient thrombotic deposition that embolizes quickly before larger thrombi can form. This is a qualitative observation that was unable to be analyzed quantitatively. While the discrete time point results suggest that SiC is less thrombogenic than Ti6Al4V at this wall shear rate, the accompanying real-time video suggests that SiC has material properties that encourage embolization and may present a clinical risk should the phenomenon occur *in vivo* and allow the shedding of emboli large enough to trigger tissue ischemia. Hoffman et al. reported similar material properties with hydrogel coatings where blood-contacting materials implanted in animals would lack obvious deposition onto the test surfaces at the time of explant, but where the animals had infarcts in tissue beds distal to the hydrogels.[115]

Trial and error approaches to materials selection and flow path design may be used by device manufacturers in an effort to reduce thrombogenicity complications. Such methods are

time-consuming and expensive, with often unpredictable outcomes. Computational models have been developed to reduce the time and cost of designing and producing safe, effective blood-wetted devices.[70, 72, 73, 116, 117] Flamm et al. [117] performed a multiscale simulation of platelet deposition onto collagen under flow. The images produced from this simulation were visually similar to the real-time images of platelet deposition onto Ti6Al4V in the current report, suggesting that this computational model might also be applicable to synthetic biomaterials. The data collected from this study could be used to advance the accuracy and utility of such predictive models of thrombosis in blood-wetted cardiovascular devices.

## 2.5 LIMITATIONS

An obvious limitation to this study is its acute, *in vitro* nature. Test materials were subjected to blood analogue perfusion for five min, whereas the tested materials would be implanted for much longer periods of time. However, when screening an array of alternative materials for *in vivo* testing, those forming large thrombi or experiencing substantial embolization acutely might be eliminated in favor of less reactive alternatives. A possible alternative to using a single-pass experiment would be utilizing a recirculating flow loop. This would allow for longer perfusion times and increase individual platelet interactions with the material surface through multiple passes. However, the blood would also contact larger areas of non-test surfaces, introducing artifact in the system.

Another potential limitation in this study is the use of a dilute suspension of red blood cells (25% hematocrit). Although this is lower than the average hematocrit for healthy individuals, it is not atypical for patients implanted with VADs.[118] Sodium citrate was used to

limit the platelet activation caused by the blood draw. This may have reduced bulk phase platelet activation and microaggregate formation during the experiment. Heparin could have been used to mimic the anticoagulants given to VAD patients; however, studies have shown that the *in vitro* use of heparin as an anticoagulant can result in a greater incidence of spontaneous platelet aggregation and activation when compared to sodium citrate.[119, 120]

When RBC ghosts are prepared, the majority of their contents are released and replaced with a saline solution. Thus RBC ghosts contain markedly less adenosine diphosphate (ADP) when compared to native RBCs, raising concerns that they may not be a suitable model because this platelet agonist could not be released as in the native RBCs. However, because the flow produced in the flow chamber is steady laminar flow and the wall shear rates to which the RBCs are exposed are physiological, there should be limited hemolysis or shear-induced ADP release.

A final limitation of note is that thrombus growth in the vertical direction and total platelet deposition was not quantified in these experiments. While earlier work has shown that the overall fluorescence intensity of the microscopic field of view might be used as a correlate of platelet deposition, this was not possible with the current system.[121] High background fluorescence from free quinacrine dihydrochloride in the clear perfusate was a confounding factor here, as was the lack of opaque RBCs to quench this free fluorophore. The temporal measurements of platelet adhesion should thus be considered in the context of the video data, which demonstrate that the platelet adhesion was reflective of the formation of distinct thrombi. The observation that the thrombi grow in elliptical patterns in the downstream direction is in agreement with similar studies investigating mural thrombus formation.[122] These thrombi would presumably also grow in the vertical direction as later arriving platelets preferred to join existing thrombi rather than adhere to patches of the surface where platelets were not adhering.

## 2.6 CONCLUSIONS

Mixing of RBC ghosts with fluorescently-labeled platelets creates an effective blood analogue with which the acute thrombogenicity of opaque blood-contacting materials can be assessed. This method was used to evaluate several materials under consideration for utilization in blood-contacting medical devices, such as VADs. The reduced platelet deposition at elevated wall shear rate that was observed in this study suggests that the blood biocompatibility of VADs might be improved by minimizing the areas of low shear blood contact. Furthermore, this technique revealed that MPC-Ti6Al4V and ZTA have improved thromboresistance when compared to Ti6Al4V and, thus, may be alternatives for consideration in future VAD designs.

### **3.0 VISUALIZATION AND ANALYSIS OF BIOMATERIAL-CENTERED THROMBUS FORMATION WITHIN A DEFINED CREVICE UNDER FLOW**

#### **3.1 INTRODUCTON**

Geometric irregularities, such as steps and crevices, within the flow path of continuous flow VADs serve as a nidus for thrombus formation.[49] Manufacturers make a great effort to reduce the presence of such features within their devices prior to implantation through precise machining and polishing. However, VADs are comprised of multiple parts that serve to create the blood contacting surfaces. So, the introduction of internal steps and crevices is unavoidable, at some level. Also, there is the possibility that surface imperfections can be introduced during the operation of some devices, for instance when a non-fixed VAD impeller collides with a housing surface and creates a scratch.[123]

Understanding how surface irregularities affect the development of thrombotic deposition on clinically relevant biomaterials would provide a useful tool for improving the blood flow path design and materials selection process for VADs and other blood-contacting medical devices. Such data could be used directly or in the development of mathematical models that seek to predict thrombotic deposition risk for a given biomaterial/geometry combination. To date, the use of flow visualization technologies such as particle image velocimetry (PIV) have become routine in blood pump design, as has the early evaluation of candidate biomaterials by acute blood contact under well-defined flow conditions or simple mixing.[6] There have been a limited

number of *in vitro* studies that have examined real-time platelet deposition onto biomaterials in regions of disturbed flow.[72, 124] These reports did not evaluate geometries associated with device joints or surface imperfections and generally evaluated disturbances on a much larger scale. Further, these reports did not evaluate the opaque metallic materials used in the rotary blood pumps in common clinical use today. The objective of this report was to quantify human platelet deposition onto Ti6Al4V alloys, as well as positive and negative control surfaces, in the region of crevices (~50-150  $\mu\text{m}$  in width) that might be encountered in many VADs or other cardiovascular devices. To achieve this, reconstituted fresh human blood with hemoglobin-depleted red blood cells (RBC ghosts, to achieve optical clarity while maintaining relevant rheology), long working optics, and a custom designed parallel plate flow chamber were employed.

## **3.2 MATERIALS AND METHODS**

### **3.2.1 Blood analog preparation**

Fresh whole blood was collected after informed consent from 12 healthy donors (7 male, 5 female), who had refrained from taking any platelet altering medications 14 days prior to collection, with a mean age of  $27 \pm 6$  years in accordance with Institutional Review Board guidelines. Platelet rich plasma (PRP) was collected by centrifuging citrated blood (collected into 5 mL Vacutainer tubes, [0.105M] citrate, BD, Franklin Lakes, NJ, USA) at 250xg for 15 min. Platelets were fluorescently labeled by the addition of quinacrine dihydrochloride (0.5  $\mu\text{M}$  final concentration, Sigma-Aldrich, St. Louis, MO, USA) to the PRP. Packed RBCs (type O-,

Valley Biomedical Products & Services, Inc., Winchester, VA, USA) were utilized to create RBC ghosts through an established protocol.[125] The blood analog used as the perfusate was made by mixing the fluorescently labeled PRP with the RBC ghosts to produce a final hematocrit of 25% and a final platelet concentration of  $2.7 \pm 0.30 \times 10^8$  per mL.

### 3.2.2 Parallel plate flow chamber

A custom parallel plate chamber was designed for this study. Flow channels containing crevices of defined dimensions were prepared from polydimethylsiloxane (PDMS) using a photo-etched silicon mold. The perfusion apparatus is shown in **Figure 15**. The main flow channel is 3 x 8 mm and includes one of three crevice dimensions ( $53 \pm 7 \times 122 \pm 4 \mu\text{m}^2$  (n=7),  $90 \pm 12 \times 122 \pm 4 \mu\text{m}^2$  (N=7), or  $137 \pm 10 \times 122 \pm 4 \mu\text{m}^2$  (N=80)). Silicon tubing (Silicon® Med-X Tubing; United States Plastic Corporation, Lima, Ohio, USA) was connected to the PDMS channel as inlet and outlet connectors. A titanium alloy sample (Ti6Al4V; LaunchPoint Technologies Inc., Goleta, CA, USA) acted as the bottom plate of the chamber. Ti6Al4V was selected for study since it is employed by several current and experimental VADs for blood-contacting surfaces.[84] Platelet deposition on rat tail, type I collagen coated glass coverslips (Neuvitro Corporation, Vancouver, WA, USA; N=5) and a TiAl6V4 surface that had been modified with methacryloyloxyethyl phosphorylcholine polymer (MPC-Ti6Al4V, N=5) were employed as positive and negative thrombogenic control surfaces respectively. The control surfaces were employed in perfusions utilizing the 90  $\mu\text{m}$  wide crevice. MPC-Ti6Al4V was prepared in the authors' laboratory using previously reported protocols.[46] A simple clamping mechanism held the plates together and acrylic shim stock was placed between the plates to provide a precisely defined channel height of 0.1 mm (**Figure 15B**). The flow within this chamber was assumed to be one-dimensional laminar parallel plate flow (Reynolds numbers between 0.1 and 0.4).[43, 92]

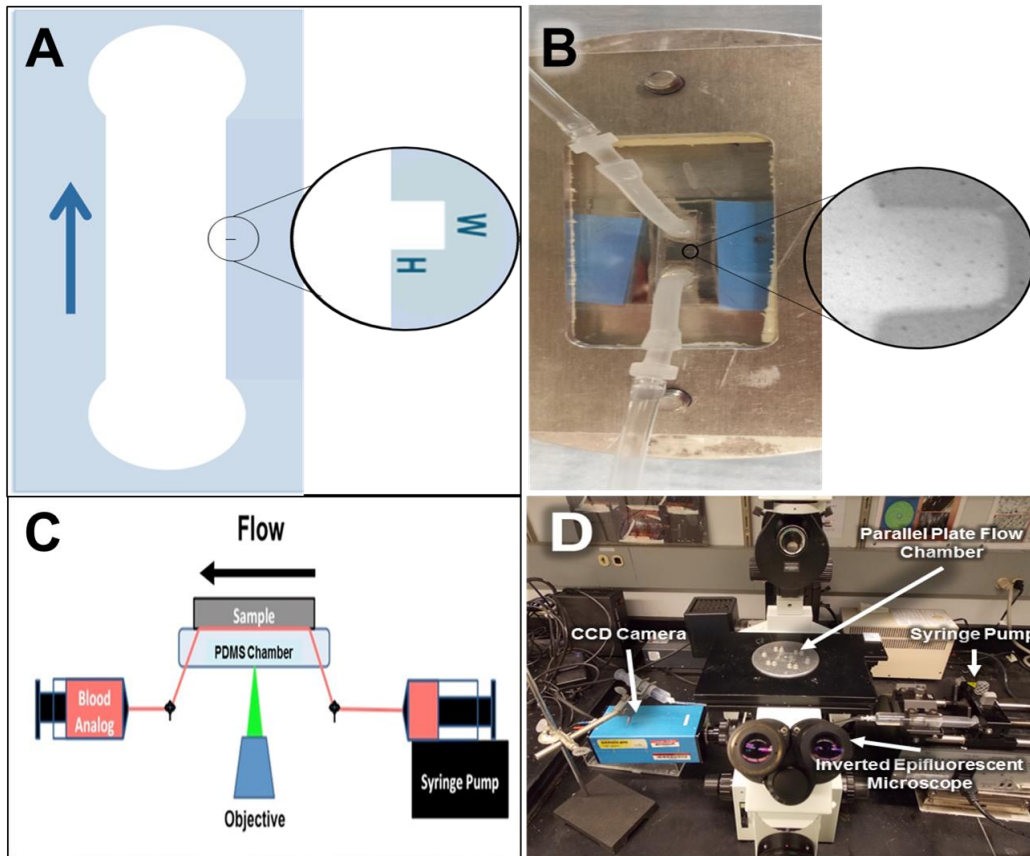


**Figure 15.** *Experimental Setup. A) Schematic of the flow path utilized in this study with magnified view of the rectangular crevice. The arrow indicates the direction of flow B) Photograph of parallel plate chamber with magnified view of the rectangular crevice. C) Schematic of the experimental layout. D) Photograph of the actual experimental layout.*

### 3.2.3 Blood analog perfusion and image acquisition

All non-test surfaces were passivated by incubation with 1% bovine serum albumin (BSA, microbiological grade powder; MP Biomedicals, LLC, Solon, OH, USA) in PBS for 20 min prior to perfusion. The whole blood analog was collected into a 20 mL polystyrene syringe (BD Biosciences) and pushed through the parallel plate flow chamber by syringe pump (Harvard Apparatus, Holliston, Massachusetts, USA) for 10 min at flow rates of 0.125 and 0.310 mL/min

(wall shear rates of  $400 \text{ sec}^{-1}$  and  $1000 \text{ sec}^{-1}$  respectively at the center of the channel). Platelet deposition was visualized within the crevices, in real time, using an inverted epifluorescence microscope (Olympus IX FLA, Olympus Corporation, Shinjuku, Tokyo, Japan) with a 40x super long working distance objective (PlanFL, phase contrast, working distance 6.5 mm - 8.3 mm, numerical aperture 0.55; Olympus Corporation) and a 103W HBO short arc mercury lamp light source (OSRAM GmbH, Munich, Germany). Images were acquired every 0.4 sec beginning at one min after the start of perfusion using a CCD camera (PCO-TECH Inc., Romulus, Michigan, USA).

#### **3.2.4 Fluorescent image analysis**

The percent of the surface covered by deposited platelets was computed through established protocols.[125] Images were also analyzed to determine the probability of platelets adhering to a specific region within the crevice and the average intensity of the adherent platelets utilizing ImageJ (NIH, Bethesda, MD, USA) and custom designed MatLab (MathWorks, Inc., Natick, MA, USA) programs. Briefly, to calculate the probability of platelet adhesion, images were converted from grayscale to binary. All pixels that were brighter than a predetermined threshold were rendered white (platelets) and given a value of 1, whereas all pixels below that threshold were rendered black and given the value of 0. At discrete time points, the corresponding values of the pixels from each test were summed and divided by the total number of experiments. Intensity color maps were generated by averaging the intensity of the deposited platelets at discrete time points.

### 3.2.5 Statistical analysis

All data are presented as mean  $\pm$  standard error of the mean. Data were analyzed by two-way, repeated measures ANOVA with specific post- hoc testing using the Bonferroni correction. SPSS v23 (IBM Corp, Armonk, NY) was used for all statistical analyses.

## 3.3 RESULTS

### 3.3.1 Probability of acute platelet adhesion

The probability maps generated from the acquired fluorescent images of platelet deposition within the various crevice sizes on Ti6Al4V are displayed in **Figures 16** and **17**. In all color map images, flow in the main channel was directed downward. When the blood analog was perfused at a wall shear rate of  $400 \text{ sec}^{-1}$ , the region with the greatest probability of adhesion for all three crevice sizes occurred at the distal corner, nearest the main channel (**Figure 16**). This region increased in area over time. After 10 min of perfusion a region on the proximal corner, nearest the main channel of the  $53 \text{ }\mu\text{m}$  and  $90 \text{ }\mu\text{m}$  crevices also contained a high probability of platelet adhesion ( $>75\%$ ). Adhesion was least likely to occur in the largest crevice ( $137 \text{ }\mu\text{m}$ ).

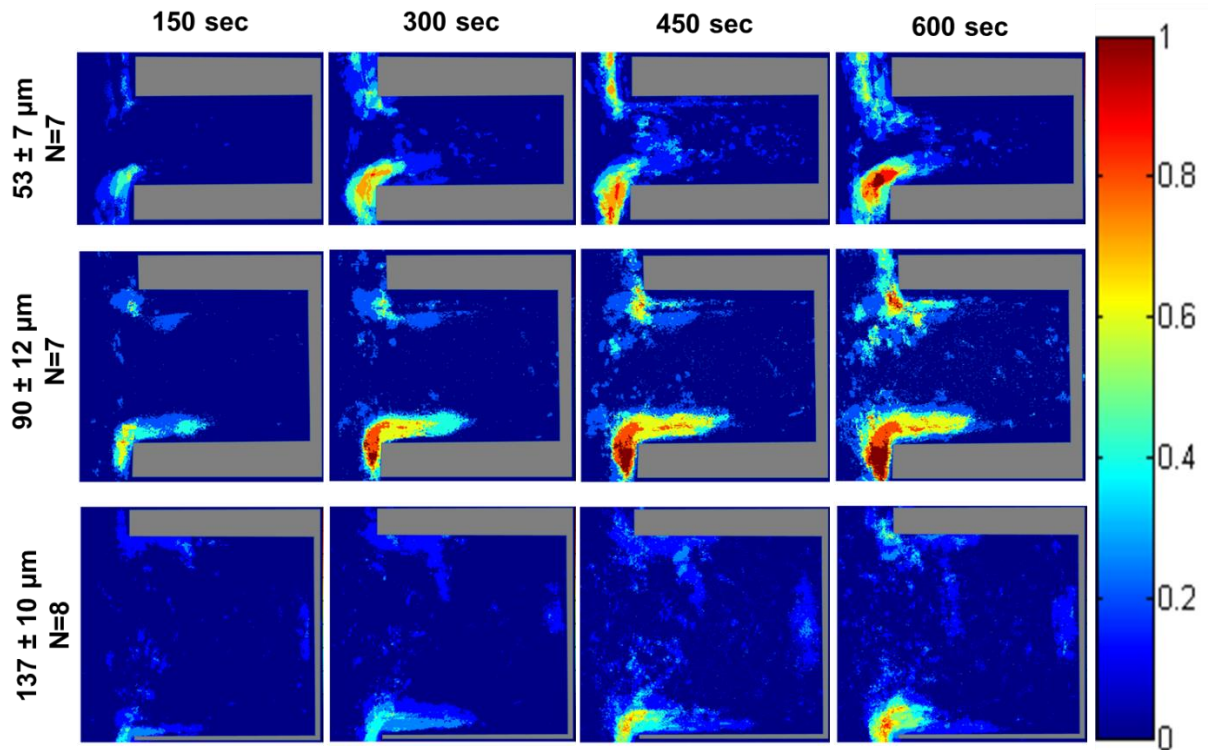


**Figure 16.** Color maps depicting the local probability of platelet deposition within each crevice size, over time, at a perfusion rate of  $125 \mu\text{L}/\text{min}$  and a wall shear rate of  $400 \text{ sec}^{-1}$ . The direction of flow is down for the main channel, outside of the crevice.

Increasing the wall shear rate to  $1000 \text{ sec}^{-1}$  resulted in the greatest probability of platelet adhesion again being located at the distal corner, nearest the main channel for the  $53$  and  $90 \mu\text{m}$  crevices (**Figure 17**). However, this region did decrease in size with the increase in wall shear rate. Within the  $137 \mu\text{m}$  crevice, the platelets mainly adhered along the distal wall with a maximum probability of adhesion  $<50\%$ .

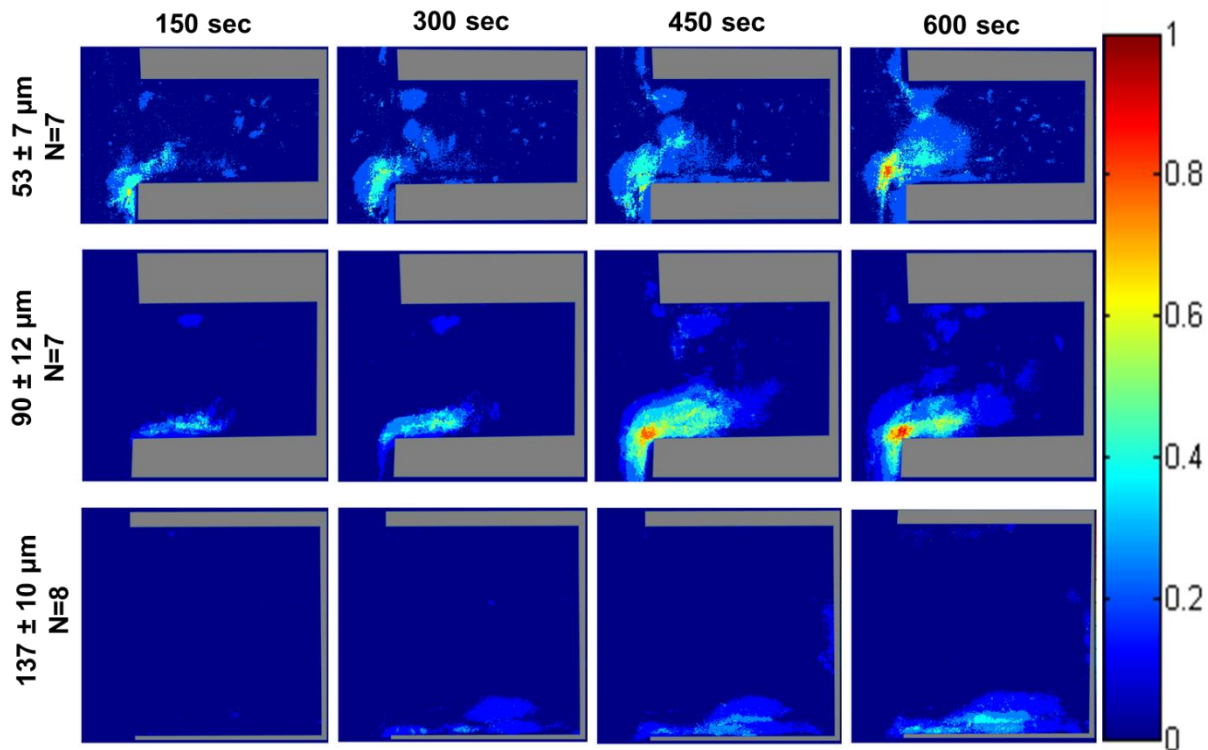


**Figure 17.** Color maps depicting the probability of platelets depositing within each crevice size, over time, at a perfusion rate of 310  $\mu\text{L}/\text{min}$  and a wall shear rate of  $1000 \text{ sec}^{-1}$ . The direction of flow is down for the main channel, outside of the crevice.

When comparing different surfaces at both wall shear rates, the greatest adhesion occurred on the type I collagen with regions having a high probability ( $>75\%$ ) of platelet adhesion being located at both the distal and proximal corner, nearest the main channel. Similar to Ti6Al4V, these regions of platelet adhesion increased with time. MPC-Ti6Al4V was the least thrombogenic with a maximum probability of platelet adhesion  $<30\%$  in the limited region where this occurred (**Figures 18 and 19**). Upon increasing the wall shear rate from 400 to  $1000 \text{ sec}^{-1}$ , platelets were more likely to adhere along the distal wall of MPC-Ti6Al4V instead of at the distal corner.

The fluorescent images were further analyzed to determine the percent of the analyzed blood contacting surface covered by adherent platelets over time (**Figure 20**). At the  $400 \text{ sec}^{-1}$  wall shear rate, the  $53 \text{ }\mu\text{m}$  and  $90 \text{ }\mu\text{m}$  crevice had significantly greater adhesion compared to the  $137 \text{ }\mu\text{m}$  crevice, with a platelet surface coverage of  $19.9 \pm 1.6\%$  ,  $16.7 \pm 2.9\%$  and  $10.4 \pm 1.4\%$  respectively. ( $P=0.01$ , **Figure 20A**). Comparing the materials, collagen had the greatest surface coverage with  $23.1 \pm 3.2\%$  after 10 min of perfusion and MPC-Ti6Al4V had the least amount of adherent platelets with a maximum surface coverage of  $1.1 \pm 0.2 \%$  ( $P<0.01$ , **Figure 20B**).

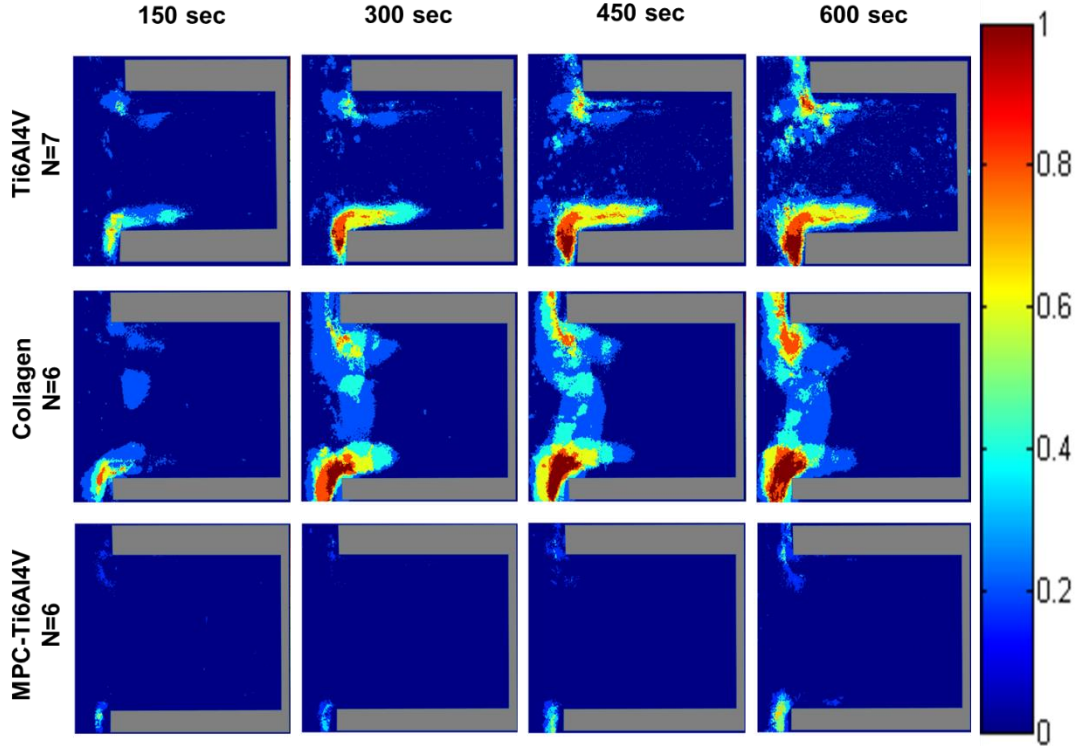


**Figure 18.** Color maps depicting the probability of platelets depositing on each material, over time, at a perfusion rate of  $125 \text{ }\mu\text{L}/\text{min}$  and a wall shear rate of  $400 \text{ sec}^{-1}$ . Crevice size of  $90 \pm 12 \text{ }\mu\text{m}$ . The direction of flow is down for the main channel, outside of the crevice.

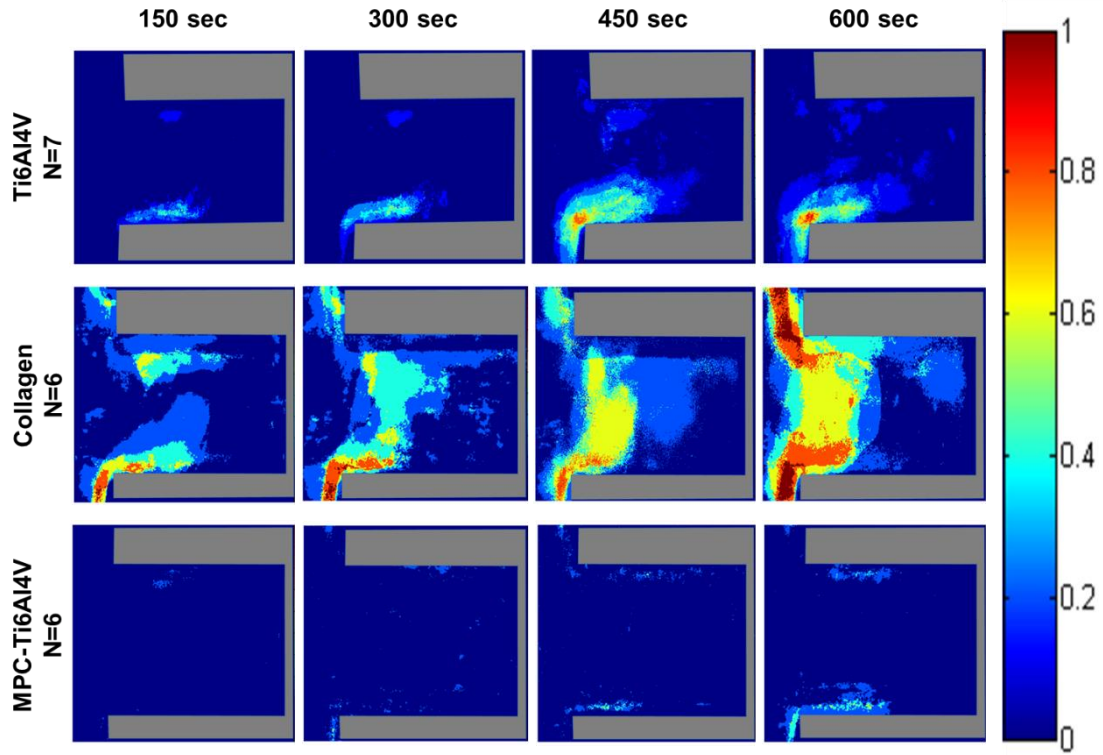


**Figure 19.** Color maps depicting the probability of platelets depositing on each material, over time, at a perfusion rate of  $310 \mu\text{L}/\text{min}$  and a wall shear rate of  $1000 \text{ sec}^{-1}$ . Crevice size of  $90 \pm 12 \mu\text{m}$ . The direction of flow is down for the main channel, outside of the crevice.

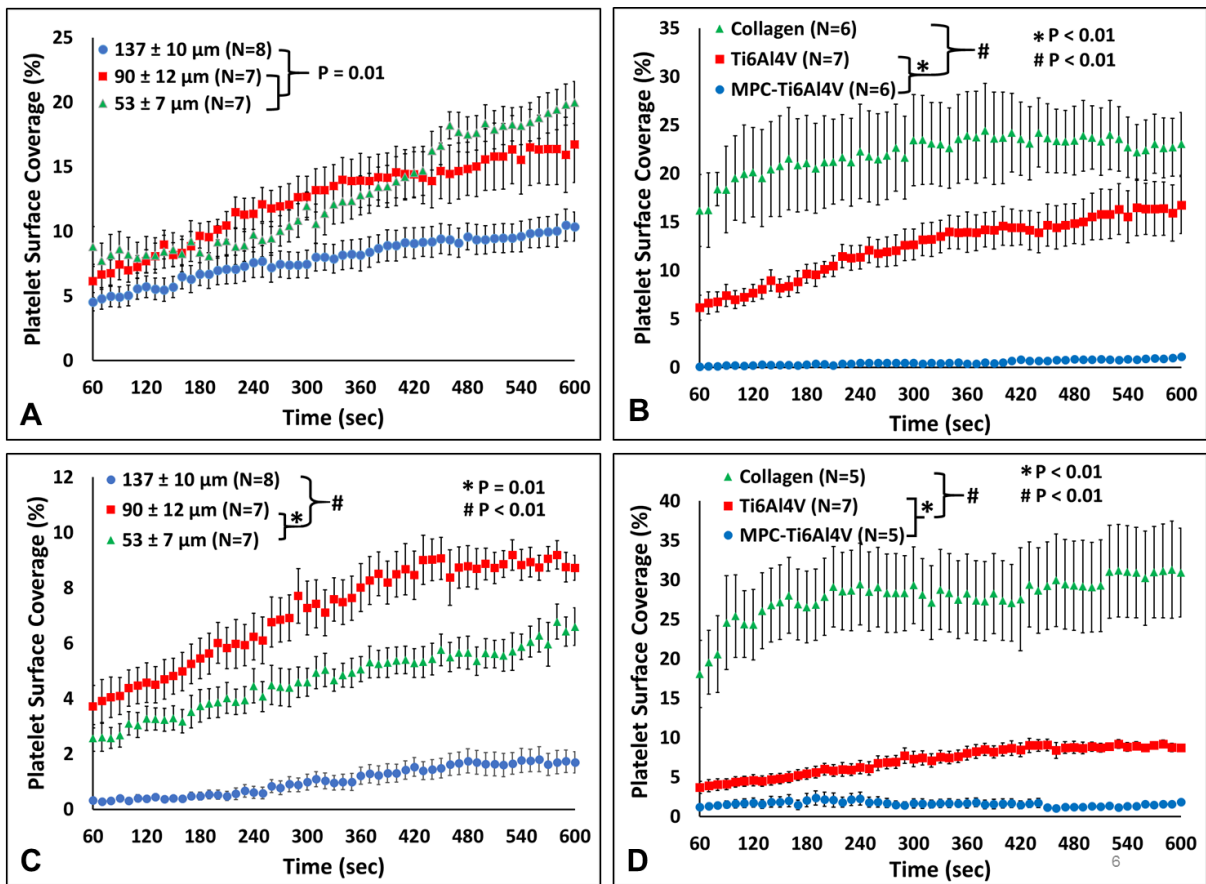


**Figure 20.** The percent of the surface covered by deposited platelets. A) The effect of crevice size on platelet surface coverage at a wall shear rate of  $400 \text{ sec}^{-1}$ . B) The effect of material on platelet surface coverage at a wall shear rate of  $400 \text{ sec}^{-1}$ . Crevice size of  $90 \pm 12 \mu\text{m}$ . C) The effect of crevice size on platelet surface coverage at a wall shear rate of  $1000 \text{ sec}^{-1}$ . D) The effect of material on platelet surface coverage at a wall shear rate of  $1000 \text{ sec}^{-1}$ . Crevice size of  $90 \pm 12 \mu\text{m}$ .

Increasing the wall shear rate to  $1000 \text{ sec}^{-1}$  significantly decreased the percent platelet coverage within the  $53 \text{ }\mu\text{m}$ ,  $90 \text{ }\mu\text{m}$  and the  $137 \text{ }\mu\text{m}$  ( $P < 0.01$ , **Figure 21**). However, the increase in wall shear rate did not result in a significant change in adhesion for the collagen and MPC-Ti6Al4V samples. At the higher wall shear rate, the  $137 \text{ }\mu\text{m}$  crevice had least amount of platelet adhesion compared to the other crevice sizes at  $1.7 \pm 1.1\%$  ( $P < 0.01$ ). The  $90 \text{ }\mu\text{m}$  crevice had significantly greater platelet coverage at  $8.7 \pm 0.5\%$  compared to the  $137 \text{ }\mu\text{m}$  and  $53 \text{ }\mu\text{m}$  crevices ( $1.7 \pm 1.1\%$  and  $6.6 \pm 0.6\%$  respectively,  $P < 0.01$ ).

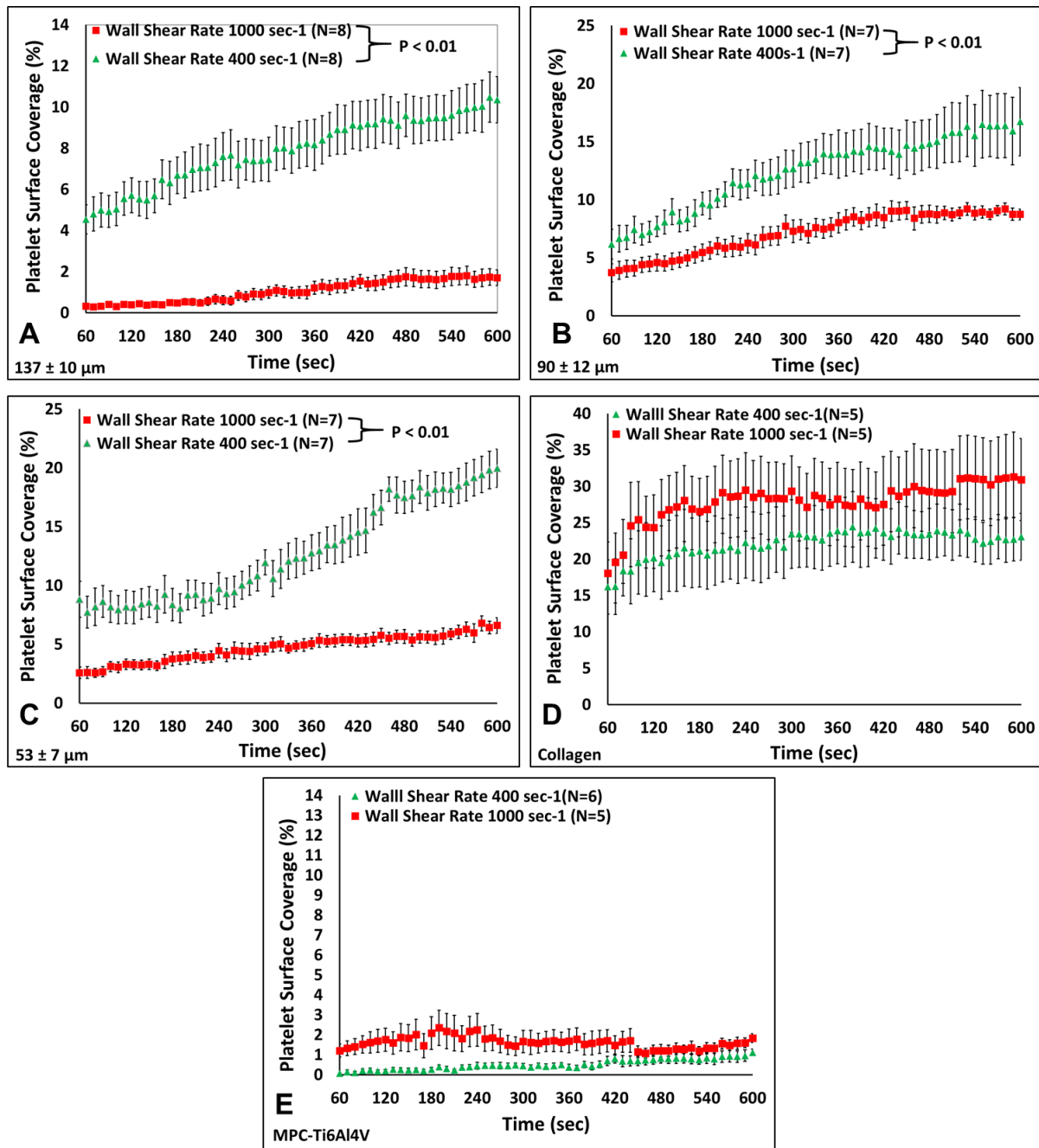


**Figure 21.** Effect of wall shear rate on platelet surface coverage. A)  $137 \pm 10 \mu\text{m}$ . B)  $90 \pm 12 \mu\text{m}$ . C)  $53 \pm 7 \mu\text{m}$ . D) Collagen. E) MPC-Ti6Al4V.

### 3.3.2 Average intensity of deposited platelets

Color maps depicting the average fluorescence intensity from deposited platelets on Ti6Al4V (**Figure 22** and **Figure 23**) and the control materials (**Figure 24** and **Figure 25**) within the crevices were generated to provide a 3-dimensional approximation of thrombus formation, assuming that stacked platelets led to higher local fluorescence intensity.[121] The greatest platelet deposition occurred on the collagen surface and the 90  $\mu\text{m}$  crevice often became completely occluded after 10 min of perfusion. The images were thus normalized to the greatest average intensity exhibited by those collagen control surfaces that were completely occluded. At both wall shear rates the region of high platelet deposition (intensity  $>15$ ; maximum intensity  $=25$ ) occurred at the distal corner of the crevice nearest the main channel in the 53 and 90  $\mu\text{m}$  crevices. However these regions of high platelet deposition were smaller in size when the blood analog was perfused at a higher wall shear rate. Platelets were least likely to deposit in the 137  $\mu\text{m}$  crevice, and when the wall shear rate was increased to  $1000 \text{ sec}^{-1}$  for this crevice size, the average intensity decreased to  $<15$ .

The greatest platelet deposition occurred on the type I collagen samples. The intensity images revealed that large thrombi formed along the entire entrance of the crevice, on the collagen coverslip. The least amount of deposition occurred on the MPC-Ti6Al4V samples with an average intensity  $<10$ .

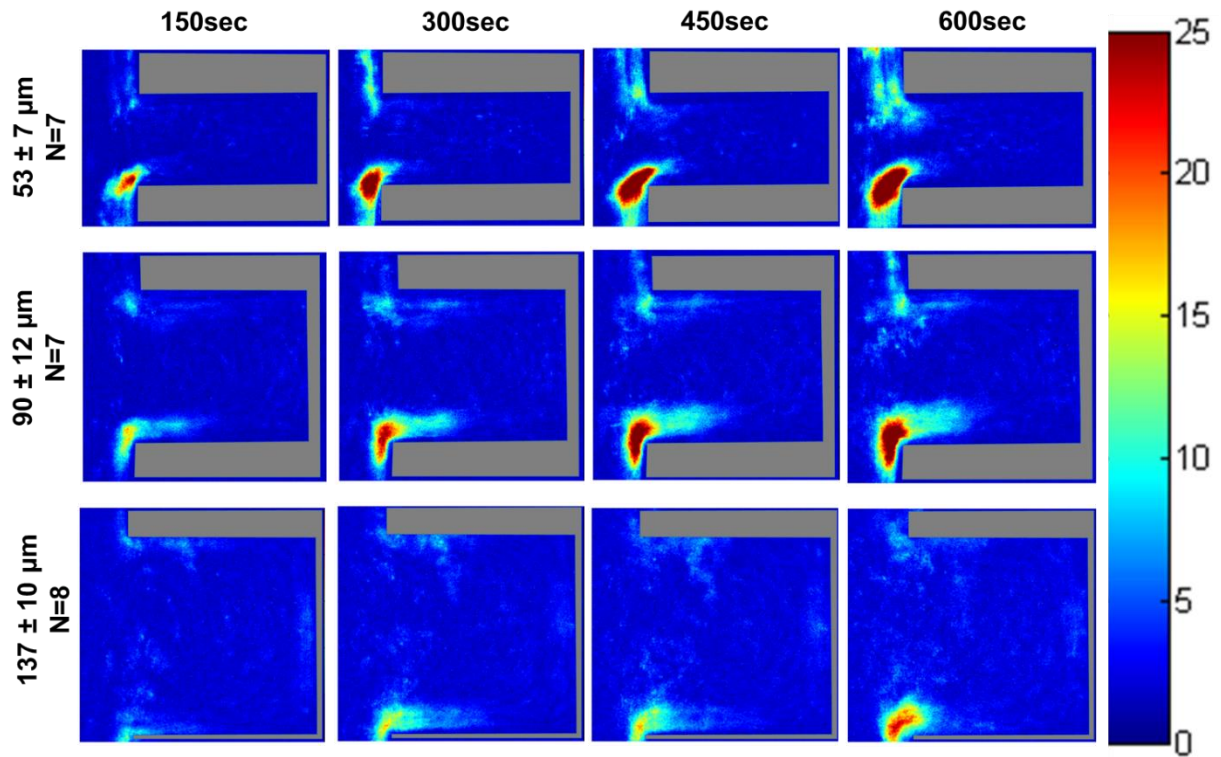


**Figure 22.** Color maps depicting the average intensity of the platelet deposition within each crevice size, over time, at a perfusion rate of 125  $\mu\text{L}/\text{min}$  and a wall shear rate of  $400 \text{ sec}^{-1}$ . The direction of flow is down for the main channel, outside of the crevice.

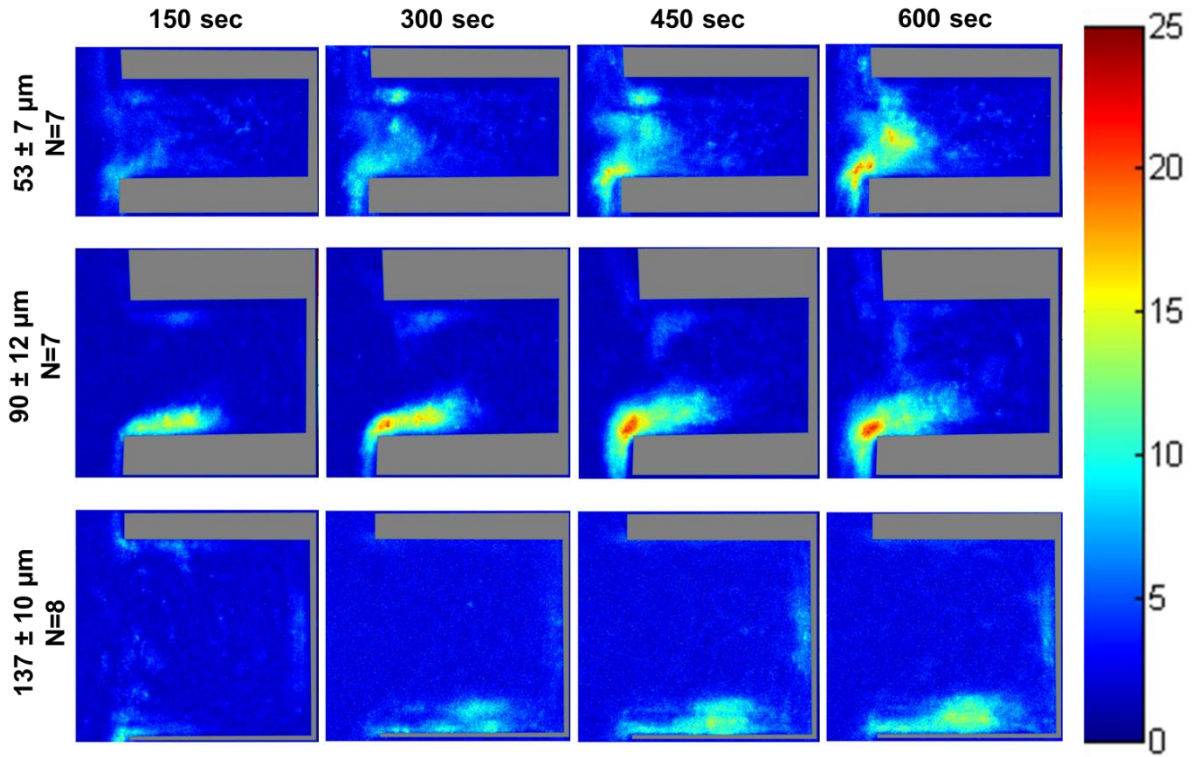


**Figure 23.** Color maps depicting the average intensity of the platelet deposition within each crevice size, over time, at a perfusion rate of 310  $\mu\text{L}/\text{min}$  and a wall shear rate of  $1000 \text{ sec}^{-1}$ . The direction of flow is down for the main channel, outside of the crevice.

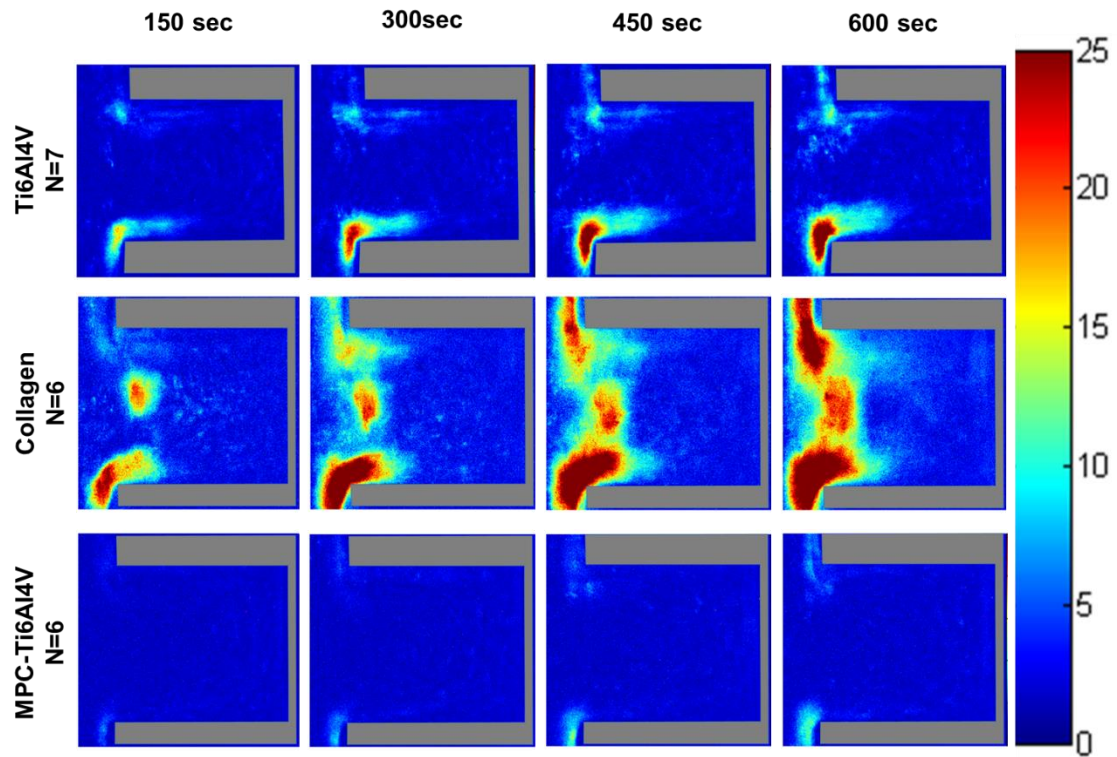


**Figure 24.** The direction of flow is down. Color maps depicting the average intensity of the platelet deposition on each material over time, at a perfusion rate of 125  $\mu\text{L}/\text{min}$  and a wall shear rate of  $400 \text{ sec}^{-1}$ . Crevice size of  $90 \pm 12 \mu\text{m}$ .

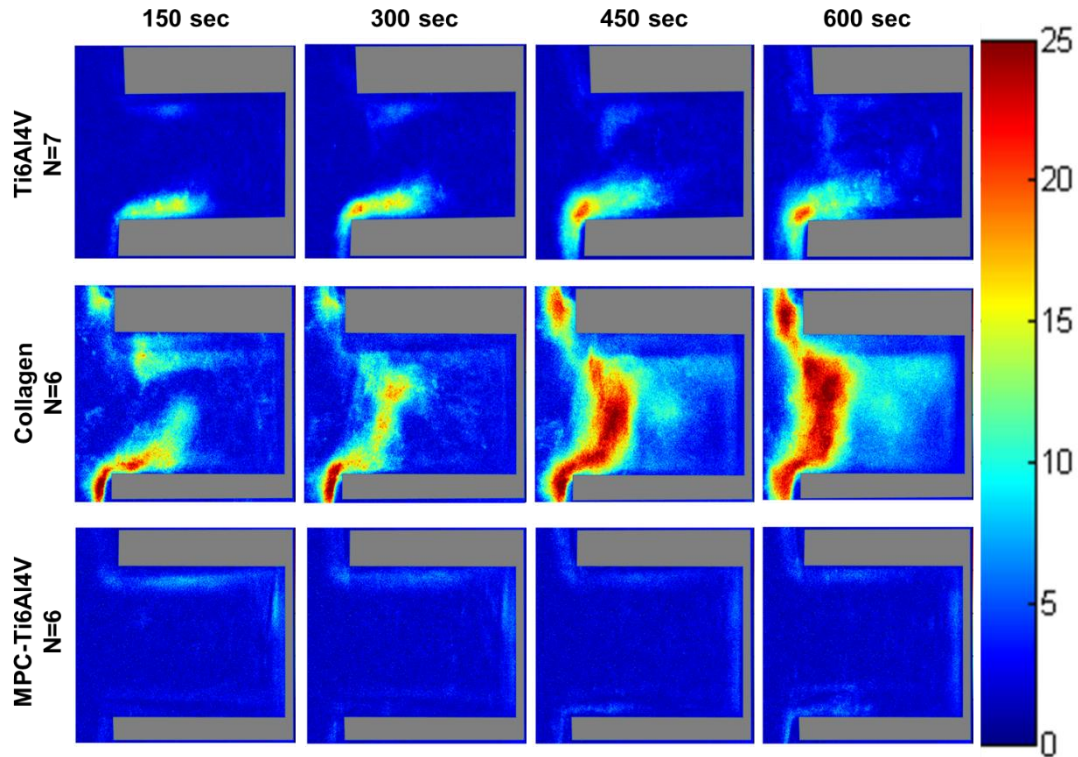


**Figure 25.** The direction of flow is down. Color maps depicting the average intensity of the platelet deposition on each material over time, at a perfusion rate of 310  $\mu\text{L}/\text{min}$  and a wall shear rate of  $1000 \text{ sec}^{-1}$ . Crevice size of  $90 \pm 12 \mu\text{m}$ .

### 3.3.3 Representative real-time perfusion videos

Representative accelerated videos of platelets depositing within the crevices for different materials and the two wall shear rates are available in the supplemental material of this report (**Videos 3.1-3.7**). At both wall shear rates, two flow regimes are visible within the crevice: the primary flow path that curves into the crevice from the main channel flow at the proximal corner and rejoins the main channel flow at the distal corner, and a secondary vortex that forms further within the crevice. The diameter of the vortex decreased in size with the decrease in crevice width. In the  $53 \mu\text{m}$  and  $90 \mu\text{m}$  crevices

(**Videos 3.1** and **3.2**), the platelets initially adhered to the distal corner, nearest the main channel, and grew upward toward the center of the crevice. As the thrombi grew and partially occluded the crevice, the vortex was disturbed and the flow within the crevice became more unstable. When the wall shear rate was increased to  $1000 \text{ sec}^{-1}$ , the stability of the thrombi decreased and more embolization events were observed (**Video 3.3** and **Video 3.4**). Only a few embolization events were noted within the  $137 \mu\text{m}$  crevice or on the MPC-Ti6Al4V at both wall shear rates (**Video 3.5** and **Video 3.6**).

### 3.4 DISCUSSION

The fluid flow pathway within a blood-wetted medical device is an important determinant of the likelihood for thrombus development and subsequent embolization. According to Virchow's triad, it is one of the three major factors that affect thrombosis along with surface and the status of the blood.[126] Therefore, it is important to consider blood flow patterns when designing cardiac devices and selecting blood contacting biomaterials. Several studies have used PIV to characterize fluid flow within irregular geometries, such as bifurcations, steps, and crevices, and in specific cardiovascular devices in order to identify regions that could potentially promote thrombus formation.[49, 57, 127-129] Studies using this method have been able to ascertain potentially hazardous flow patterns (i.e. recirculation and stagnation). However, platelet-sized particles [57, 129] or red blood cells in platelet poor plasma [49, 127] are used in this technique as the tracing particles instead of biologically active platelets.

Many microfluidic devices have been designed to investigate the effect of the blood flow pathway on the development of thrombi. Unlike PIV, this technique utilizes active platelets to characterize how disturbed flow contributes to platelet adhesion and aggregation.[14, 31-33] The majority of these studies examine platelet deposition onto collagen-coated or uncoated glass coverslips after backward steps, sudden expansions, or stenosis.[50, 55, 130, 131]

Few studies have examined how complex flow paths affect the adhesion or deposition of platelets onto a biomaterial.[72, 124] Goodman et al. [72] used an experimental flow cell consisting of polyethylene tubing with sudden constrictions. Heparinized human blood was perfused through flow cells and thrombus growth was observed with video-microscopy. It was found that there were three regions of substantial platelet deposition; at the point of contraction, at the point of expansion, and at the flow reattachment point. Schaller et al. [124] developed a stagnation flow chamber to examine how flow stagnation and a continuum of wall shear rates affected platelet adhesion onto glass coverslips that were thinly coated with commercial polyurethanes or adsorbed von-Willebrand factor as their test materials. Although these techniques provide a way to examine real-time platelet deposition onto biomaterials, the flow conditions are not related to the defects or design attributes of many cardiovascular devices

Previous PIV studies of sudden expansions and constrictions revealed that the highest concentration of platelet sized particles was in the corners, where there were regions of recirculating flow.[49, 72] These results would suggest that the greatest platelet deposition would have been located towards the back of the crevices where the secondary vortices formed. However, it was found here that the regions of greatest deposition occurred on the distal corners of the crevices toward the main channel. This may have occurred because the distal corner is the first area the platelets impact, and the secondary flow vortex pattern increases the cumulative

time that platelets can interact with this area. Once platelets adhere and activate within this region, they release their granules and initiate biochemical pathways that result in a local flux of platelet agonists, creating a positive feedback loop that promotes further deposition. Ha et al. [130] and Taylor et al. [132] found that platelet deposition onto collagen initially occurred on the edge of a sudden expansion but then progressed into the corner. The crevices are similar to a sudden expansion followed quickly by a sudden constriction. This creates two distinct flow paths: the secondary flow vortex pattern and the primary flow path that curves into the crevice from the main channel flow at the proximal corner and then rejoins the main channel flow at the distal corner. This primary flow path would transport platelets away from the crevice after some potential interaction with the distal corner, and may be why the thrombus does not grow into the bottom of the crevice.

Cardiovascular device manufactures generally try to minimize the size of discontinuities and crevices within their devices to intuitively reduce their potential to promote thrombus formation. However, in the size range examined, it was found that the largest crevice was the least thrombogenic. The real-time videos show that platelets tended to remain trapped in the vortices of the 53 and 90  $\mu\text{m}$  crevices for an extended period of time when compared to the 137  $\mu\text{m}$  crevice. Therefore platelets in the 137  $\mu\text{m}$  crevice were exposed to the disturbed flow patterns, artificial material, and biochemical agonist for a shorter period of time when compared to the other crevice sizes, making it less likely they would activate and adhere.

Although this was an acute study, the real-time visualization method employed provides the ability to investigate the initiation and potentiation of thrombus deposition generated by irregular geometries with opaque materials. For example, the color maps and surface coverage analysis suggest that when one increases the shear rate to  $1000 \text{ sec}^{-1}$ , platelet adhesion within the

53  $\mu\text{m}$  crevice decreases. However, the videos show that the thrombi that form in the crevice are not stable. In **Video 3.5** the thrombus that formed in the 53  $\mu\text{m}$  crevice rotates with the secondary vortex. Often times this unstable thrombus would embolize, an effect not perceivable with endpoint analysis. This method also provides a way to investigate how the growth of thrombi affects the flow pattern within the crevice. As the deposition increases within the 53  $\mu\text{m}$  and 90  $\mu\text{m}$  crevices the flow becomes erratic, altering the shape of the secondary vortex.

Several mathematical and computer models have been developed to try to predict platelet deposition and thrombus formation with simple flow paths.[72, 133] Some researchers have even incorporated flow over a step as part of their modeling.[133] However, the interpretation of these models is limited by the lack of experimental data characterizing the effects of steps and crevices, or the effect of common clinical biomaterials on thrombus formation. A robust predictive model of device thrombosis would reduce the time and resources spent in empirically seeking to design more blood-biocompatible cardiovascular devices. The methodology employed in this study and the type of data generated provides a means for the refinement and fitting of models that seek to simulate the thrombotic deposition process in blood-wetted devices.

### **3.5 LIMITATIONS**

Some limitations of the current report are worth noting. Aside from the aforementioned acute nature of the blood perfusion experiments, the results are also limited by the 2D nature of the flow pathway. The biomaterial only comprised the bottom (imaged) surface of the flow chamber. The other surfaces of the channel were albumin-passivated PDMS, in an effort to minimize any effects from platelet deposition onto non-test material. Etching the flow path directly into a

Ti6Al4V surface may be possible to create only one non-test surface, however etch techniques that were evaluated (data not shown) were not able to achieve the precision or tolerance necessary to make a crevice with smooth, well defined walls. Further, the use of a PDMS channel allowed multiple materials to be tested with a consistently shaped geometry. Another limitation was that only three crevice sizes were investigated. Limitations on the size range evaluated were the tolerance of the photo-etching technique employed and the field of view associated with the optical system. A rectangular geometry was chosen to represent an idealized crevice because the fluid flow within it has been well-characterized and this geometry is readily amenable to computational modeling.[134] There was some slight geometric distortions in the crevice shape due to the clamping mechanism used to seal the chamber, causing the edges to be slightly rounded. Finally, this study used a dilute suspension of red blood cells (25% hematocrit). Although this is lower than the average hematocrit for healthy individuals, it is not atypical for patients implanted with VADs.[118]

### 3.6 CONCLUSIONS

The employed method provides a viable means for quantifying the effect of common geometric irregularities found in cardiovascular devices on platelet deposition. Interestingly, the least amount of deposition occurred in the largest crevice size. While the most deposition occurred in the 90  $\mu\text{m}$  and 53  $\mu\text{m}$  crevices at the lower wall shear rate. This suggests that the crevice size might be tailored, depending on the flow condition, to reduce the risk of thromboembolic events. These data could be used to improve the accuracy of a predictive model of thrombotic deposition in VADs to help determine the tolerable limits of these features. These limits could then be incorporated in to the design of blood-wetted, implantable cardiovascular devices to improve their hemocompatibility.

## **4.0 CHARACTERIZING THE EFFECT OF SUB-THRESHOLD CONCENTRATIONS OF ADP ON PLATELET DEPOSITION ONTO CLINICALLY RELEVANT OPAQUE MATERIALS**

### **4.1 INTRODUCTON**

Heart failure patients often have abnormal coagulation that increases their risk of stroke and thrombotic events prior to VAD implantation. This hypercoagulable state may be caused by many factors. One factor is that heart failure patients often have elevated levels of biochemical agonists, such as thrombin, thromboxane, and adenosine diphosphate (ADP) that are known to promote thrombus formation.[58-60] Biochemical agonists can be categorized as either weak or strong depending on how strongly they promote platelet aggregation.[7] Although ADP is considered a weak agonist it plays an important role in thrombus formation. When a platelet is activated it releases dense granules, which contain a high concentration of ADP. This creates a positive feedback loop, promoting further platelet activation and aggregation. ADP induces an influx of extracellular  $Ca^{++}$ , an important co-factor for platelet activation.[8] ADP has also been shown to work synergistically with other agonists to promote platelet aggregation.[7-9] ADP-induced platelet aggregation is such a significant clinical concern that an anti-platelet medication has been developed to target the interaction between platelets and ADP. Clopidogrel (Plavix) reduces platelet activation through inhibiting the P2Y<sub>12</sub> (ADP) receptor.[58]

Platelet aggregometry data show that platelets can either be reversibly aggregated or irreversibly aggregated depending on the concentration of biochemical agonist added to the sample. For ADP, platelets are reversibly aggregated when exposed to an ADP concentration of less than 1.5  $\mu\text{M}$ . [135-137] However, a sub-threshold concentration of agonist may interact with other factors, such as shear stress and blood contact with artificial surfaces, to irreversibly aggregate platelets and cause thrombosis in VADs. Understanding the functional relationship between shear stress, biochemical agonists, and artificial surfaces would be a useful tool in assessing the hemocompatibility of blood-wetted devices. The aim of this report is to investigate the effect of sub-threshold concentrations of ADP in conjunction with flow on platelet deposition onto clinically relevant opaque materials.

## **4.2 MATERIALS AND METHODS**

### **4.2.1 Blood analog preparation**

Fresh whole blood was collected after informed consent from 12 healthy donors (8 male, 4 female), who had refrained from taking any platelet altering medications 14 days prior to collection, with a mean age of  $28 \pm 5$  years in accordance with Institutional Review Board guidelines. Platelet rich plasma (PRP) was collected by centrifuging heparinized blood (collected into 10 mL Vacutainer tubes, (158 USP lithium heparin, PD biosciences, Franklin Lakes, NJ, USA) at 250xg for 15 min. Platelets were fluorescently labeled by the addition of quinacrine dihydrochloride (0.5  $\mu\text{M}$  final concentration, Sigma-Aldrich, St. Louis, MO, USA) to the PRP. Packed RBCs (type O-, Valley Biomedical Products & Services, Inc., Winchester, VA, USA)

were utilized to create RBC ghosts through the protocol established in section 2.2.2 of this report.[125] The blood analog used as the perfusate was made by mixing the fluorescently labeled PRP with the RBC ghosts to produce a final hematocrit of 25% and a final platelet concentration of  $2.6 \pm 0.43 \times 10^8$  per mL.

#### **4.2.2 Parallel plate flow chamber and membrane based agonist delivery system**

A parallel plate flow chamber that was described in Chapter 2.2.4 was modified for this study.[125] Briefly, the chamber consisted of a clear acrylic top plate with angled nylon inflow and outflow barbed connectors. A titanium alloy sample (Ti6Al4V; LaunchPoint Technologies Inc., Goleta, CA, USA) or zirconia toughened alumina (ZTA) acted as the bottom plate of the chamber. Ti6Al4V was selected for study because it is employed by several current and experimental VADs for blood-contacting surfaces.[46] ZTA was chosen because previous studies have shown it to be significantly less thrombogenic than Ti6Al4V.[125] A simple clamping mechanism held the plates together, with a silicone gasket outlining the channel width and length (5 x 8 mm). Aluminum shim stock was placed between the plates to provide a precisely defined channel height of 0.076 mm.

A membrane based agonist delivery system was designed to evenly introduce specific concentrations of adenosine diphosphate (ADP) into the blood analog over time (**Figure 26 and Video 4.1**). A thin walled, expanded polytetrafluoroethylene tubular membrane (Aeos ePTFE Extruded Sub-Lite-Wall®, inner diameter  $0.91 \pm 0.05$  mm, wall thickness  $0.01 \pm 0.03$  mm, Zeus Industrial Products, Inc., Orangeburg, SC, USA) was inserted through the polyvinyl chloride tubing (PVC; Saint-Gobain™ Vincon™ Flexible PVC Tubing, inner diameter 3.20 mm, wall thickness 6.40 mm, Fisher Scientific, Pittsburgh, PA, USA), directly before the barbed inlet of

the parallel plate chamber, using a 21 G needle (BD™ General Use and Precision Glide Hypodermic Needles, Fisher Scientific, Pittsburgh, PA, USA). A 1 µm pore size was chosen because it allows the agonist to be perfused into the blood analog while preventing the blood cells from entering the membrane. The membrane is secured to the needle using miniature heat-shrink tubing (McMaster-Carr, Aurora, OH, USA) and the holes, made by the needle, in the PVC were sealed by non-toxic sealant (ECO-BOND Pet Safe, Eco-Bond Adhesives, LLC, Pewaukee, WI, USA).

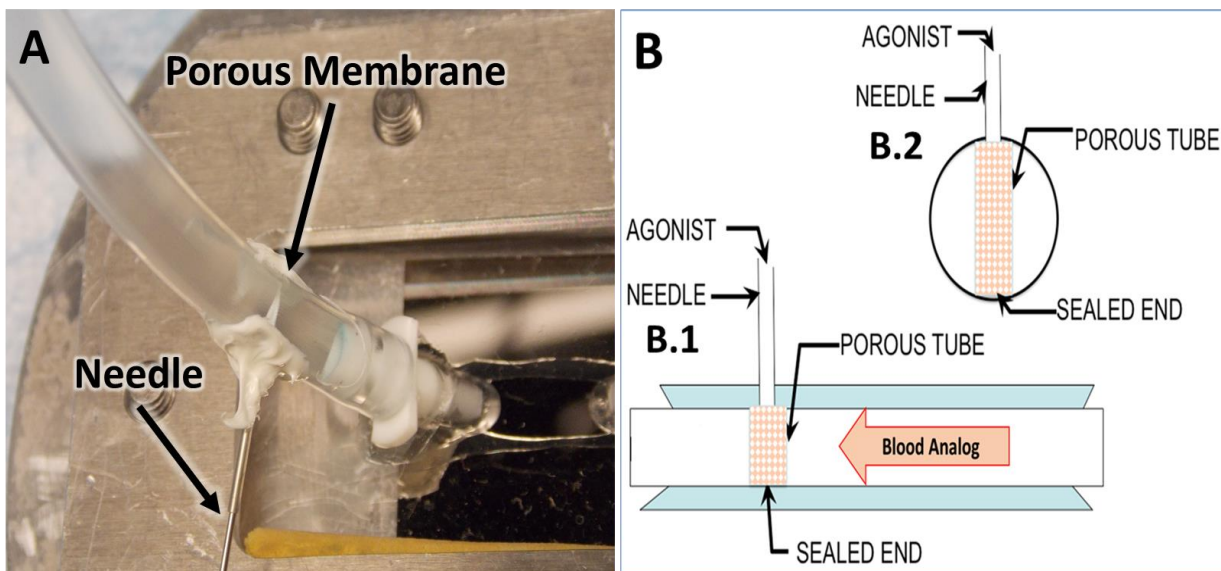


**Figure 26.** Membrane based biochemical agonist delivery system. A) Photo of the membrane based biochemical agonist delivery system. B) Schematic of the agonist delivery system. B.1) Side view of the system schematic. B.2) Front view of the system schematic.

### 4.2.3 Blood analog and agonist perfusion

All non-test surfaces were passivated by incubation with 1% bovine serum albumin (BSA, microbiological grade powder; MP Biomedicals, LLC, Solon, OH, USA) in PBS for 20 min prior to perfusion. The whole blood analog was collected into a 20 mL polystyrene syringe (BD Biosciences) and pushed through the parallel plate flow chamber by syringe pump (Harvard Apparatus, Holliston, Massachusetts, USA) for 10 min at flow rates of 0.117 and 0.289 mL/min (wall shear rates of  $400 \text{ sec}^{-1}$  and  $1000 \text{ sec}^{-1}$  respectively at the center of the channel). 0, 115, or 230  $\mu\text{M}$  of ADP (adenosine 5'-diphosphate, BD Biosciences) in PBS was collected into a 20 mL polystyrene syringe (BD Biosciences) and pushed through a syringe pump (Harvard Apparatus, Holliston, Massachusetts, USA) simultaneously with the blood analog. Depending on the wall shear rate of the blood analog, the ADP solution was either perfused at a blood flow rate of 5 or 12.5  $\mu\text{L}/\text{min}$  ( $400$  and  $1000 \text{ sec}^{-1}$  respectively) so that the final concentration of ADP would be 0, 5, or 10 nM/min at the site of the membrane. The blood analog was forced to flow around the membrane to promote mixing and even distribution of the agonist.

#### **4.2.4 Image acquisition**

Platelet deposition was visualized within the crevices, in real time, using an inverted epifluorescence microscope (Olympus IX FLA, Olympus Corporation, Shinjuku, Tokyo, Japan) with a 40x super long working distance objective (PlanFL, phase contrast, working distance 6.5 mm - 8.3 mm, numerical aperture 0.55; Olympus Corporation) and a 103W HBO short arc mercury lamp light source (OSRAM GmbH, Munich, Germany). Images were acquired every 0.4 sec beginning at one min after the start of perfusion using a CCD camera (PCO-TECH Inc., Romulus, Michigan, USA).

#### **4.2.5 Fluorescent image analysis**

The percent of the surface covered by deposited platelets was computed through the protocols established in section 2.2.5 of this report protocols.[125] These images were also analyzed to determine the average area of the individual thrombi adhered to the surfaces over time.

#### **4.2.6 Statistical analysis**

All data are presented as mean  $\pm$  standard error of the mean. Data were analyzed by two-way, repeated measures ANOVA with specific post- hoc testing using the Bonferroni correction. SPSS v23 (IBM Corp, Armonk, NY) was used for all statistical analyses.

## 4.3 RESULTS

### 4.3.1 Acute platelet deposition

The fluorescent images were analyzed to determine the percent of the blood contacting surface covered by adherent platelets over time (**Figure 27**). At a wall shear rate of 400 sec<sup>-1</sup> (**Figure 27A**), the addition of 10 nM of ADP caused a significant increase in platelet deposition onto Ti6Al4V (Ti6Al4V: 10 nM) with  $35.5 \pm 2.1\%$  of the surface covered after 10 min of perfusion (N=6, P < 0.01). However, at the same ADP concentration, ZTA had the least amount of platelet deposition with a maximum platelet surface coverage of  $10.1 \pm 1.2\%$  (ZTA: 10 nM, N=5, p < 0.01). The addition of 5 nM of ADP did not significantly increase platelet deposition on Ti6Al4V (Ti6Al4V: 5nM) compared to the control (Ti6Al4V: 0 nM) with  $9.9 \pm 1.1\%$  of the surface covered by platelets after 10 min of perfusion ( N=5, P < 0.01).

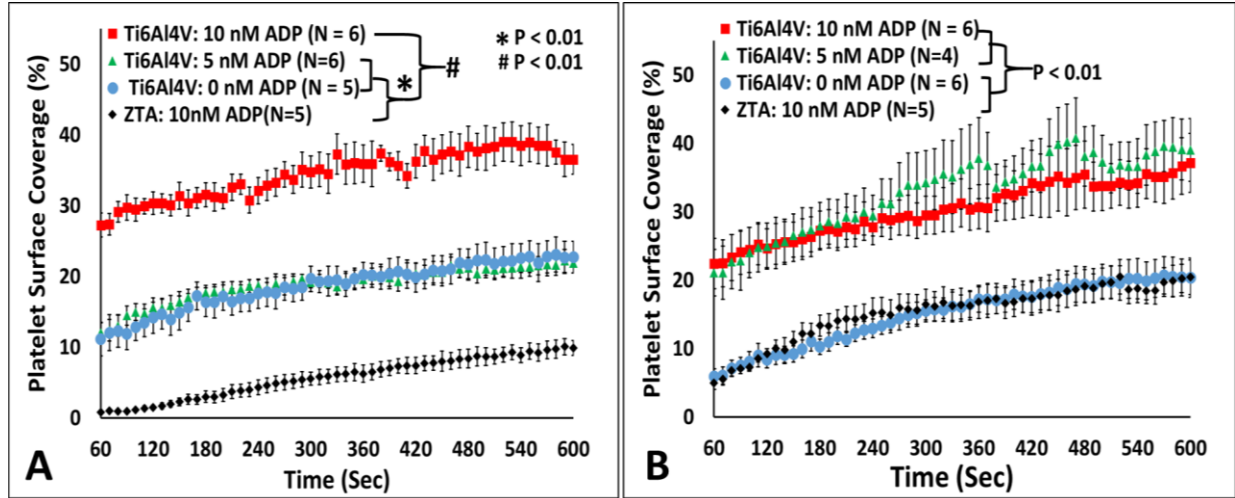


**Figure 27.** Percent of the test surface covered by deposited platelets. A) Wall shear rate  $400 \text{ sec}^{-1}$ . B) Wall shear rate  $1000 \text{ sec}^{-1}$ .

At a wall shear rate of  $1000 \text{ sec}^{-1}$  (**Figure 27B**) the Ti6Al4V: 5 nM and Ti6Al4V: 10 nM samples had significantly increased platelet deposition when compared to the control with  $39.0 \pm 4.6\%$ ,  $37.1 \pm 4.3\%$  and  $20.4 \pm 2.9\%$  of the surface covered after 10 min of perfusion respectively (N=6,  $P < 0.1$ ). There is no significant difference in the platelet deposition between the Ti6Al4V: 5 nM and Ti6Al4V: 10 nM samples. After 10 min of perfusion, the platelet deposition on ZTA: 10 nM was significantly less than the Ti6Al4V: 5 nM and Ti6Al4V: 10 nM samples at  $20.4 \pm 2.5$  (N=5,  $P < 0.01$ ). However, the thrombogenicity of ZTA was essentially equivalent to that of the control Ti6Al4V sample. When examining the effect of wall shear rate (**Figure 28**), platelet deposition increased with the increase in shear rate for the Ti6Al4V: 5 nM and ZTA: 10 nM samples ( $P < 0.01$ , **Figure 28B** and **28D** respectively). At both shear rates the platelet surface coverage significantly increased with time on all of the samples ( $P < 0.01$ ).

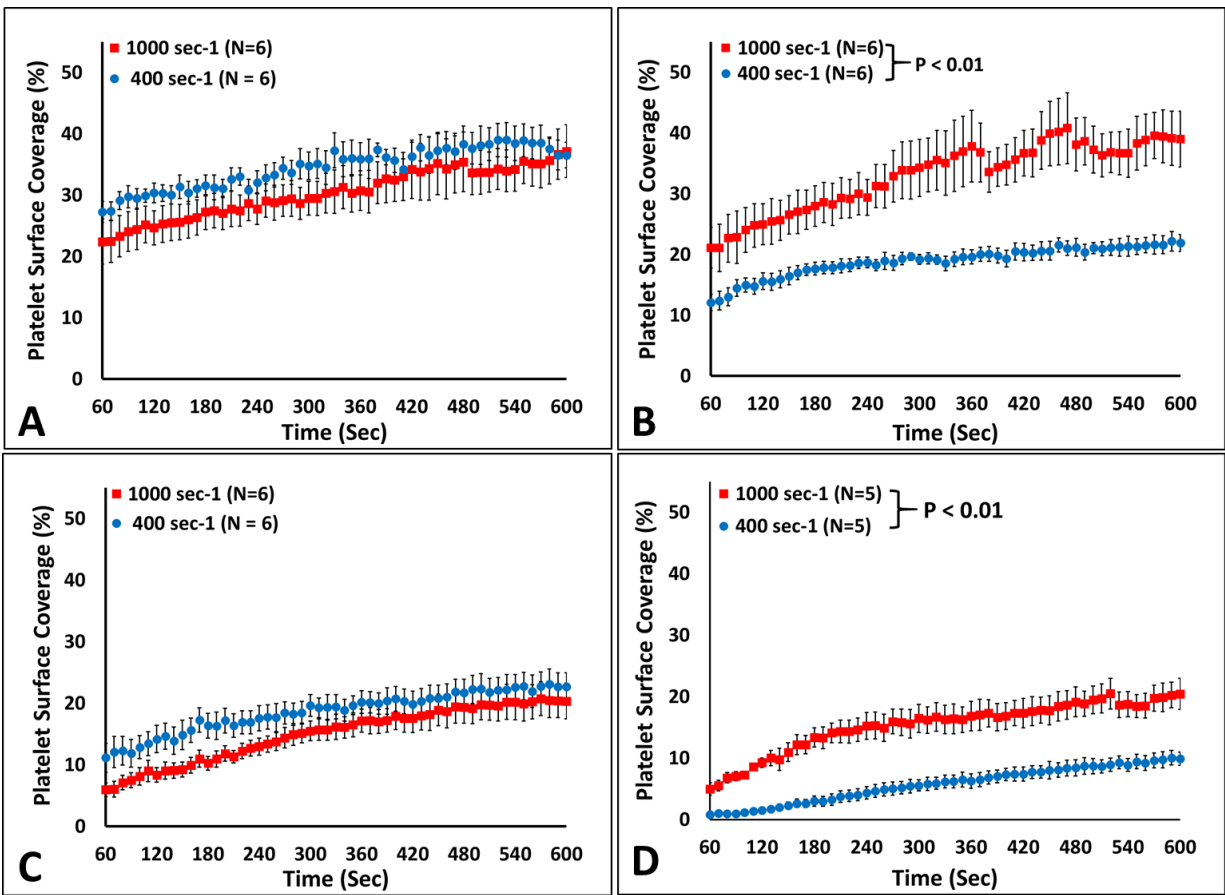


**Figure 28.** Effect of wall shear rate on the percent of the test surface covered by deposited platelets. A) Ti6Al4V: 10 nM ADP. B) Ti6Al4V: 5 nM ADP. C) Ti6Al4V: 0 nM ADP. D) ZTA: 10 nM ADP

The average area of individual thrombi adhered to the surface was also examined using the fluorescent images (**Figure 29**). At a wall shear rate of 400 sec<sup>-1</sup> (**Figure 29A**), there was no significant difference in thrombi size between the Ti6Al4V: 5 nM, Ti6Al4V: 0 nM, and ZTA: 10 nM samples with an average individual thrombi area of  $192 \pm 20$ ,  $146 \pm 7$ , and  $152 \pm 17 \mu\text{m}^2$  respectively. The largest thrombi were adhered to Ti6Al4V: 10 nM samples with an average area of  $328 \pm 51 \mu\text{m}^2$  at the end of the perfusion experiment ( $P = 0.01$ ).

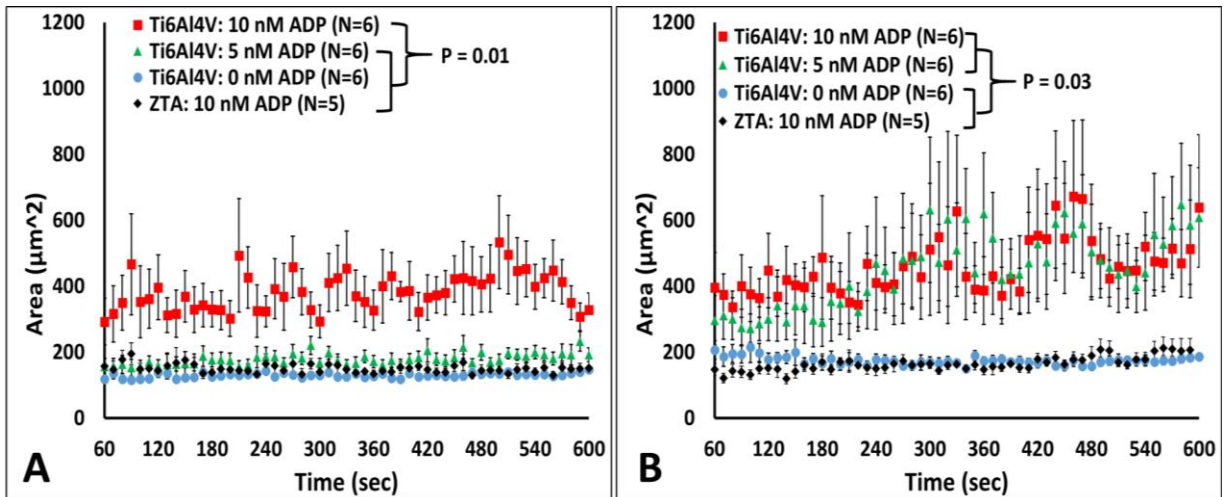


**Figure 29.** Average area of individual thrombi over time. A) Wall shear rate  $400 \text{ sec}^{-1}$ . B) Wall shear rate  $1000 \text{ sec}^{-1}$

At a shear rate of  $1000 \text{ sec}^{-1}$  (**Figure 29B**) the largest thrombi were found on the Ti6Al4V: 5 nM and Ti6Al4V: 10 nM samples with an average individual thrombi area of  $639 \pm 220$  and  $608 \pm 151 \mu\text{m}^2$  respectively. The thrombi generated on these samples were significantly larger than the Ti6Al4V: 0 nM and ZTA: 10 nM samples ( $P = 0.03$ ). The area of the thrombi on ZTA: 10 nM was not significantly different from the titanium control with an average individual thrombi area of  $152 \pm 17$  and  $186 \pm 10 \mu\text{m}^2$  after 10 min of perfusion. When comparing the effect of wall shear rate the average individual area of the adherent thrombi increased with the increase in shear rate for the Ti6Al4V samples (**Figure 30B**). However, the average area of thrombi on the other samples is not significantly affected by shear rate (**Figure 30**).

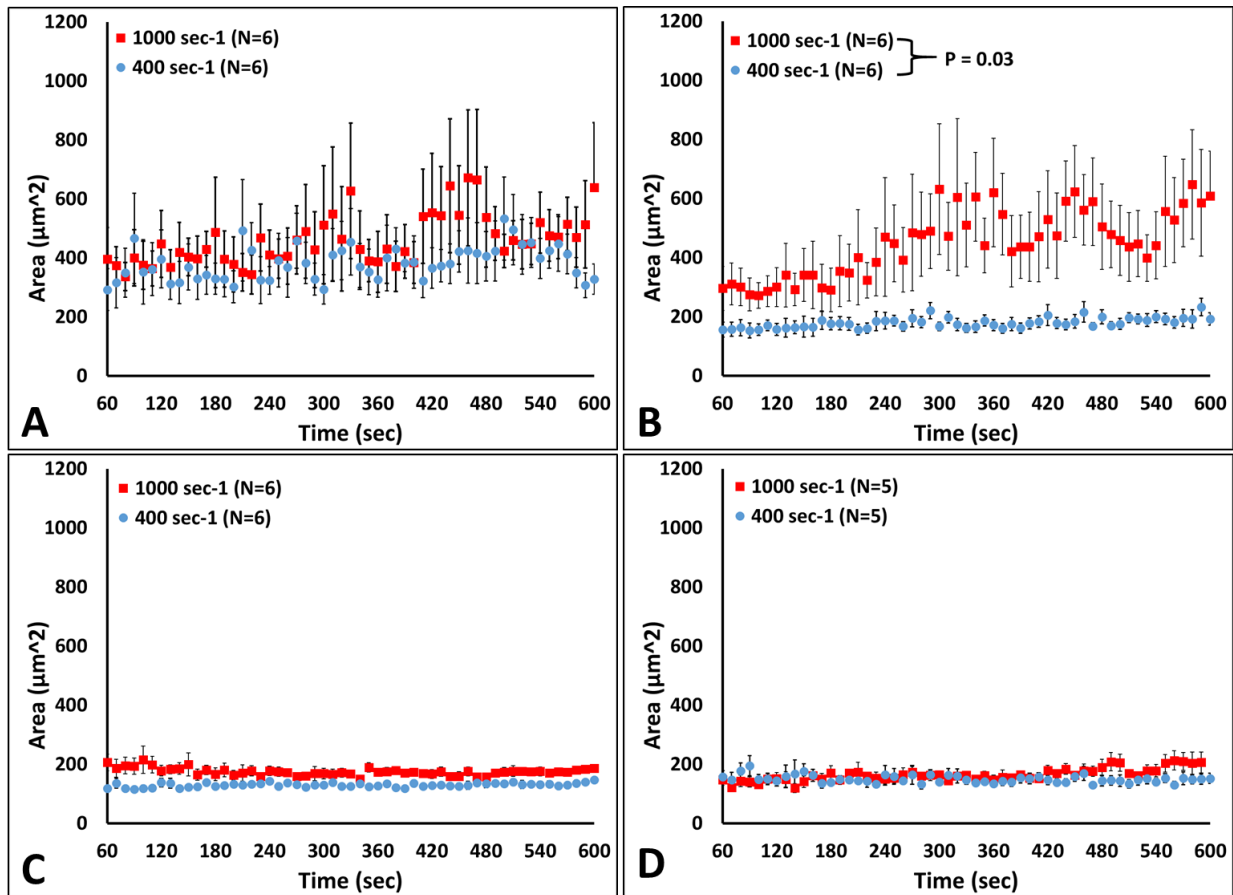


**Figure 30.** Effect of wall shear rate on average area of individual thrombi over time. A) Ti6Al4V: 10 nM ADP. B) Ti6Al4V: 5 nM ADP. C) Ti6Al4V: 0 nM ADP. D) ZTA: 10 nM ADP.

#### 4.3.2 Representative real-time perfusion videos

Representative real-time perfusion videos of platelet deposition at each experimental flow condition are available in the supplemental material of this report (**Videos 4.1-4.8**). At the lower wall shear rate the videos of the Ti6Al4V: 5 nM, Ti6Al4V: 0 nM, and ZTA: 10 nM looked similar with the thrombi growing in elliptical patterns, with the long axis aligned in the direction of flow (**Videos 4.1-4.3**). However, the ZTA: 10 nM video shows that few platelets adhere to the surface when compared to the other videos. Platelets rapidly adhered

to the Ti6Al4V:10nM surface, at both wall shear rates, and Ti6Al4V: 5nM surface, at the higher shear rate. The thrombi form in a more spherical pattern on these samples (**Video 4.4, 4.5** and **4.8**). Embolization of thrombi with a diameter of greater than 20  $\mu\text{m}$  was observed sporadically with the Ti6Al4V: 10 nM samples, at both shear rates, and Ti6Al4V: 5 nM samples the wall shear rate of 1000  $\text{sec}^{-1}$ . An example of these emboli is shown in **Figure 31** and **Figure 32**. This sporadic embolization may be why the standard error for these samples is more than 2 fold greater than the other surfaces. Examination of the length of the flow path following perfusion indicated that platelets reacted uniformly with the test materials and were not diffusion-limited by the rapid depletion of platelets onto the surface at the inlet of the chamber. [77]

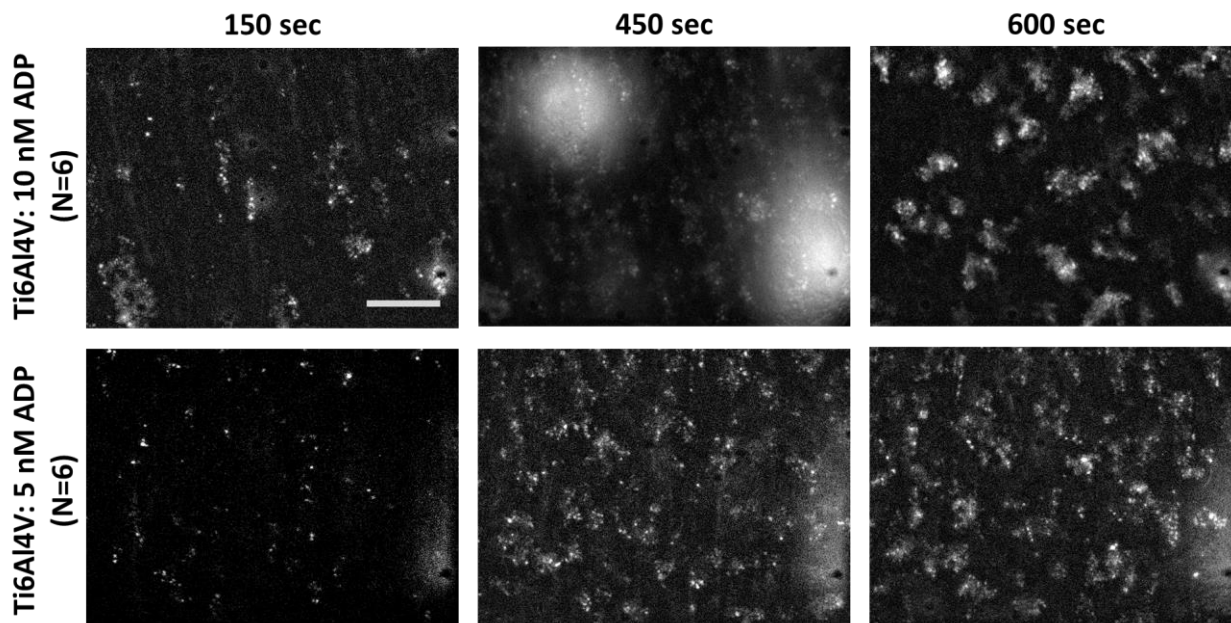


**Figure 31.** Representative fluorescent images of embolization at a wall shear rate of 400  $\text{sec}^{-1}$ . Embolization was only seen when 10 nM of ADP was added to the blood analog perfusing over the Ti6Al4V surface. Scale bar = 40  $\mu\text{m}$

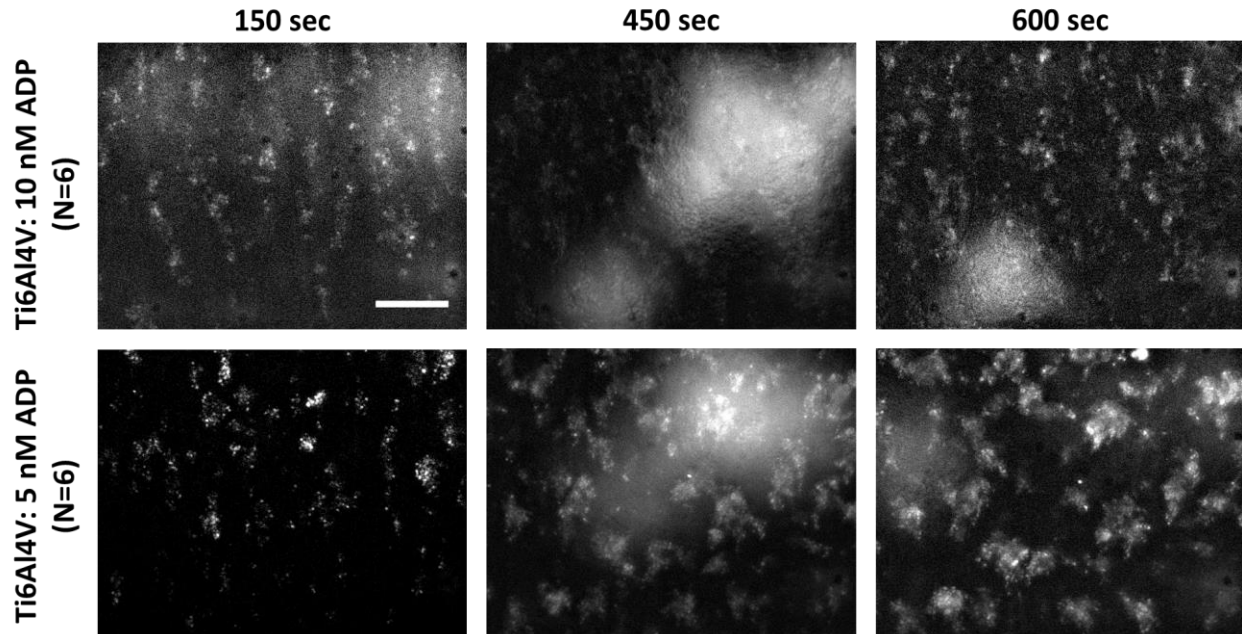


**Figure 32.** Representative fluorescent images of embolization at a wall shear rate of  $1000 \text{ sec}^{-1}$ . Embolization was seen when 5 nM or 10 nM of ADP was added to the blood analog perfusing over the Ti6Al4V surface. Scale bar =  $40 \mu\text{m}$ .

#### 4.4 DISCUSSION

The study described in this report is one of the few studies that examines all three factors that contribute to thrombus formation in blood-wetted devices as defined by Virchow's triad (material reactivity, blood composition, and blood flow). Specifically, this report describes a method for investigating the effect of ADP induced platelet aggregation prior to contact with clinically relevant VADs. VAD patients often experience several hematological events, such as hemolysis, that increase the concentration of ADP within the blood that could lead to increased thrombus formation within the devices.[39] Studies have shown that ADP released during hemolysis can increase platelet aggregation and adhesion. Alkhamis et al. investigated the

release of ADP, from whole blood, when it is subjected to a shear stress. The investigators utilized a cone and plate viscometer to produce laminar shear stress (0.7 uM-5uM of ADP).[138, 139] Numerical modeling studies have suggested that ADP released from already formed thrombi may contribute to platelet activation and downstream thrombi formation.[140-142] Although the experiments described in this report only utilize ADP to sensitize the platelets prior to material contact, it is still applicable to “pre-activation” of platelets with other agonist. Platelet activation may be initiated by a variety of agonists including, but not limited to, thrombin, serotonin, and thromboxane.[136, 143-145]

Furthermore, heart failure patients tend to be associated with a hypercoagulable state. Reduced myocardial contractility leads to low cardiac output and abnormal blood flow that can initiate coagulation. Patients with heart failure often have dysfunctional endothelium, which can no longer act as an anticoagulant barrier. Furthermore, VAD patients have elevated plasma levels of clotting factors, adhesion molecules, and growth factors, such as von Willebrand factor (vWf), P-selectin, and vascular endothelial growth factor.[58] Infection, which occurs at a rate of 9.96 events/ 100 patient months in the first 12 months post-implant, can elevate plasma levels of inflammatory cytokines, such as tumor necrosis factor alpha and interleukin-1 (IL-1), that are known to activate platelets.[1, 58]

Several studies have utilized platelet aggregometry to analyze the effect of biochemical agonists, such as ADP, on platelet aggregation.[135-137, 146] There are two main types of platelet aggregometry: impedance and light transmission. For impedance aggregometry, an agonist is added to an aliquot of whole blood and two electrodes are inserted into the sample. Platelet aggregation is measured by the increase in electrical impedances generated by platelets adhering to and aggregating on the electrodes. Light transmission aggregometry uses a

photometer to measure the light transmitted through a sample of PRP after the addition of a biochemical agonist. The light transmission through the sample increases as the sample aggregates due to the precipitation of platelet aggregates. In both methods, the blood is continuously mixed through stirring or shaking of the sample.[147] Aggregometry is a useful method for examining platelet aggregation. However, the blood is not exposed to flow conditions typically found in cardiac devices. Furthermore, this assay does not examine the effect of biomaterials on aggregation.

Few studies have examined the effect of biochemical agonist on platelet aggregation, under flow. Bell et al. examined ADP-induced platelet aggregation under flow in polyethylene tubes. They measured the quantity and size of platelet aggregates formed when 0.2 or 1  $\mu\text{M}$  of ADP was added to the blood. They found that an increase in ADP concentration caused an increase in the quantity and size of ADP.[148] A major limitation to their study is that the agonist was mixed rapidly with the blood by a magnetic stir prior to being perfused through the tubing. The flow conditions caused by the mixing, along with platelets interacting with the artificial surface of the stir bar, may have contributed to the formation of platelet aggregates. Also, they only investigated platelet aggregation and did not examine platelet adhesion to the surface of the tubing.[148]

Neeves et al. developed a membrane-based device that allowed for the introduction of ADP into flowing blood at three defined fluxes. The device consisted of a fibrinogen coated polycarbonate membrane that was reversibly sealed between two parallel plate flow chambers. One chamber contained the flowing blood and the other contained the agonist. Utilizing fluorescent microscopy, they examined the effect of introducing ADP.[149] Importantly, the study performed by Neeves et al. did not evaluate platelet deposition onto a biomaterial because

the membrane was coated in fibrinogen. This method could be used to examine platelet deposition onto a biomaterial. However, due the design of the device, platelet adhesion could only be examined on the membrane surface, limiting the utility of the technique. Specifically, the method could not be used to examine the metallic surface currently utilized in most implantable continuous flow VADs, Additionally, Neeves et al. only examined platelet aggregation at one wall shear rate ( $250 \text{ sec}^{-1}$ ). Expectantly, they found that the increase in ADP flux resulted in an increase in platelet aggregation.[149]

The most significant result of these studies was the discovery of the synergistic amplification of biochemical agonists by shear. This is illustrated in **Figure 27**. This figure shows that at a wall shear rate  $400 \text{ sec}^{-1}$  the addition of 5 nM ADP did not significantly increase platelet deposition. However increasing the wall shear rate to  $1000 \text{ sec}^{-1}$  resulted in nearly a 2.5 fold increase in deposition on the titanium surface. Furthermore, the real-time fluorescent videos showed that this same dilute quantity of ADP increased the frequency of embolization, as well as the size of the emboli. This is particularly interesting because numerical modeling studies have suggested that local concentrations of ADP downstream of where the agonist was introduced would be lower at a higher wall shear rate.[140-142] This would suggest that platelets perfused at  $400 \text{ sec}^{-1}$  would be exposed to a higher local concentration of ADP at the surface of the titanium compared to the higher shear rate and, therefore, would be more likely to aggregate and adhere to the surface.

One explanation for this discontinuity may be that the local ADP concentration at the surface of the titanium is great enough when combined with the reactivity of the surface to cause platelet aggregation and adhesion at both wall shear rates. Therefore, the increase in platelet deposition at the higher shear rate may be due to the increased transportation of platelets to the

Ti6Al4V surface. Also, 5 nM is 300 times lower than the threshold value measured by aggregometry.[135-137] Thus, any platelets aggregated initially by the addition of this concentration are likely to be reversibly aggregated. At a wall shear rate of  $400 \text{ sec}^{-1}$ , the platelets may return to their resting state prior to contact with the titanium. While at  $1000 \text{ sec}^{-1}$ , the platelets may not have time to return to resting state before they are further activated by contact with the artificial surface.

The addition of 10 nM of ADP did not cause any embolization. Furthermore, even at  $1000 \text{ sec}^{-1}$  platelet deposition on the ZTA: 10 nM sample was not significantly different than the control (Ti6Al4V: 0 nM). This suggests that this synergistic effect of shear and agonist can be negated through the utilization of a less thrombogenic material.

Several mathematical and computer models have been developed to try to predict platelet deposition and thrombus formation with simple flow paths.[72, 78, 133] Some models, such as the ones described in Sorensen et al. and Goodman et al. have incorporated biochemical agonists into their analysis.[72, 78] However, these models require the agonist to be at critical level to affect platelet activation and do not consider the combined effect of material contact and agonist exposure. The study described in this report illustrated that a sub-critical level of ADP, in conjunction with flow and material contact, can cause a significant increase in platelet deposition. The data generated from this analysis could be used to improve the utility and accuracy to these and other predictive models of thrombosis.

## 4.5 LIMITATIONS

A major limitation to this report is the acute nature of the study. The test materials are only exposed to the blood for 10 min. However, the real-time visualization method employed provides the ability to investigate thrombus formation and embolization caused by the addition of a sub-threshold agonist. Another limitation is the emboli witnessed during this study are not hazardous due to their small size. However, these emboli could continue to grow downstream to a dangerous size. Wilhelm et al. utilized transcranial Doppler ultrasound to measure microembolic signals in VAD patients before, during, and after implantation. They also analyzed the patients' coagulation state during this time. They found that patients who experienced microembolic showering had increased levels of prothrombin fragment F1.2. These data suggesting that microembolic showering is an indicator of increased coagulation activity that could result in a detrimental thromboembolic event.

## 4.6 CONCLUSIONS

The employed method provides a viable means for qualifying the functional effect of biochemical agonist, blood flow, and biomaterials on platelet deposition. This report found that the addition of a sub-threshold level of ADP resulted in a 2.5 fold increase in increase thrombus formation on Ti6Al4V. Furthermore, increasing the wall shear rate from 400 to 1000  $\text{sec}^{-1}$  significantly increased the effect of adding 5 nM of ADP. This indicates a synergistic

amplification of biochemical agonists by shear. It was also found that the thrombogenicity of the system could be significantly reduced by replacing Ti6Al4V with a ZTA. This suggests that utilizing ZTA as the blood contacting surface of VADs may help to improve the overall hemocompatibility of the device. Finally, the data generated could be utilized to validate and calibrate predictive models of device thrombosis.

## **5.0 CONTINUED RESEARCH AND FUTURE DIRECTIONS**

The studies presented in the previous section add to the scientific knowledge of thrombosis development in blood-wetted devices. The techniques described in these studies enable additional research to be performed in this area that will continue to advance the field. The following research opportunities outside of the objectives of this dissertation are possible due to the results of the work contained in this report.

### **5.1 SYNERGISTIC EFFECT OF BIOCHEMICAL AGONIST ON PLATELET DEPOSITION ONTO CLINICALY RELEVANT MATERIALS**

The results generated from the study described in Chapter 4.0 of this report show that there is a synergistic effect between ADP, material contact, and shear. Aggregometry studies have also shown that sub-threshold levels of ADP work synergistically with other agonists and proteins to promote platelet aggregation.[135, 136, 150] However, few studies have investigated the effect of multiple agonists, as sub-threshold concentrations, on platelet adhesion onto biochemical agonist, under flow. The biochemical agonist delivery system described in chapter 4.2.2 could be modified to infuse multiple agonists simultaneously and used to study wider variety of combinations of agonists, shear, and surface chemistry. Periodic collection of the effluent and subsequent analysis with flow cytometry may aid in the mapping of the emboli composition. As

described previously, Bell et al examined ADP-induced platelet aggregation under flow in polyethylene tubes. They employed an electronic particle counter to quantify the number and size of single platelets and aggregates.[148] This technique could be incorporated into this study to provide further information on the dynamics of platelet embolization.

As discussed in section 1.3.3 the different anticoagulant and anti-platelet medications inhibit platelet aggregation and thrombus formation through a variety of different pathways.[61-69] Therefore, the technique described in section 4.2 could also be employed to investigate how commonly utilized anticoagulation and anti-platelet medications affect agonists-induced thrombus formation. The data generated from the proposed study could be used to incorporate the effect of anticoagulation therapies into a model of device thrombosis, increasing its utility.

## **5.2 CHARACTERIZING THE EFFECT OF GEOMETRIC IRREGULARITIES ON PLATELET DEPOSITION ONTO CLINICALLY RELEVANT SURFACES**

### **5.2.1 Investigating the effect of crevice size and geometry**

As discussed in Chapter 3.0, geometric irregularities within the flow path of continuous flow VADs serve as a nidus for thrombus formation.[49] A rectangular crevice was chosen because the flow patterns generated within it is well characterized and this geometry is readily amenable to computational modeling.[134] However, the majority of these features are the unintended consequence of merging multiple components. The resulting crevices are probably a variety of irregular geometries. The study described in Chapter 3.0 could be expanded to include numerous geometries (i.e. triangular or semicircular crevices). Several of the studies that have examined

the effect of steps on platelet deposition incorporated sharp corners into their features.[50, 55, 130, 131] Rounding the corners of these regions produce a less rapid change of the contours of the flow path. This should reduce the erratic flow patterns generated by this change and may reduce thrombogenicity of that feature. The effect of the slope of the corner can also be investigated in the proposed study. These suggested experiments could help determine particularly thrombogenic geometries.

The majority of VAD manufacturers try to limit the size of the steps and crevices within the blood flow path by precision polishing and machining. Intuitively, the sizes of the generated crevices would be on the micron scale ( $< 50 \mu\text{m}$ ). Furthermore, if a non-fixed VAD impeller collided with the housing surface it would likely create a microscopic scratch.[123] A limitation to the study described in Chapter 3.0 was that the smallest crevice sized evaluated was around  $50 \mu\text{m}$ . Limitations on the size range evaluated were the tolerance of the photo-etching technique employed and the field of view associated with the optical system. However, the development of new technologies such as 3D nano-printers may make such an analysis possible. Investigating  $< 50 \mu\text{m}$  sized crevices will generate additional data that could be used to determine the tolerable limits of these geometric irregularities.

### **5.2.2 Pulsatile flow**

As discussed in Chapter 1, continuous flow VADs have improved mechanical durability, are smaller and have decreased power requirements compared to pulsatile VADS.[10] However, continuous flow VADS significantly decreased the pulsatile flow in the vascular system. Studies have shown that some patients supported by continuous flow VADs have experienced adverse cardiac events, such as aortic insufficiency, right heart failure, and gastrointestinal bleeding,

which were not witnessed in patients supported by pulsatile VADs.[151-153] Some research groups are attempting to develop a method to modulate the speed of continuous flow VADs to mimic pulsatile flow and potentially reduce these adverse effects.[151, 152].

Currently there is a debate among scientific members of the VAD community on the effect of pulsatility on thrombus formation in continuous flow VADs. Some studies suggest that increasing the pulsatility of continuous flow VADs will allow the aortic valve to frequently open and provide regular washing of the pump.[152] Yang et al. performed a high-speed visualization of the flow patterns within the HeartMate II at steady and pulsatile flow conditions. They found that pulsatile flow induced a periodic disturbance within the device that created flow patterns known to contribute to thrombus formation.[57] These findings are supported by a recent report noting an increase in pump thrombosis when operating the pump at a lower speed during the weaning phase of a ventricular recovery study.[154] Incorporating pulsatile flow into the study described in Chapter 3.0 would provide a method for visualizing the effect of pulsatile flow on platelet deposition within a defined crevice. The proposed study could potentially determine if pulsatility improves washing within the crevice or contributes to the potentially hazardous flow patterns.

### **5.3 COMPARATIVE ANALYSIS OF HUMAN, BOVINE AND OVINE BLOOD**

The use of animal models to evaluate the biocompatibility of cardiovascular devices is an essential part of device development and must be conducted to ensure safety before a clinical trial can begin. However, the coagulation systems vary between different species.[96, 155-157] Few studies have performed a comparative analysis of species specific platelet activation and

thrombus formation. Baker et al. and Johnson et al. developed flow cytometry assays to investigate platelet activation and aggregation using bovine and ovine blood respectively, however they did not investigate platelet adhesion.[96, 157]

Palagalli et al. investigated species specific (buffalos, horses, pig, sheep, and human) platelet adhesion onto fibrinogen *in vitro*. They found that horse platelets were most likely to adhere to the fibrinogen, whereas sheep (ovine) platelets were unable to adhere to autologous fibrinogen unless activated with ADP.[156] Goodman et al. compared how human, ovine, and porcine platelets adhered to biomaterials *in vitro*. The biomaterials investigated in that study were pyrolytic carbon mechanical heart valve leaflets, National Institutes of Health-reference polyethylene and silicone rubber, and Formvar<sup>TM</sup>. The study found that platelet responses were strongly dependent on biomaterial and species. For example, both human and porcine blood spread extensively on pyrolytic carbon, while human platelets spread extensively on polyethylene but porcine platelets did not.[155] Although these studies offer a comparative analysis of species specific platelet adhesion, both studies were performed under stagnant conditions. Furthermore, they did not utilize whole blood or PRP. Instead the platelets were isolated from the blood through centrifugation and filtering. This process could have affected platelet function before blood contact with the test surface.

The method described in Chapter 2.0-3.0 could be utilized to perform comparative analysis of the effect of blood donor species on platelet deposition under flow. Therefore, using these techniques as a method for comparing different animal models would be a useful tool in selecting the appropriate model based on the blood contacting material and blood flow patterns.

## 5.4 IN VIVO VALIDATION OF IN VITRO VISUALIZATION AND ANALYSIS OF BIOMATERIAL-CENTERED THROMBUS FORMATION WITHIN A DEFINED CREVICE

### 5.4.1 Visualization of platelet adhesion

The *in vitro* method employed in Chapter 3 of this report provides a viable means for quantifying the effect of common geometric irregularities found in cardiovascular devices on platelet deposition. However, due to its acute nature the results would need to be validated *in vivo* to prove the clinical significance of the study. This *in vivo* analysis could be achieved through the modifications of the visualization technique described by Wagner et al. and Schaub et al. (**Figure 33**).[8, 43] They developed a fiber optic remote microscope to visualize and quantify platelet deposition onto an opaque surface, in a continuous manner. They also modified a polycarbonate centrifugal blood pump to include septums at the top and bottom to allow the fiber optic camera to be inserted into the blood flow path so that platelet deposition could be visualized.[8, 43] A similar pump could be designed to introduce a crevice of defined dimensions into the blood flow path. This device could then be implanted into a bovine animal model using percutaneous inlet and outlet cannula so that the pump remains visible similar to that of the CentriMag (Thoratec Corp, Pleasanton, CA, USA) continuous flow VAD. The thrombus formation within a crevice could then be visualized by the fiber optic remote microscope and the results could be compared to the *in vitro* analysis.

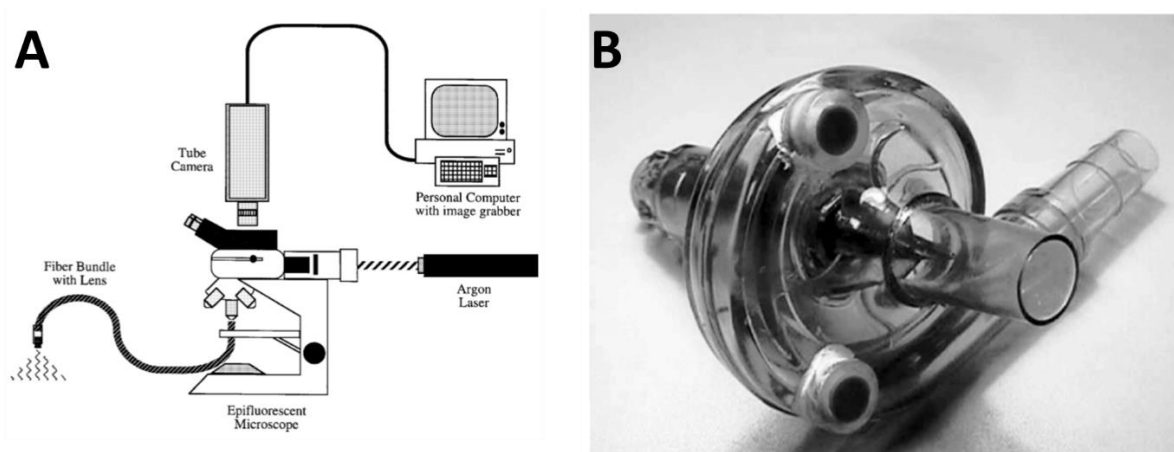


**Figure 33.** Method for *in vivo* visualization. A) Fiber optic remote microscope. B) Modified a polycarbonate centrifugal blood pump. From Wagner et al.[8]

#### 5.4.2 Hematological analysis of test subject's blood

It is difficult to diagnosis pump thrombosis and it is usually characterized by a pattern of clinical symptoms, laboratory findings, echocardiograph data, and device settings.[65] An increased serum lactate dehydrogenase (LDH) level, is often the associated with late stage pump thrombosis, however there are few markers for early stage pump thrombosis. Furthermore, most continuous flow VADs are composed of opaque materials, making it impossible to visually detect pump thrombosis.[65, 158, 159] In order to investigate potential markers for early pump thrombosis, periodic samples could be taken from the pump described in the previous section and analyzed for coagulation markers (i.e thrombin and LDH). Since thrombus formation might be visually monitored via the fiber optic microscope, specific samples could be taken at the initiation of thrombosis and when the thrombosis grows to a potential hazardous size. The data generated could potentially identify biological markers that are associated with early development of pump thrombosis.

## 6.0 FINAL CONCLUSIONS

VADs have become an established treatment option for patients with advanced heart failure. The first generation of VADs were pulsatile, positive displacement pumps that were designed to mimic the biphasic flow of the native heart. They were utilized as a bridge to transplant for heart failure patients waiting for a donor organ.[19] Due to their large size, first generation pumps could only be used in a limited patient population. Additionally, the durability of these devices was limited. In order to produce pulsatile flow, pumps were complex with multiple moving parts.[12, 19, 160, 161] The introduction of continuous flow blood pumps decreased the size and power requirements and increased the mechanical life of VADs. This allowed pump utilization in a broader patient population. However, these devices are still plagued by thrombosis. The incidence of thrombosis, bleeding, and neurologic dysfunction experienced by patients supported by continuous flow VADs continues to limit the cost-effectiveness and clinical acceptance of the technology.[1, 2, 11, 12]

The creation of a computational model to predict thrombosis would reduce the time and cost of designing and producing safe, effective blood-wetted devices. Such a model could be used to determine prothrombogenic areas of devices prior to implantation. While several mathematical models have been developed to predict platelet activation and adhesion, there is still no computational model that can predict thrombosis in an actual device with any mathematical certainty.[70-75] The data generated from the studies described in this report could be used to improve the accuracy and advance the utility of such a predictive model.

The method described in Chapter 2.0 provides a method for side-by-side biomaterial analysis. This is a useful tool for the selection and design of materials for use as a blood contacting surface. The results from this study show a reduction in platelet deposition at elevated wall shear rate. This suggests that the blood biocompatibility of VADs might be improved by minimizing the areas of low shear blood contact. Furthermore, this technique revealed that MPC-TI6AL4V and ZTA have improved thromboresistance when compared to Ti6Al4V and, thus, may be alternatives for consideration in future VAD designs.

The method employed in Chapter 3.0 provides a viable means for quantifying the effect of common geometric irregularities found in cardiovascular devices on platelet deposition. Interestingly, the least amount of deposition occurred in the largest crevice size. At the higher shear rate, the most deposition occurred in the 90  $\mu\text{m}$  crevice (medium size crevice). This suggests that the crevice size might be tailored, depending on the flow condition, to reduce the risk of thromboembolic events. As described in the future directions section of this report, this study could be advanced to incorporate more clinically relevant crevice sizes and shapes, thus generating additional data that could be used to determine the tolerable limits of these geometric irregularities. The *in vivo* study described in the future directions section could be used to validate this *in vitro* study, thus improving its clinical significance.

The method described in Chapter 2.0-3.0 could be utilized to perform comparative analysis of the effect of blood donor species on platelet deposition under clinically relevant flow conditions. Studies have shown that platelet adhesion is dependent on both species and material.[27] Therefore, using these techniques as a method for comparing different animal models would be a useful tool in selecting the appropriate model based on the blood contacting material and blood flow patterns. This is clinically relevant because an improved *in vivo* animal model would result in a more accurate assessment of the biocompatibility of a blood wetted device under investigation. Therefore, it would be less likely that an unexpected adverse event would occur when the device is implanted in patients.

According to Virchow's triad, there are three factors that contribute to thrombosis in blood wetted devices: the composition of the blood, the blood flow, and biomaterial contact. [37, 38] Although the triad was developed in 1856, the functional relationship of all three factors is not well characterized. The study described in Chapter 4 incorporated all aspects of the triad into

the analysis. It was found that shear and ADP work synergistically to increase platelet aggregation and deposition. This was indicated by the nearly 2.5 fold increase in platelet deposition with the addition of a sub-threshold level of ADP. It was also found that this synergistic effect could be negated through the utilization of a less thrombogenic material.

Currently there is no accurate way of detecting the early stages of pump thrombosis. Furthermore, it is impossible to visually detect pump thrombosis in most continuous flow VADs because the pump housings are made of opaque materials.[7, 33, 34] In order to investigate potential markers for early pump thrombosis, periodic samples could be taken from the pump described in the future directions section of this report and analyzed for coagulation markers (i.e. thrombin and LDH). The thrombus formation could be visually monitored via the fiber optic microscope, therefore it could be known if a thrombus has formed in the pump at the time the sample is collected. The data generated could potentially identify biological markers that are associated with early development of pump thrombosis.

Although there are still many aspects of pump thrombosis that are unknown, from the results of this report, I hypothesize that the blood biocompatibility of VADs can be improved by coating the Ti6Al4V surface with MPC. This would allow the manufacturers to continue to utilize the easily machined titanium alloy, while improving the blood compatibility of their device. Furthermore, future VADs might have fewer regions of potentially hazardous flow conditions by intentionally producing larger crevices in the areas where multiple materials are combined. Incorporating more favorable crevice geometries and sizes into the VAD design could improve the overall blood biocompatibility of the device.

## APPENDIX A

### REPRESENTATIVE REAL-TIME PERFUSION VIDEOS

As previously mentioned, representative real-time perfusion videos of platelet deposition are available in the supplemental material of this report. Below are the descriptions that accompany those videos.

#### A.1 REAL TIME VISUALIZATION AND CHARACTERIZATION OF PLATELET DEPOSITION UNDER FLOW ONTO CLINICALLY RELEVANT OPAQUE SURFACES

**Video 2.1:** Representative real-time perfusion video of platelets adhering to Ti6Al4V, at a wall shear rate of  $400 \text{ sec}^{-1}$ . The video speed was increased by a factor of 9. Flow is up. Scale bar =  $20 \mu\text{m}$ .

**Video 2.2:** Representative real-time perfusion video of platelets adhering to SiC, at a wall shear rate of  $400 \text{ sec}^{-1}$ . The video speed was increased by a factor of 9. Flow is up. Scale bar =  $20 \mu\text{m}$ .

**Video 2.3:** Representative real-time perfusion video of platelets adhering to  $\text{Al}_2\text{O}_3$ , at a wall shear rate of  $400 \text{ sec}^{-1}$ . The video speed was increased by a factor of 9. Flow is up. Scale bar =  $20 \mu\text{m}$ .

**Video 2.4:** Representative real-time perfusion video of platelets adhering to YZTP, at a wall shear rate of  $400 \text{ sec}^{-1}$ . The video speed was increased by a factor of 9. Flow is up. Scale bar =  $20 \mu\text{m}$ .

**Video 2.5:** Representative real-time perfusion video of platelets adhering to ZTA, at a wall shear rate of  $400 \text{ sec}^{-1}$ . The video speed was increased by a factor of 9. Flow is up. Scale bar =  $20 \mu\text{m}$ .

**Video 2.6:** Representative real-time perfusion video of platelets adhering to MPC-Ti6Al4V, at a wall shear rate of  $400 \text{ sec}^{-1}$ . The video speed was increased by a factor of 9. Flow is up. Scale bar =  $20 \mu\text{m}$ .

**Video 2.7:** Representative real-time perfusion video of platelets adhering to Ti6Al4V, at a wall shear rate of  $1000 \text{ sec}^{-1}$ . The video speed was increased by a factor of 9. Flow is up. Scale bar =  $20 \mu\text{m}$ .

**Video 2.8:** Representative real-time perfusion video of platelets adhering to SiC, at a wall shear rate of  $1000 \text{ sec}^{-1}$ . The video speed was increased by a factor of 9. Flow is up. Scale bar =  $20 \mu\text{m}$ .

**Video 2.9:** Representative real-time perfusion video of platelets adhering to  $\text{Al}_2\text{O}_3$ , at a wall shear rate of  $1000 \text{ sec}^{-1}$ . The video speed was increased by a factor of 9. Flow is up. Scale bar =  $20 \mu\text{m}$ .

**Video 2.10:** Representative real-time perfusion video of platelets adhering to YZTP, at a wall shear rate of  $1000 \text{ sec}^{-1}$ . The video speed was increased by a factor of 9. Flow is up. Scale bar =  $20 \mu\text{m}$ .

**Video 2.11:** Representative real-time perfusion video of platelets adhering to ZTA, at a wall shear rate of  $1000 \text{ sec}^{-1}$ . The video speed was increased by a factor of 9. Flow is up. Scale bar =  $20 \mu\text{m}$ .

**Video 12:** Representative real-time perfusion video of platelets adhering to MPC-Ti6Al4V, at a wall shear rate of  $1000 \text{ sec}^{-1}$ . The video speed was increased by a factor of 9. Flow is up. Scale bar =  $20 \mu\text{m}$ .

## **A.2 VISUALIZATION AND ANALYSIS OF BIOMATERIAL-CENTERED THROMBUS FORMATION WITHIN A DEFINED CREVICE UNDER FLOW**

**Video 3.1:** Representative real-time perfusion video of platelets depositing onto Ti6Al4V, within the  $53 \mu\text{m}$  crevice, at a wall shear rate of  $400 \text{ sec}^{-1}$ . The video speed was increased by a factor of 18. Flow is down. Scale bar =  $40 \mu\text{m}$ .

**Video 3.2:** Representative real-time perfusion video of platelets depositing onto Ti6Al4V, within the  $90 \mu\text{m}$  crevice, at a wall shear rate of  $400 \text{ sec}^{-1}$ . The video speed was increased by a factor of 18. Flow is down. Scale bar =  $40 \mu\text{m}$ .

**Video 3.3:** Representative real-time perfusion video of platelets depositing onto Ti6Al4V, within the  $53 \mu\text{m}$  crevice, at a wall shear rate of  $1000 \text{ sec}^{-1}$ . The video speed was increased by a factor of 18. Flow is down. Scale bar =  $40 \mu\text{m}$ .

**Video 3.4:** Representative real-time perfusion video of platelets depositing onto Ti6Al4V, within the 90  $\mu\text{m}$  crevice, at a wall shear rate of  $1000 \text{ sec}^{-1}$ . The video speed was increased by a factor of 18. Flow is down. Scale bar = 40  $\mu\text{m}$ .

**Video 3.5:** Representative real-time perfusion video of platelets depositing onto Ti6Al4V, within the 137  $\mu\text{m}$  crevice, at a wall shear rate of  $1000 \text{ sec}^{-1}$ . The video speed was increased by a factor of 18. Flow is down. Scale bar = 40  $\mu\text{m}$ .

**Video 3.6:** Representative real-time perfusion video of platelets depositing onto MPC-Ti6Al4V, within the 90  $\mu\text{m}$  crevice, at a wall shear rate of  $1000 \text{ sec}^{-1}$ . The video speed was increased by a factor of 18. Flow is down. Scale bar = 40  $\mu\text{m}$ .

**Video 3.7:** Representative real-time perfusion video of platelets depositing onto Collagen, within the 90  $\mu\text{m}$  crevice, at a wall shear rate of  $1000 \text{ sec}^{-1}$ . The video speed was increased by a factor of 18. Flow is down. Scale bar = 40  $\mu\text{m}$ .

### A.3 CHARACTERIZING THE EFFECT OF SUB-THRESHOLD

#### CONCENTRATIONS OF ADP ON PLATELET DEPOSITION ONTO CLINICALLY RELEVANT OPAQUE MATERIALS

**Video 4.1:** Example of diffusion through the membrane-based biochemical agonist delivery system. Colored water is pushed through the membrane into a PVC tube containing flowing, unaltered water.

**Video 4.2:** Representative real-time perfusion video of platelets depositing onto Ti6Al4V, after the addition of 5 nM of ADP, at a wall shear rate of  $400 \text{ sec}^{-1}$ . The video speed was increased by a factor of 18. Flow is down. Scale bar = 40  $\mu\text{m}$ .

**Video 4.3:** Representative real-time perfusion video of platelets depositing onto Ti6Al4V, after the addition of 0 nM of ADP, at a wall shear rate of  $400 \text{ sec}^{-1}$ . The video speed was increased by a factor of 18. Flow is down. Scale bar = 40  $\mu\text{m}$ .

**Video 4.4:** Representative real-time perfusion video of platelets depositing onto ZTA, after the addition of 10 nM of AD, at a wall shear rate of  $400 \text{ sec}^{-1}$ . The video speed was increased by a factor of 18. Flow is down. Scale bar = 40  $\mu\text{m}$ .

**Video 4.5:** Representative real-time perfusion video of platelets depositing onto Ti6Al4V, after the addition of 10 nM of ADP, at a wall shear rate of  $400 \text{ sec}^{-1}$ . The video speed was increased by a factor of 18. Flow is down. Scale bar = 40  $\mu\text{m}$ .

**Video 4.6:** Representative real-time perfusion video of platelets depositing onto Ti6Al4V, after the addition of 5 nM of ADP, at a wall shear rate of 1000 sec<sup>-1</sup>. The video speed was increased by a factor of 18. Flow is down. Scale bar = 40 μm.

**Video 4.7:** Representative real-time perfusion video of platelets depositing onto Ti6Al4V, after the addition of 0 nM of ADP, at a wall shear rate of 1000 sec<sup>-1</sup>. The video speed was increased by a factor of 18. Flow is down. Scale bar = 40 μm.

**Video 4.8:** Representative real-time perfusion video of platelets depositing onto ZTA, after the addition of 10 nM of ADP, at a wall shear rate of 1000 sec<sup>-1</sup>. The video speed was increased by a factor of 18. Flow is down. Scale bar = 40 μm.

**Video 4.9:** Representative real-time perfusion video of platelets depositing onto Ti6Al4V, after the addition of 10 nM, of ADP, at a wall shear rate of 1000 sec<sup>-1</sup>. The video speed was increased by a factor of 18. Flow is down. Scale bar = 40 μm.

## BIBLIOGRAPHY

1. Kirklin, J.K., et al., *Sixth INTERMACS annual report: a 10,000-patient database*. J Heart Lung Transplant, 2014. **33**(6): p. 555-64.
2. Eckman, P.M. and R. John, *Bleeding and Thrombosis in Patients With Continuous-Flow Ventricular Assist Devices*. Circulation, 2012. **125**(24): p. 3038-3047.
3. Adzic, A., S.R. Patel, and S. Maybaum, *Impact of Adverse Events on Ventricular Assist Device Outcomes*. Curr Heart Fail Rep, 2013. **10**(1): p. 89-100.
4. Slaughter, M.S., *Hematologic effects of continuous flow left ventricular assist devices*. J Cardiovasc Transl Res, 2010. **3**(6): p. 618-24.
5. Bluestein, D., K.B. Chandran, and K.B. Manning, *Towards Non-thrombogenic Performance of Blood Recirculating Devices*. Ann Biomed Eng, 2010. **38**(3): p. 1236-1256.
6. Li, S. and J.J. Henry, *Nonthrombogenic approaches to cardiovascular bioengineering*. Annu Rev Biomed Eng, 2011. **13**: p. 451-75.
7. Stevenson, L.W., *Crisis Awaiting Heart Transplantation: Sinking the Lifeboat*. JAMA Intern Med, 2015. **175**(8): p. 1406-9.
8. Wagner, W.R., et al., *Blood biocompatibility analysis in the setting of ventricular assist devices*. J Biomater Sci Polym Ed, 2000. **11**(11): p. 1239-59.
9. Puehler, T., et al., *Mechanical circulatory support devices as destination therapy-current evidence*. Ann Cardiothorac Surg, 2014. **3**(5): p. 513-24.
10. Shreenivas, S.S., J.E. Rame, and M. Jessup, *Mechanical circulatory support as a bridge to transplant or for destination therapy*. Curr Heart Fail Rep, 2010. **7**(4): p. 159-66.
11. de Mel, A., B.G. Cousins, and A.M. Seifalian, *Surface modification of biomaterials: a quest for blood compatibility*. Int J Biomater, 2012. **2012**: p. 707863.
12. Iii, J.R.F. and Y.J. Woo, *Mechanical circulatory assistance*. Circ J, 2011. **75**(1): p. 38-46.

13. Kirklin, J.K., et al., *Fifth INTERMACS annual report: risk factor analysis from more than 6,000 mechanical circulatory support patients*. J Heart Lung Transplant, 2013. **32**(2): p. 141-56.
14. Kirklin, J.K., et al., *INTERMACS database for durable devices for circulatory support: first annual report*. J Heart Lung Transplant, 2008. **27**(10): p. 1065-72.
15. INTERMACS, *Manual of Operations and Procedures, Version 4.0*. Available at <https://www.uab.edu/medicine/intermacs/mop-4-0>, 2014.
16. Friedrich, E.B. and M. Bohm, *Management of end stage heart failure*. Heart, 2007. **93**(5): p. 626-31.
17. Cheng, A., M.F. Swartz, and H.T. Massey, *VADoscopy: a novel intraoperative technique to evaluate HeartMate II left ventricular assist device inflow obstruction and thrombosis*. ASAIO J, 2013. **59**(6): p. 671-4.
18. Topkara, V.K., et al., *HeartWare and HeartMate II left ventricular assist devices as bridge to transplantation: a comparative analysis*. Ann Thorac Surg, 2014. **97**(2): p. 506-12.
19. Stewart, G.C. and M.M. Givertz, *Mechanical circulatory support for advanced heart failure: patients and technology in evolution*. Circulation, 2012. **125**(10): p. 1304-15.
20. Miller, L.W., et al., *Use of a Continuous-Flow Device in Patients Awaiting Heart Transplantation*. N Engl J Med, 2007. **357**(9): p. 885-96.
21. Pagani, F.D., et al., *Extended mechanical circulatory support with a continuous-flow rotary left ventricular assist device*. J Am Coll Cardiol, 2009. **54**(4): p. 312-21.
22. Starling, R.C., et al., *Results of the post-U.S. Food and Drug Administration-approval study with a continuous flow left ventricular assist device as a bridge to heart transplantation: a prospective study using the INTERMACS (Interagency Registry for Mechanically Assisted Circulatory Support)*. J Am Coll Cardiol, 2011. **57**(19): p. 1890-8.
23. Slaughter, M.S., et al., *Advanced heart failure treated with continuous-flow left ventricular assist device*. N Engl J Med, 2009. **361**(123): 241-51.
24. Esmore, D., et al., *A prospective, multicenter trial of the VentrAssist left ventricular assist device for bridge to transplant: safety and efficacy*. J Heart Lung Transplant, 2008. **27**(6): p. 579-88.

25. Strueber, M., et al., *Multicenter evaluation of an intrapericardial left ventricular assist system*. J Am Coll Cardiol, 2011. **57**(12): p. 1375-82.
26. Slaughter, M.S., et al., *HeartWare ventricular assist system for bridge to transplant: combined results of the bridge to transplant and continued access protocol trial*. J Heart Lung Transplant, 2013. **32**(7): p. 675-83.
27. Dell'Aquila, A.M., et al., *Initial clinical experience with the HeartWare left ventricular assist system: a single-center report*. Ann Thorac Surg, 2013. **95**(1): p. 170-7.
28. Wu, L., et al., *Outcomes of HeartWare Ventricular Assist System support in 141 patients: a single-centre experience*. Eur J Cardiothorac Surg, 2013. **44**(1): p. 139-45.
29. Rogers, J.G., et al., *Chronic mechanical circulatory support for inotrope-dependent heart failure patients who are not transplant candidates: results of the INTrEPID Trial*. J Am Coll Cardiol, 2007. **50**(8): p. 741-7.
30. Rose, E.A., et al., *Long-term use of a left ventricular assist device for end-stage heart failure*. N Engl J Med, 2001. **345**(20): p. 1435-43.
31. Witt, B.J., et al., *The incidence of ischemic stroke in chronic heart failure: a meta-analysis*. J Card Fail, 2007. **13**: p. 489-96.
32. Starling, R.C., et al., *Unexpected abrupt increase in left ventricular assist device thrombosis*. N Engl J Med, 2014. **370**(1): p. 33-40.
33. Kirklin, J.K., et al., *Interagency Registry for Mechanically Assisted Circulatory Support (INTERMACS) analysis of pump thrombosis in the HeartMate II left ventricular assist device*. J Heart Lung Transplant, 2014. **33**(1): p. 12-22.
34. FDA, *Serious Adverse Events with Implantable Left Ventricular Assist Devices (LVADs): FDA Safety Communication*. Available at <http://www.fda.gov/MedicalDevices/Safety/AlertsandNotices/ucm457327.htm>, 2015.
35. DeVore, A.D., C.A. Milano, and J.G. Rogers, *VAD therapy 20/20: moving beyond the myopic view of a nascent therapy*. Ann Cardiothorac Surg, 2014. **3**(6): p. 603-5.
36. Chung, I. and G.Y. Lip, *Virchow's Triad Revisited: Blood Constituents*. Pathophysiol Haemost Thromb, 2003. **35**: p. 449-54.
37. Wolberg, A.S., et al., *Procoagulant activity in hemostasis and thrombosis: Virchow's triad revisited*. Anesth Analg, 2012. **114**(2): p. 275-85.
38. Gatti, A.M., et al., *In-vivo short- and long-term evaluation of the interaction material-blood*. J Mater Sci Mater Med, 2005. **16**(12): p. 1213-9.

39. Gorbet, M.B. and M.V. Sefton, *Biomaterial-associated thrombosis: roles of coagulation factors, complement, platelets and leukocytes*. *Biomaterials*, 2004. **25**(26): p. 5681-703.
40. Basmadjian, D., M.V. Sefton, and S.A. Baldwin, *Coagulation on biomaterials in flowing blood: some theoretical considerations*. *Biomaterials*, 1997. **18**(23): p. 1511-22.
41. Sefton, M.V., et al., *Does surface chemistry affect thrombogenicity of surface modified polymers?* *J Biomed Mater Res.*, 2001. **55**(4): p. 447-59.
42. Dion, I., et al., *Haemocompatibility of Ti6Al4V alloy*. *Biomaterials*, 1993. **14**: p. 122-6.
43. Schaub, R.D., et al., *Assessing acute platelet adhesion on opaque metallic and polymeric biomaterials with fiber optic microscopy*. *J Biomed Mater Res A*, 2000. **49**: p. 460-8.
44. Riedel, N.A., et al., *Improved thrombogenicity on oxygen etched Ti6Al4V surfaces*. *Mater Sci Eng C* 2012. **32**: p. 1196–1203.
45. Walkowiak-Przybyło, M., et al., *Adhesion, activation, and aggregation of blood platelets and biofilm formation on the surfaces of titanium alloys Ti6Al4V and Ti6Al7Nb*. *J Biomed Mater Res A* 2012. **1000**: p. 768–775.
46. Ye, S.H., et al., *Simple surface modification of a titanium alloy with silanated zwitterionic phosphorylcholine or sulfobetaine modifiers to reduce thrombogenicity*. *Colloids Surf B Biointerfaces*, 2010. **79**(2): p. 357-64.
47. Sheriff, J., et al., *Evaluation of shear-induced platelet activation models under constant and dynamic shear stress loading conditions relevant to devices*. *Ann Biomed Eng*, 2013. **41**(6): p. 1279-96.
48. Nesbitt, W.S., et al., *A shear gradient-dependent platelet aggregation mechanism drives thrombus formation*. *Nat Med*, 2009. **15**(6): p. 665-73.
49. Zhao, R., et al., *Micro-flow visualization of red blood cell-enhanced platelet concentration at sudden expansion*. *Ann Biomed Eng*, 2008. **36**(7): p. 1130-41.
50. Karino, T. and H.L. Goldsmith, *Adhesion of human platelets to collagen on the walls distal to a tubular expansion* *Microvasc Res*, 1979. **17**(3): p. 238-62.
51. Karino, T. and H.L. Goldsmith, *Aggregation of human platelets in an annular vortex distal to a tubular expansion*. *Microvasc Res*, 1979. **17**(3): p. 217-37.
52. Mandrusov, E., et al., *Separated Flows in Artificial Organs: A Cause of Early Thrombogenesis?* *ASAIO J*, 1996. **42**(5): p. M506-13.

53. Alemu, Y. and D. Bluestein, *Flow-induced platelet activation and damage accumulation in a mechanical heart valve: numerical studies*. *Artif Organs*, 2007. **31**(9): p. 677-88.
54. Ahn, T., et al., *Influence of stent expansion states on platelet deposition in an extracorporeal porcine arteriovenous shunt model using a multichannel perfusion chamber*. *J Korean Med Sci*, 2001. **16**: p. 31-8.
55. Wootton, D.M., et al., *A Mechanistic Model of Acute Platelet Accumulation in Thrombotic Stenoses*. *Annals of Biomedical Engineering*, 2001. **29**(4): p. 321-329.
56. Yin, W., et al., *Flow-induced platelet activation in bileaflet and monoleaflet mechanical heart valves*. *Ann Biomed Eng*, 2004. **32**(8): p. 1058-66.
57. Yang, F., R.L. Kormos, and J.F. Antaki, *High-speed visualization of disturbed pathlines in axial flow ventricular assist device under pulsatile conditions*. *J Thorac Cardiovasc Surg*, 2015.
58. Fatullayev, J., et al., *Continuous-Flow Left Ventricular Assist Device Thrombosis: A Danger Foreseen is a Danger Avoided*. *Med Sci Monit Basic Res*, 2015. **21**: p. 141-4.
59. Chong, A.Y. and G.Y. Lip, *Viewpoint: the prothrombotic state in heart failure: a maladaptive inflammatory response?* *Eur J Heart Fail*, 2007. **9**(2): p. 124-8.
60. Lip, G.Y. and C.R. Gibbs, *Does heart failure confer a hypercoagulable state? Virchow's triad revisited*. *J Am Coll Cardiol*, 1999. **35**(5): p. 1424-6.
61. Toeg, H., M. Ruel, and H. Haddad, *Anticoagulation strategies for left ventricular assist devices*. *Curr Opin Cardiol*, 2015.
62. Chuang, Y.J., et al., *Heparin enhances the specificity of antithrombin for thrombin and factor Xa independent of the reactive center loop sequence. Evidence for an exosite determinant of factor Xa specificity in heparin-activated antithrombin*. *J Biol Chem*, 2001. **276**(18): p. 14961-71.
63. Baumann Kreuziger, L.M., B. Kim, and G.M. Wieselthaler, *Antithrombotic therapy for left ventricular assist devices in adults: a systematic review*. *J Thromb Haemost*, 2015. **13**(6): p. 946-55.
64. Fitchett, D., et al., *Antiplatelet therapy and cardiac surgery: review of recent evidence and clinical implications*. *Can J Cardiol*, 2013. **29**(9): p. 1042-7.

65. Jennings, D.L. and P.A. Weeks, *Thrombosis in continuous-flow left ventricular assist devices: pathophysiology, prevention, and pharmacologic management*. *Pharmacotherapy*, 2015. **35**(1): p. 79-98.
66. Joshi, A., et al., *Anticoagulant monitoring in ventricular assist device patients: a feasibility study*. *Interact Cardiovasc Thorac Surg*, 2008. **7**(6): p. 1035-8.
67. Stehlik, J., S.A. Johnson, and C.H. Selzman, *Gold standard in anticoagulation assessment of left ventricular assist device patients?: how about bronze*. *JACC Heart Fail*, 2015. **3**(4): p. 323-6.
68. Ansell, J., et al., *Pharmacology and management of the vitamin K antagonists: American College of Chest Physicians Evidence-Based Clinical Practice Guidelines (8th Edition)*. *Chest*, 2008. **133**(6 Suppl): p. 160S-198S.
69. Tello-Montoliu, A., et al., *Impact of aspirin dose on adenosine diphosphate-mediated platelet activities. Results of an in vitro pilot investigation*. *Thromb Haemost*, 2013. **110**(4): p. 777-84.
70. Bluestein, D., S. Einav, and M.J. Slepian, *Device thrombogenicity emulation: A novel methodology for optimizing the thromboresistance of cardiovascular devices*. *J Biomech.*, 2013. **46**(2): p. 338-344.
71. Filipovic, N., M. Kojic, and A. Tsuda, *Modelling thrombosis using dissipative particle dynamics method*. *Philos Trans A Math Phys Eng Sci*, 2008. **366**(1879): p. 3265-79.
72. Goodman, P.D., et al., *Computational Model of Device-Induced Thrombosis and Thromboembolism*. *Ann Biomed Eng*, 2005. **33**(6): p. 780-797.
73. Hund, S.J. and J.F. Antaki, *An extended convection diffusion model for red blood cell-enhanced transport of thrombocytes and leukocytes*. *Phys Med Biol*, 2009. **54**(20): p. 6415-35.
74. Xenos, M., et al., *Device Thrombogenicity Emulator (DTE)--design optimization methodology for cardiovascular devices: a study in two bileaflet MHV designs*. *J Biomech*, 2010. **43**(12): p. 2400-9.
75. Xu, Z., et al., *A multiscale model of thrombus development*. *J R Soc Interface*, 2008. **5**(24): p. 705-22.
76. Fogelson, A.L., *Continuum models of platelet aggregation: formulation and mechanical properties*. *SIAM J. Appl. Math.*, 1992. **52**: p. 1089-1110.
77. Sorensen, E.N., et al., *Computational simulation of platelet deposition and activation: II. Results for Poiseuille flow over collagen*. *Ann Biomed Eng*, 1999. **27**: p. 449-58.

78. Sorensen, E.N., et al., *Computational simulation of platelet deposition and activation: I. Model development and properties*. Ann Biomed Eng, 1999. **27**: p. 436-48.
79. Bedekar, A.S., *A computational model combining vascular biology and haemodynamics for thrombosis prediction in anatomically accurate cerebral aneurysms*. Food Bioprod. Process, 2005. **83**(2): p. 118-126.
80. Jordan, A., et al., *The effects of margination and red cell augmented platelet diffusivity on platelet adhesion in complex flow*. Biorheology, 2004. **41**(5): p. 641-653.
81. Anand, M., K. Rajagopal, and K.R. Rajagopal, *A model for the formation and lysis of blood clots*. Pathophysiol Haemost Thromb, 2005. **34**: p. 109-120.
82. Goodman, P.D., et al., *Computational model of device-induced thrombosis and thromboembolism*. Ann Biomed Eng, 2005. **33**(6): p. 780-797.
83. Leiderman, K. and A.L. Fogelson, *“Grow with the flow: a spatial–temporal model of platelet deposition and blood coagulation under flow*. Math. Med. Biol., 2010. **28**(1): p. 47-84.
84. Sin, D.C., H.L. Kei, and X. Miao, *Surface coatings for ventricular assist devices*. Expert Rev Med Devices, 2009. **6**(1): p. 51-60.
85. Savage, B., E. Saldívar, and Z.M. Ruggeri, *Initiation of platelet adhesion by arrest onto fibrinogen or translocation on von Willebrand factor*. Cell, 1996. **84**(4): p. 289-97.
86. Dise, C.A., J.W. Burch, and D.B. Goodman, *Direct interaction of mepacrine with erythrocyte and platelet membrane phospholipid*. J BiolChem, 1982. **257**(9): p. 4701-4.
87. Schwach, G. and H. Passow, *Preparation and properties of human erythrocyte ghosts*. Mol Cell Biochem, 1973. **2**: p. 197-218.
88. Aarts, P.A., et al., *Blood platelets are concentrated near the wall and red blood cells, in the center in flowing blood*. Arteriosclerosis, 1988. **8**(6): p. 819-824.
89. Goldsmith, H.L., et al., *Physical and Chemical Effects of Red Cells in the Shear-induced Aggregation of Human Platelets*. Biophys J, 1995. **69**: p. 1584-95.
90. Bozzo, J., et al., *Comparison of the effects of human erythrocyte ghosts and intact erythrocytes on platelet interactions with subendothelium in flowing blood*. Biorheology, 2001. **38**: p. 429-37.

91. Johnson, C.A., et al., *Biocompatibility assessment of the first generation PediaFlow pediatric ventricular assist device*. *Artif Organs*, 2011. **35**(1): p. 9-21.
92. Kent, N.J., et al., *Microfluidic device to study arterial shear-mediated platelet-surface interactions in whole blood: reduced sample volumes and well-characterised protein surfaces*. *Biomed Microdevices*, 2010. **12**(6): p. 987-1000.
93. Song, X., et al., *Quantitative Evaluation of Blood Damage in a Centrifugal VAD by Computational Fluid Dynamics*. *J. Fluids Eng* 2004. **126**(3): p. 410-18.
94. Wu, J., et al., *Computational fluid dynamics analysis of blade tip clearances on hemodynamic performance and blood damage in a centrifugal ventricular assist device*. *Artif Organs*, 2010. **34**(5): p. 402-11.
95. Zhang, Y., et al., *Design optimization of an axial blood pump with computational fluid dynamics*. *ASAIO J*, 2008. **54**(2): p. 150-5.
96. Johnson, C.A., Jr., et al., *Flow cytometric assays for quantifying activated ovine platelets*. *Artif Organs*, 2008. **32**(2): p. 136-45.
97. Deible, C.R., et al., *Molecular barriers to biomaterial thrombosis by modification of surface proteins with polyethylene glycol*. *Biomaterials*, 1999. **20**: p. 101-9.
98. Lei, L., et al., *Photo-immobilized heparin micropatterns on Ti–O surface: preparation, characterization, and evaluation in vitro*. *J Mater Sci*, 2011. **46**(21): p. 6772-6782.
99. Godo, M.N. and M.V. Sefton, *Characterization of transient platelet contacts on a polyvinyl alcohol hydrogel by video microscopy*. *Biomaterials*, 1999. **20**: p. 1117-26.
100. Otto, M., et al., *Modification of human platelet adhesion on biomaterial surfaces by protein preadsorption under static and flow conditions*. *J Mater Sci Mater Med* 2004. **15**: p. 35-42.
101. Xu, C. and D.M. Wootton, *Platelet near-wall excess in porcine whole blood in artery-sized tubes under steady and pulsatile flow conditions*. *Biorheology*, 2004. **41**: p. 113-25.
102. Tokarev, A.A., A.A. Butylin, and F.I. Ataullakhanov, *Platelet adhesion from shear blood flow is controlled by near-wall rebounding collisions with erythrocytes*. *Biophys J*, 2011. **100**(4): p. 799-808.
103. Kim, S., et al., *The cell-free layer in microvascular blood flow*. *Biorheology*, 2009. **46**: p. 181-9.

104. Sherwood, J.M., et al., *The effect of red blood cell aggregation on velocity and cell-depleted layer characteristics of blood in a bifurcating microchannel*. *Biomicrofluidics*, 2012. **6**(2): p. 24119.
105. Baskurt, O.K., et al., *Parameterization of red blood cell elongation index--shear stress curves obtained by ektacytometry*. *Scand J Clin Lab Invest*, 2009. **69**(7): p. 777-88.
106. Szarvas, M., et al., *Differential platelet deposition onto collagen in cone-and-plate and parallel plate flow chambers*. *Platelets*, 2006. **17**(3): p. 185-90.
107. Wang, S., et al., *Biomimetic fluorocarbon surfactant polymers reduce platelet adhesion on PTFE/ePTFE surfaces*. *J Biomater Sci Polym Ed*, 2009. **20**(5-6): p. 619-35.
108. Uchida, M., et al., *Reduced platelet adhesion to titanium metal coated with apatite, albumin-apatite composite or laminin-apatite composite*. *Biomaterials*, 2005. **26**(34): p. 6924-31.
109. Milner, K.R., A.J. Snyder, and C.A. Siedlecki, *Sub-micron texturing for reducing platelet adhesion to polyurethane biomaterials*. *J Biomed Mater Res A*, 2006. **76**(3): p. 561-70.
110. Furukawa, K.S., et al., *Quantitative analysis of human platelet adhesions under a small-scale flow device*. *Artif Organs*, 2010. **34**(4): p. 295-300.
111. Tsai, W.B., et al., *Platelet adhesion to polystyrene-based surfaces preadsorbed with plasmas selectively depleted in fibrinogen, fibronectin, vitronectin, or von Willebrand's factor*. *J Biomed Mater Res A*, 2002. **60**(3): p. 348-59.
112. Tsai, W.B., J.M. Grunkemeier, and T.A. Horbett, *Variations in the ability of adsorbed fibrinogen to mediate platelet adhesion to polystyrene-based materials: a multivariate statistical analysis of antibody binding to the platelet binding sites of fibrinogen*. *J Biomed Mater Res A*, 2003. **67**(4): p. 1255-68.
113. Colace, T., et al., *Analysis of morphology of platelet aggregates formed on collagen under laminar blood flow*. *Ann Biomed Eng*, 2011. **39**: p. 922-9.
114. Tonda, R., et al., *Platelets interact with tissue factor immobilized on surfaces: effects of shear rate*. *Eur J Clin Invest*, 2008. **38**(1): p. 34-42.
115. Hoffman, A.S., et al., *Application of radiation-grafted hydrogels as blood-contacting biomaterials*. *Radiat Phys Chem*, 1983. **22**: p. 267-83.
116. Hund, S.J., J.F. Antaki, and M. Massoudi, *On the Representation of Turbulent Stresses for Computing Blood Damage*. *Int J Eng Sci* 2010. **48**: p. 1325-31.

117. Flamm, M.H. and S.L. Diamond, *Multiscale systems biology and physics of thrombosis under flow*. Ann Biomed Eng, 2012. **40**(11): p. 2355-64.
118. Woolley, J.R., et al., *Temporal leukocyte numbers and granulocyte activation in pulsatile and rotary ventricular assist device patients*. Artif Organs, 2014. **38**(6): p. 447-55.
119. Golański, J., et al., *Molecular insights into the anticoagulant-induced spontaneous activation of platelets in whole blood-various anticoagulants are not equal*. Thromb Res 1996. **83**: p. 199-216.
120. Harding, S.A., et al., *Flow cytometric analysis of circulating platelet-monocyte aggregates in whole blood: methodological considerations*. Thromb Haemost, 2007. **98**(2): p. 451-6.
121. Wagner, W.R. and J.A. Hubbell, *Local thrombin synthesis and fibrin formation in an in vitro thrombosis model result in platelet recruitment and thrombus stabilization on collagen in heparinized blood*. J Lab Clin Med, 1990. **116**(5): p. 636-50.
122. Jackson, S.P., *The growing complexity of platelet aggregation*. Blood, 2007. **109**(12): p. 5087-95.
123. Timms, D., et al., *Evaluation of left ventricular assist device performance and hydraulic force in a complete mock circulation loop*. Artif Organs, 2005. **29**(7): p. 573-80.
124. Schaller, J., et al., *Biocompatibility Material Test for Cardiovascular Devices using Stagnation Point Flow*. Biomed Tech (Berl), 2013.
125. Jamiolkowski, M.A., et al., *Real time visualization and characterization of platelet deposition under flow onto clinically relevant opaque surfaces*. J Biomed Mater Res A, 2015. **103**(4): p. 1303-11.
126. Lowe, G.D., *Virchow's triad revisited: abnormal flow*. Pathophysiol Haemost Thromb, 2003. **33**(5-6): p. 455-7.
127. Sherwood, J.M., et al., *Hematocrit, viscosity and velocity distributions of aggregating and non-aggregating blood in a bifurcating microchannel*. Biomech Model Mechanobiol, 2014. **13**(2): p. 259-73.
128. Wereley, S.T. and C.D. Meinhart, *Recent Advances in Micro-Particle Image Velocimetry*. Annu Rev Fluid Mech., 2010. **42**(1): p. 557-576.
129. Burgreen, G., et al., *A computational and experimental comparison of two outlet stators for the Nimbus LVAD. Left ventricular assist device*. ASAIO J, 1999. **45**(4): p. 328-33.

130. Ha, H. and S.J. Lee, *Hemodynamic features and platelet aggregation in a stenosed microchannel*. *Microvasc Res*, 2013. **90**: p. 96-105.
131. Li, M., D.N. Ku, and C.R. Forest, *Microfluidic system for simultaneous optical measurement of platelet aggregation at multiple shear rates in whole blood*. *Lab Chip*, 2012. **12**(7): p. 1355-62.
132. Taylor, J.O., et al., *In vitro quantification of time dependent thrombus size using magnetic resonance imaging and computational simulations of thrombus surface shear stresses*. *J Biomech Eng*, 2014. **136**(7).
133. Tamagawa, M., et al., *Simulation of thrombus formation in shear flows using Lattice Boltzmann Method*. *Artif Organs*, 2009. **33**(8): p. 604-10.
134. Dyke, M.V., *An album of fluid motion* 1982, Stanford, CA: Parabolic Press.
135. Razi, M., et al., *Synergism between collagen-adenosine diphosphate and collagen-epinephrine in platelets' aggregation: different dose response relationships*. *J Pak Med Assoc*, 2009. **56**: p. 368-71.
136. Huang, E. and T. Detwiler, *Characteristics of the synergistic actions of platelet agonists*. *Blood*, 1981. **57**: p. 685-91.
137. McGlasson, D.L. and G.A. Fritsma, *Whole blood platelet aggregometry and platelet function testing*. *Semin Thromb Hemost*, 2009. **35**(2): p. 168-80.
138. Alkhamis, T.M., R.L. Beissinger, and J.R. Chediak, *Artificial surface effect on red blood cells and platelets in laminar shear flow*. *Blood*, 1990. **75**(7): p. 1568-75.
139. Helms, C.C., et al., *Mechanisms of hemolysis-associated platelet activation*. *J Thromb Haemost*, 2013. **11**(12): p. 2148-54.
140. Hubbell, J.A. and L.V. McIntire, *Platelet active concentration profiles near growing thrombi. A mathematical consideration*. *Biophys J*, 1986. **50**(5): p. 937-45.
141. Hubbell, J.A. and L.V. McIntire, *Visualization and analysis of mural thrombogenesis on collagen, polyurethane and nylon*. *Biomaterials*, 1986. **7**(5): p. 354-63.
142. Folie, B.J. and L.V. McIntire, *Mathematical analysis of mural thrombogenesis. Concentration profiles of platelet-activating agents and effects of viscous shear flow*. *Biophys J*, 1989. **56**(6): p. 1121-41.
143. Gear, A.R., *Preaggregation reactions of platelets*. *Blood*, 1981. **58**(3): p. 477-90.
144. Stalker, T.J., et al., *Hierarchical organization in the hemostatic response and its relationship to the platelet-signaling network*. *Blood*, 2013. **121**(10): p. 1875-85.

145. Fegghi, S. and N.J. Sniadecki, *Mechanobiology of platelets: techniques to study the role of fluid flow and platelet retraction forces at the micro- and nano-scale*. Int J Mol Sci, 2011. **12**(12): p. 9009-30.
146. Thompson, N.T., M.C. Scrutton, and R.B. Wallis, *Synergistic responses in human platelets. Comparison between aggregation, secretion and cytosolic Ca<sup>2+</sup> concentration*. Eur J Biochem, 1986. **161**(2): p. 399-408.
147. Paniccia, R., et al., *Platelet function tests: a comparative review*. Vasc Health Risk Manag, 2015. **11**: p. 133-48.
148. Bell, D.N., S. Spain, and H.L. Goldsmith, *Adenosine diphosphate-induced aggregation of human platelets in flow through tubes. II. Effect of shear rate, donor sex, and ADP concentration*. Biophys J, 1989. **56**(5): p. 829-43.
149. Neeves, K.B. and S.L. Diamond, *A membrane-based microfluidic device for controlling the flux of platelet agonists into flowing blood*. Lab Chip, 2008. **8**(5): p. 701-9.
150. Rozalski, M., M. Nocun, and C. Watala, *Adenosine diphosphate receptors on blood platelets - potential new targets for antiplatelet therapy*. Acta Biochim Pol, 2005. **52**: p. 411-5.
151. Soucy, K.G., et al., *Rotary pump speed modulation for generating pulsatile flow and phasic left ventricular volume unloading in a bovine model of chronic ischemic heart failure*. J Heart Lung Transplant, 2015. **34**(1): p. 122-31.
152. Soucy, K.G., et al., *Rotary pumps and diminished pulsatility: do we need a pulse?* ASAIO J, 2013. **59**(4): p. 355-66.
153. da Rocha, E.S.J.G., et al., *Influence of aortic valve opening in patients with aortic insufficiency after left ventricular assist device implantation*. Eur J Cardiothorac Surg, 2015.
154. Hurst, T.E., N. Moazami, and R.C. Starling, *Left ventricular assist device thrombosis in the setting of left ventricular recovery*. J Heart Lung Transplant, 2015. **34**(4): p. 622-3.
155. Goodman, S.L., *Sheep, pig, and human platelet-material interactions with model cardiovascular biomaterials*. J Biomed Mater Res., 1999. **45**(3): p. 240-50.
156. Pelagalli, A., et al., *Adhesive properties of platelets from different animal species*. J Comp Pathol, 2003. **126**: p. 127-31.
157. Baker, L.C., et al., *Flow cytometric assays to detect platelet activation and aggregation in device-implanted calves*. J Biomed Mater Res, 1997. **42**(2): p. 312-21.

158. Toda, K. and Y. Sawa, *Clinical management for complications related to implantable LVAD use*. Gen Thorac Cardiovasc Surg, 2015. **63**(1): p. 1-7.
159. Tchanchaleishvili, V., et al., *Evaluation and treatment of pump thrombosis and hemolysis*. Ann Cardiothorac Surg, 2014. **3**(5): p. 490-5.
160. Pepper, J.R., *Update on mechanical circulatory support in heart failure*. Heart, 2012. **98**(8): p. 663-9.
161. Spiliopoulos, K., et al., *Current status of mechanical circulatory support: a systematic review*. Cardiol Res Pract, 2012. **2012**: p. 574198.